HYDROLOGICAL IMPACT OF LAND USE AND CLIMATE CHANGE ON THE WEST COAST RIVER BASINS OF KARNATAKA

Thesis
Submitted in partial fulfillment of the requirements for the degree of

DOCTOR OF PHILOSOPHY
by
SHARANNYA T.M.

DEPARTMENT OF WATER RESOURCES AND OCEAN ENGINEERING
NATIONAL INSTITUTE OF TECHNOLOGY KARNATAKA
SURATHKAL, MANGALORE- 575 025
DECEMBER 2022

HYDROLOGICAL IMPACT OF LAND USE AND CLIMATE CHANGE ON THE WEST COAST RIVER BASINS OF KARNATAKA

Thesis
Submitted in partial fulfillment of the requirements for the degree of

DOCTOR OF PHILOSOPHY
by
SHARANNYA T.M.

(187528AM508)

Under the guidance of

Dr. AMAI MAHESHA

Professor

Department of Water Resources and Ocean Engineering

NITK Surathkal

DEPARTMENT OF WATER RESOURCES AND OCEAN ENGINEERING

NATIONAL INSTITUTE OF TECHNOLOGY KARNATAKA

SURATHKAL, MANGALORE- 575 025

DECEMBER 2022

DECLARATION

By the Ph.D. Research Scholar

I hereby *declare* that the Research Thesis entitled **"Hydrological Impact of Land Use and Climate Change on the West Coast River Basins of Karnataka"**, which is being submitted to the National Institute of Technology Karnataka, Surathkal in partial fulfilment of the requirements for the award of the Degree of Doctor of Philosophy in the Department of Water Resources and Ocean Engineering is a *bonafide report of the research work carried out by me*. The material contained in this Research Thesis has not been submitted to any University or Institution for the award of any degree.

SHARANNYA T. M.

(Register Number: 187528AM508)

Department of Water Resources and Ocean Engineering

National Institute of Technology Karnataka, India

Place: NITK Surathkal

Date: 28/12/2022

CE R T I F I CATE

This is to *certify* that the Research Thesis entitled **"Hydrological Impact of Land Use and Climate Change on the West Coast River Basins of Karnataka"**, submitted by **SHARANNYA T M** (Register Number: 187528AM508) as the record of the research work carried out by her, is *accepted as the Research Thesis submission* in partial fulfilment of the requirements for the award of the degree of **Doctor of Philosophy**.

Dr. AMAI MAHESH 22
Professor
Research Guide

Chairman - DRPC

Chairman (DRPC)
Dept. of Water Resources & Ocean Engineering

Department of Water Resources and Ocean Engineering
National Institute of Technology Karnataka, India

ACKNOWLEDGMENTS

I must offer my profound gratitude to my supervisor, Prof. Amai Mahesha, for his unreserved help and guidance. It is his timely suggestions that lead me to finish my thesis systematically. His words can always inspire me and promote me to think and explore more in my research work.

I also extend my sincere thanks to our HoD Prof. B.M. Dodamani, our former HoD, Prof. Amba Shetty, for their support.

To my RPAC, Prof. Katta Venkataramana, and Dr. K. Varija: Thank you for your significant inputs in shaping this study and all the faculty and my friends who had helped directly or indirectly, especially Venkatesh Kolluru and Surajit Deb Barma.

I acknowledge the Indian National Committee on Climate Change (INCCC), Ministry of Jal Shakti, Government of India, and Indian Institute of Technology Bombay, for giving me the opportunity to work under the project 'Impact of Climate Change on Water Resources in River Basins from Tadri to Kanyakumari' as a research fellow and thank for their financial support for the research work.

I sincerely express my gratitude to my parents, siblings, and in-laws for their support and encouragement in completing this work.

Very special thanks to my husband for his support and assistance in every step of my research work. I would like to thank him for making my mind relax during the hard times of my research.

I am also grateful to the department staff: Balu Anna, Sweekritha Madam, Harish Anna, Anil Anna, and Jagadish Sir for their unfailing support and assistance throughout my Ph.D. Very special gratitude goes out to everyone in the Administrative block and Accounts section for their cooperation.

Above all, I wish to express my heartfelt thanks to the Almighty God for giving me the opportunity to do this work.

ABSTRACT

The Western Ghats of India is an environmental and climate-sensitive region of India. The Western Ghats are the mountainous forest range of a tropical region that play significant role in distributing Indian monsoon rains. Three west-flowing rivers of the Western Ghats representing different levels of anthropogenic influence were chosen for this study to understand the individual and combined effect of land use land cover (LULC) and climate change (CC) on the hydrology of river basins that spread over the northern, middle and southern portion of the west coast Karnataka. The study was carried out with five objectives which include (i) Assessment of satellite and India Meteorological Department (IMD) rainfall products for streamflow simulation in the study area, (ii) To investigate long-term changes in current LULC and model predicted future LULC scenarios on streamflow, (iii) To evaluate the impact of long-term climate change on regional hydrology using SWAT and to assess the river basin responses, (iv) To assess the combined impact of land use land cover change and climate change over the study area, (v) Scenario analysis of the combined effect of land-use change and climate change on blue water and green water availability.

Evaluation of satellite precipitation data was performed using the Tropical Rainfall Measuring Mission (TRMM) and Climate Hazards Group InfraRed Precipitation with Station data (CHIRPS), employing a semi-distributed hydrological model, i.e., Soil and Water Assessment Tool (SWAT), for simulating streamflow and validating them against the flows generated by the India Meteorological Department (IMD) rainfall dataset. The historical land use (LU) changes were studied for four decades (1988–2016) using the maximum likelihood algorithm and the long-term LU (2016–2100) was estimated using the Dyna-CLUE prediction model. Five General Circulation Models (GCMs) were utilized to assess the effects of climate change (CC) and the SWAT model was used for hydrological modeling of the three river basins. To characterize granular effects of LU and CC on regional hydrology, a scenario approach was adopted and three scenarios depicting near-future (2006–2040), mid-future (2041–2070), and far future (2071–2100) based on climate were established.

It was observed that the IMD rainfall-driven streamflow emerged as the best followed by the TRMM, CHIRPS-0.05, and CHIRPS-0.25. The impact of climate change was more predominant than the impact due to land use land cover. However, deforestation and the conversion of other LULC into an unorganized plantation/ agriculture with urban expansion contribute to an increase in streamflow. As per the water availability and vulnerability assessment, the Aghanashini basin was classified under the extremely vulnerable sector, Gurupura and Varahi basins under the low vulnerable sector for water scarcity. The thesis is an attempt to study the LULC comprehensively on the impact on rivers of the Western Ghats of India and is an effective tool in understanding the hydrological impacts and adopting strategies to counter the impacts of LULC and CC.

Keywords: Climate Change; Dyna CLUE; Land Use; Satellite precipitation data; SWAT; Water Scarcity; West Coast of Karnataka; Western Ghats of India

TABLE OF CONTENTS

ABSTRACT i

LIST OF FIGURES vii

LIST OF TABLES xiii

LIST OF ABBREVIATIONS xiv

CHAPTER 1 1

INTRODUCTION 1

1.1 GENERAL 1

1.2 CLIMATE CHANGE 3

1.2.1 General aspects including various scenarios 3

1.3 LAND USE LAND COVER CHANGE 4

1.3.1 General aspects and present trend 4

1.4 SATELLITE-BASED RAINFALL DATA 4

1.4.1 General aspects and significance 4

1.5 SCOPE OF THE STUDY 5

1.6 OBJECTIVES 6

1.7 ORGANIZATION OF THE THESIS 6

CHAPTER 2 9

LITERATURE REVIEW 9

2.1 GENERAL 9

2.2 ADEQUACY OF SATELLITE RAINFALL DATA FOR STREAMFLOW PREDICTION 9

2.3 LAND USE LAND COVER STUDIES 10

2.4 CLIMATE CHANGE STUDIES 12

2.5 RELATED STUDIES IN THE WESTERN GHATS 13

2.6 THE RAINFALL-RUNOFF MODELS 14

2.7 WATER SCARCITY AND VULNERABILITY ANALYSIS 14

2.8 LITERATURE GAP 15

CHAPTER 3 17

STUDY AREA 17

3.1 GENERAL 17

3.1.1 Aghanashini River Basin (ARB) 18

3.1.2 Varahi River Basin (VRB) 19

3.1.3 Gurupura River Basin (GRB) 21

CHAPTER 4 23

EVALUATION OF SATELLITE PRECIPITATION PRODUCTS IN SIMULATING STREAMFLOW ... 23

4.1 GENERAL 23

4.2 SATELLITE PRECIPITATION DATASETS 23

4.2.1 Gauge-Based Meteorological Data 23

4.2.2 TRMM Rainfall Data 24

4.2.3 CHIRPS Rainfall Data 24

4.3 METHODOLOGY 25

4.3.1 Statistical Evaluation of the Satellite Precipitation Data 25

4.3.2 Hydrologic Model 25

4.3.3 Model Calibration, Validation and Uncertainty Analysis 26

4.3.4 Performance Indices for Examining Streamflow Simulation 27

4.3.5 Streamflow Simulations Using Satellite Precipitation Datasets in SWAT 28

4.4 RESULTS AND DISCUSSION 29

4.4.1 Performance of Satellite Precipitation Datasets 29

4.4.2 Evaluation of Streamflow Generation 30

4.4.3 Hydrologic Process Simulation 34

4.5 CLOSURE 39

CHAPTER 5 41

RIVER BASIN RESPONSE ON EFFECTS OF LAND USE AND CLIMATE CHANGE 41

5.1 METHODOLOGY 41

5.1.2 Pre-processing of Landsat data 42
5.1.3 Principle of Dyna-CLUE and its structure for projection of future LULC..... 42
5.1.4 Logistic Regression 45
5.1.5 Allocation Procedure 47
5.1.6 Mapping of Input Drivers 47
5.1.7 Scenario Analysis 51
5.2 RESULTS AND DISCUSSION 52
5.2.1 GCM climate data analysis..... 52
5.2.2 LULC Change Analysis from 1988 to 2100 63
5.2.3 Calibration and Validation of the SWAT Model 67
5.2.4 Impacts of LULC changes on streamflow..... 70
5.2.5 Impact of climate change on streamflow 79
5.2.6 Combined impacts of LULC and climate change on streamflow..... 89
CHAPTER 6 101
BASIN-SCALE WATER AVAILABILITY AND VULNERABILITY ASSESSMENT 101
6.1 METHODOLOGY 101
6.2 RESULTS AND DISCUSSION 102
6.2.1 Basin-scale water availability and vulnerability assessment 102
6.3 Keen observervation for the River Basin 105
6.3.1 Keen observation for Aghanashini River Basin 105
6.3.2 Keen observation for the Varahi River Basin 107
6.3.3 Keen observation for the Gurupura River Basin 108
CHAPTER 7 111
SUMMARY AND CONCLUSIONS..... 111
7.1 EVALUATION OF SATELLITE PRECIPITATION PRODUCTS IN SIMULATING STREAMFLOW 111
7.2 RIVER BASIN RESPONSE ON EFFECTS OF LAND USE AND CLIMATE CHANGE 112
7.3 BASIN-SCALE WATER AVAILABILITY AND VULNERABILITY ASSESSMENT 115

7.4 LIMITATIONS OF THE STUDY 117

7.5 SCOPE FOR FUTURE RESEARCH 117

REFERENCES.....119

PUBLICATIONS……133

BRIEF BIO……...135

LIST OF FIGURES

Fig.No.	Figure Caption	Page No.
3.1	Study area	15
3.2	(a) Location map and sub-basins of the study area, (b) DEM (c) Soil data, (d) LULC categories, and (e) monthly average precipitation of ARB.	19
3.3	(a) Location map and sub-basins of the study area, (b) DEM (c) Soil data, (d) LULC categories, and (e) monthly average precipitation of VRB.	20
3.4	(a) Location map and sub-basins of the study area, (b) DEM (c) Soil data, (d) LULC categories, and (e) monthly average precipitation of GRB.	21
4.1	Daily simulation of streamflow for different precipitation datasets.	32
5.1	Input drivers used for predicting land use in the ARB	49
5.2	Input drivers used for predicting land use in the VRB	50
5.3	Input drivers used for predicting land use in the GRB	50
5.4	Taylor diagram for: a) rainfall (mm/month), b) Tmax (°C), and c) Tmin (°C) for (i) ARB, (ii) VRB, (iii) GRB	52
5.5	GCM variables (red) compared with observed variables (black) for daily: a) rainfall; b) maximum temperature, and c) minimum temperature from 1981 to 2005 in ARB	54
5.6	GCMs variables (red) compared with observed variables (black) for daily: a) rainfall; b) maximum temperature, and c) minimum temperature from 1981 to 2005 in VRB	55
5.7	GCMs variables (red) compared with observed variables (black) for daily: a) rainfall; b) maximum temperature, and c) minimum temperature from 1981 to 2005 in GRB	56

Fig.No.	Figure Caption	Page No.
5.8	Comparison of historical observed and GCMs simulated rainfall (1981 to 2005) and projection of future rainfall (2006 to 2100) of RCP emission scenarios in ARB	57
5.9	Comparison of historical observed and GCMs simulated rainfall (1981 to 2005) and projection of future rainfall (2006 to 2100) of RCP emission scenarios in VRB	58
5.10	Comparison of historical observed and GCMs simulated rainfall (1981 to 2005) and projection of future rainfall (2006 to 2100) of RCP emission scenarios in GRB	58
5.11	Comparison of historical observed and GCMs simulated maximum temperature (1981 to 2005) and projection of future maximum temperature (2006 to 2100) of RCP 4.5 and RCP 8.5 emission scenarios (ENS- Ensembled) for ARB	60
5.12	Comparison of historical observed and GCMs simulated maximum temperature (1981 to 2005) and projection of future maximum temperature (2006 to 2100) of RCP 4.5 and RCP 8.5emission scenarios (ENS- Ensembled) for VRB	60
5.13	Comparison of historical observed and GCMs simulated maximum temperature (1981 to 2005) and projection of future maximum temperature (2006 to 2100) of RCP 4.5 and RCP 8.5 emission scenarios (ENS- Ensembled) for GRB	61
5.14	Comparison of historical observed and GCMs simulated minimum temperature (1981 to 2005) and projection of future minimum temperature (2006 to 2100) of RCP 4.5 and RCP 8.5 emission scenarios (ENS- Ensembled) for ARB	61
5.15	Comparison of historical observed and GCMs simulated minimum temperature (1981 to 2005) and projection of future minimum temperature (2006 to 2100) of RCP 4.5 and RCP 8.5 emission scenarios (ENS- Ensembled) for VRB	62

Fig.No.	Figure Caption	Page No.
5.16	Comparison of historical observed and GCMs simulated minimum temperature (1981 to 2005) and projection of future minimum temperature (2006 to 2100) of RCP 4.5 and RCP 8.5 emission scenarios (ENS- Ensembled) for GRB	62
5.17	LULC maps for 1988, 1995, 2003, 2016 (actual), 2016 (projected), 2030, 2050, 2075 and 2100 for ARB	64
5.18	LULC maps for 1988, 1995, 2003, 2016 (actual), 2016 (projected), 2030, 2050, 2075 and 2100 for VRB	66
5.19	LULC maps for 1988, 1995, 2003, 2016 (actual), 2016 (projected), 2030, 2050, 2075 and 2100 for GRB	66
5.20	Comparison between the observed and simulated monthly streamflow value for the calibration (a) and validation (b) for ARB	69
5.21	Comparison between the observed and simulated monthly streamflow value for the calibration (a) and Validation (b) for VRB	69
5.22	Comparison between the observed and simulated monthly streamflow value for the calibration (a) and Validation (b) for GRB	70
5.23	Spatial distribution of historical mean rainfall at sub-basin scale used for simulation: (i) ARB, (ii) VRB, (iii) GRB	71
5.24	Intercomparison of simulated streamflow at the watershed outlet for the LULC from 1988 to 2100: (i) ARB, (ii) VRB, (iii) GRB	72
5.25	Spatial distribution of change in the surface runoff (m3/s) for historical LULC 1988 to 2003 (a) 1988– 1995; (b) 1988–2003; (c) 1988-2016; and for future (d) 2016 – 2030; (e) 2016 –2050; (f) 2016 – 2075; (g) 2016 – 2100 for the ARB	73

Fig.No.	Figure Caption	Page No.
5.26	Spatial distribution of change in the surface runoff (m3/s) for historical LULC 1988 to 2003 (a) 1988– 1995; (b) 1988–2003; (c) 1988-2016; and for future (d) 2016 – 2030; (e) 2016 –2050; (f) 2016 – 2075; (g) 2016 – 2100 for the VRB	74
5.27	Spatial distribution of change in the surface runoff (m3/s) for historical LULC (1988 to 2003 (a) 1988– 1995; (b) 1988–2003; (c) 1988-2016; and for future (d) 2016 – 2030; (e) 2016 –2050; (f) 2016 – 2075; (g) 2016 – 2100 for the GRB	75
5.28	Variation in streamflow owing to LULC change (a) mean monthly (b) mean seasonal and annual in the ARB	77
5.29	Variation in streamflow owing to LULC change (a) mean monthly (b) mean seasonal and annual in the VRB	77
5.30	Variation in streamflow owing to LULC change (a) mean monthly (b) mean seasonal and annual in the VRB	78
5.31	Actual rainfall distribution in ARB for different scenarios	80
5.32	Actual rainfall distribution in VRB for different scenarios	80
5.33	Actual rainfall distribution in GRB for different scenarios	81
5.34	Simulated runoff at the watershed outlet for various scenarios: (i) ARB, (ii) VRB, (iii) GRB	82
5.35	Comparison of simulated runoff at the watershed outlet of RCP scenarios for 2010 to 2100 of (i) ARB, (ii) VRB, (iii) GRB	83
5.36	Change in surface runoff for different scenarios in the ARB	84
5.37	Change in surface runoff for different scenarios in the VRB	85
5.38	Change in surface runoff for different scenarios in the GRB	85
5.39	Variation in streamflow owing to CC (a) mean monthly (b) mean seasonal and annual in the ARB	87
5.40	Variation in streamflow owing to CC (a) mean monthly (b) mean seasonal and annual in the VRB	88

Fig.No.	Figure Caption	Page No.
5.41	Variation in streamflow owing to CC (a) mean monthly (b) mean seasonal and annual in the GRB	89
5.42	Spatial distribution of rainfall of RCP emission scenarios for ARB	90
5.43	Spatial distribution of rainfall of RCP emission scenarios for VRB	91
5.44	Spatial distribution of rainfall of RCP emission scenarios for GRB	91
5.45	Spatial distribution of actual ET for RCP emission scenarios in ARB	92
5.46	Spatial distribution of actual ET for RCP emission scenarios in VRB	93
5.47	Spatial distribution of actual ET for RCP emission scenarios in GRB	93
5.48	Sub-basin level distribution of change in the surface runoff for the combined impact of LULC and CC in the ARB	94
5.49	Sub-basin level distribution of change in the surface runoff for the combined impact of LULC and CC in the VRB	95
5.50	Sub-basin level distribution of change in the surface runoff for the combined impact of LULC and CC in the GRB	96
5.51	Percentage change in streamflow due to LULC and climate change (a) mean monthly (b) mean seasonal and annual in the ARB	97
5.52	Change in streamflow due to LULC and CC (a) mean monthly (b) mean seasonal and annual in the VRB	98
5.53	Change in streamflow due to LULC and CC (a) mean monthly (b) mean seasonal and annual in the GRB	99
6.1	Changes in water scarcity for the three climate windows	104

Fig.No.	Figure Caption	Page No.
6.2	River boundary, sub-basins, and different zone for water resource management in the ARB	105
6.3	River boundary, sub-basins, and different zone for water resource management in the VRB	107
6.4	River boundary, sub-basins, and different zone for water resource management in the GRB	109

LIST OF TABLES

Table No.	Table Caption	Page No.
3.1	Salient characteristics of the study area	18
3.2	Input data used in the study	22
4.1	Categorical and continuous statistical values of precipitation datasets	29
4.2	The optimized value of each sensitive parameter for the four scenarios ("v_" and "r_" stand for replacement and a relative change to the initial parameter values, respectively)	33
4.3	Statistical indexes for Gurupura streamflow using different rainfall data	38
5.1	The GCM input data used for the future period in the present study for RCP 4.5 and 8.5 emission scenarios	42
5.2	LULC changes analysis between 1988 to 2100	65
5.3	The model performance during the calibration and validation	68
6.1	Basin-scale estimates of precipitation, Blue Water Flow (BWF), Green Water Flow (GWF), and Green Water Storage (GWS)	103
6.2	Change in rainfall and surface runoff due to LULC and climate change for RCP 4.5 and 8.5	110

LIST OF ABBREVIATIONS

Abbreviation	Description
ARB	Aghanashini River Basin
BLR	Binary Logistic Regression
BWF	Blue Water Flow
CC	Climate Change
CFSR	Climate Forecast System Reanalysis
CHIRP	Climate Hazards Group InfraRed Precipitation
CHIRPS	Climate Hazards Group InfraRed Precipitation with Station data
CLUE	Conversion of Land Use and its Effects
CN	Curve Number
CSI	Critical Success Index
CWC	Central Water Commission
DEM	Digital Elevation Model
DSS	Decision Support System
Dyna-CLUE	Dynamic Conversion of Land Use and its Effects
ERA	European Centre for Medium-Range Weather Forecasts ReAnalysis
EROS	Earth Resources Observation and Science
ET	Evapotranspiration
FAR	False Alarm Ratio
GCM	General Circulation Models
GIS	Geographic Information System
GPCC	Global Precipitation Climatology Centre
GRB	Gurupura River Basin
GWF	Green Water Flow
GWS	Green Water Storage
HRU	Hydrologic Response Unit
IMD	India Meteorological Department

IPCC	Intergovernmental Panel on Climate Change
IWRIS	India Water Resources Information System
IWRM	Integrated Water Resources Management
JAXA	Japanese Aerospace Exploration Agency
LU	Land Use
LULC	Land Use Land Cover
MSWEP	Multi-Source Weighted-Ensemble Precipitation
NBSS & LUP	National Bureau of Soil Survey & Land Use Planning
NSE	Nash-Sutcliffe Efficiency
PBIAS	Percentage Bias
PERSSIAN	Precipitation Estimation from Remotely Sensed Information
CDR	using Artificial Neural Networks- Climate Data Record
PET	Potential Evapotranspiration
POD	Probability of Detection
RCM	Regional Climate Model
RCP	Representative Concentration Pathway
RMSE	Root Mean Square Error
SCS	Soil Conservation Service
SM2-RAIN	Soil Moisture to Rain
SRTM	Shuttle Radar Topography Mission
SSP	Shared Socioeconomic Pathways
SUFI 2	Sequential Uncertainty Fitting version 2
SWAT	Soil and Water Assessment Tool
SWAT-CUP	SWAT Calibration and Uncertainty Program
TRMM	Tropical Rainfall Measuring Mission
TS	Threat score
USGS	United States Geological Survey
VRB	Varahi River Basin
WG	Western Ghats

CHAPTER 1

INTRODUCTION

1.1 GENERAL

Hydrologists and water managers are experiencing the problem of adequate water supply to the inhabitants due to the exploding population and exhausting water resources. Land Use Land Cover (LULC) and Climate Change (CC) and their potential hydrological impacts are predominantly contributing to this scarcity. The LULC change amends the precipitation process into runoff by changing hydrological parameters like surface runoff, lateral flow, return flow, percolation, and evapotranspiration (Sajikumar and Remya 2015). In contrast, the CC alters rainfall, the water content in the atmosphere, and soil moisture (Hung *et al*. 2020; Mekonnen *et al*. 2018). Hence, evaluating the effects of LULC and CC on hydrology is essential for river basin planning and management. These can be accomplished by the application of hydrological modelling, which is dependent on land use, precipitation and climatic conditions (Khairul *et al.* 2018; Venkatesh and Ramesh 2018).

Assessing changes to LULC over time provides an insight into some of the main drivers of water scarcity. It is a known phenomenon that greenhouse gas levels have grown dramatically, warming the surface and having other repercussions on CC. Human pressures on land use (LU) and CC, both individually and in combination, could lead to various disruptive ecological cascades (IPCC 2012, 2018). The impacts range from reducing crop and livestock productivity to a rapid expansion of invasive species to increased chances of wildfire occurrence, as is evident from catastrophes worldwide (https://www.c2es.org/content/wildfires-and-climate-change/). The combination of pressures coming from anthropogenic CC and LULC changes will contribute to food deprivation, the prevalence of dementia, and potential conflicts (IPCC 2012, 2018). It is thus vital to study the combined effect of LU changes and CC, and hence this study adopts a detailed modeling approach with forecasted scenarios for LU and CC.

Studies suggest that high water scarcity is observed in locations with either large population density or the existence of highly irrigated agriculture or their combination (Boretti and Rosa 2019; Status *et al*. 2021). With agriculture and its allied sectors being the single largest contributor to India's economy and further considering the high population density in India, it is imperative to carry out detailed regional studies on water scarcity. Especially in Karnataka, a southern Indian state, it is vitally pertinent to study water scarcity, as the absence of surface water in most locations elevates groundwater abstractions (Varghese *et al*. 2013).

In India, the Western Ghats (WG) is one of the highest rainfall receiving regions, has unique characteristics of mountainous terrain, and is characterized by complex precipitation patterns. Variability in precipitation is an important climatic aspect for society, agriculture, and the environment. Variation in precipitation results from atmospheric circulation and complex region-specific biological, geological, and climatic changes (Diodato 2005). There are different methods of precipitation measurement such as ground readings from rain gauges, satellite observations, numerical weather prediction models and other sources (Michaelides *et al*. 2009). Spatial rainfall data is a critical input to distributed hydrological models and a significant source of model uncertainty. Satellite-based precipitation products are increasingly being used as a substitute for ground-based rainfall predictions, in which case a thorough product evaluation is necessary before adoption.

Major inputs of the hydrologic cycle are rainfall and other sources of precipitation. All the land-mining, agriculture, urban development, and other anthropogenic activities within a watershed affect the quality and quantity of stormwater. Since various watershed processes are interdependent and highly variable concerning time and space, predicting watershed processes is challenging (Wagener *et al.* 2011). Understanding the potential implications of LULC and CC on water resources is critical for effective management and consumption.

1.2 CLIMATE CHANGE

1.2.1 General aspects including various scenarios

Climate change, according to the Intergovernmental Panel on Climate Change (IPCC-2007), is a change in the state of the climate that can be detected (through statistical tests) through changes in the mean and/or variability of its attributes and that lasts for a long time, generally decades or more. Since pre-industrial times, greenhouse gas concentration in the atmosphere has grown dramatically, warming the surface and causing other climatic changes. Changes in weather and climate accompanied by the rising global temperature are clear-cut evidence of CC. Extreme events especially increased flood and drought occurrence rates, hot and cold waves are CC's results. CC has the potential to alter the prevalence and severity of extreme meteorological events like storms, floods, and droughts.

The hydrologic cycle is inextricably related to climate, as is widely known, and changes in the climate system are expected to impact water resources and regional development. Traditional water resource management techniques presume that a hydrologic time series is steady, but "stationarity is dead" because "significant anthropogenic alteration of Earth's climate is affecting the means and extremes of precipitation, evapotranspiration, and river discharge rates" (Milly *et al.* 2008). GCMs (General Circulation Models) simulate the earth's climate system in three dimensions under rising greenhouse gas emission scenarios. GCMs work at a coarse resolution by modeling climatic factors and hence their estimates for precipitation or other hydrologic variables at more minor scales are unreliable. Furthermore, coarse-scale precipitation models are ineffective in India, where the summer monsoon rainfall is characterized by increased geographical variability (Ghosh *et al.* 2012). This necessitates downscaling, or the extraction of finer-scale hydroclimatic variables from large-scale GCM simulations, to assess the underlying impacts.

1.3 LAND USE LAND COVER CHANGE

1.3.1 General aspects and present trend

Land-use change can lead to undesirable effects on ecosystems. It is one of the significant factors for water, soil, and air pollution that deteriorate the health of water bodies inside the river basin. LU changes can be classified into hydrologic, socio-economic, ecological, and environmental effects. Many river basins across the globe have undergone massive changes due to various LU activities. LULC changes are more rapid in developing countries than in developed ones. The main factor responsible for LULC changes in developing countries is the urban sprawl. Deforestation and degradation of vegetated land can lead to soil erosion and an increase in nitrogen, phosphorous, and sediments transport into streams, resulting increased sedimentation, turbidity, and eutrophication. In a watershed, the type of LU, such as agricultural fields, forests, and urban settlements, influences the quantity of available water.

Being a developing country, India has enormous rural mitigation from rural to urban regions. Because of intense urbanization, rapid LULC changes have occurred in recent decades. Therefore, when considering LU changes and vegetation restoration, studying the effect of future LULC changes on surface runoff is crucial. This can ultimately lead to better management of the agriculture system and water resources.

Furthermore, variable varieties and coverages of the vegetative surface can alter land surface features, water balance and surface water temperature through the constituents of the hydrological cycle. As a result, runoff, streamflow, groundwater flow, and physical, chemical, and biological processes in water bodies may be altered.

1.4 SATELLITE-BASED RAINFALL DATA

1.4.1 General aspects and significance

Satellite-based remote sensing offers spatial and temporal rainfall measurements worldwide. Rainfall estimates generated from satellites cover most of the earth's crust (both over land and water). This capacity meets the need for near-real-time precipitation

data, resulting in an ever-increasing number of satellite-based rainfall products that fulfill various applications (Kidd and Levizzani 2011).

At the moment, products based on a mix of infrared and microwave data are better capable of generating precise and dependable precipitation estimations (Ebert *et al*. 2007). The topic of much recent research has been combining the high sampling rate of geostationary satellites with the improved precision afforded by many passive microwave sensors. As a result, various global-scale high-resolution rainfall products are now accessible.

It is widely accepted that places with high rain gauge density may obtain more reliable precipitation estimates than areas with low rain gauge densities (Chappell *et al*. 2013). However, due to economic or geographical constraints, ground-based observations are relatively few or unevenly dispersed. The incorporation of additional data such as radar, satellite, and topographic information, on the other hand, has been demonstrated to increase the estimation of spatial rainfall distribution. Furthermore, several research studies have employed high-resolution satellite rainfall estimates as a critical data source for hydrologic applications.

1.5 SCOPE OF THE STUDY

The Western Ghats play a critical role in regulating the hydroclimatic regime of the southern part of peninsular India. Their mountainous river basins are the principal drivers of river flows in the region. India's west coast basin is the source of many small river basins, which are primarily fed by precipitation. Especially Karnataka, a southern Indian state, is vitally pertinent to study water scarcity, as the absence of surface water in most locations elevates groundwater abstractions (Varghese *et al*. 2013). Increased temperatures, variations in precipitation intensity and magnitude, and LULC are expected to alter evapotranspiration rates and river runoff (Kiprotich *et al*. 2021). According to Fadnavis *et al*. (2020), the forests in the northern and central regions of Western Ghats of India are most vulnerable to CC, with temperatures rising disproportionately faster than rainfall. As a result, assessing variations in streamflow and their impact on the hydrological features of river basins is critical for watershed

development and management and flood and drought mitigation. Several investigations have been conducted to assess the trends in meteorological variables such as rainfall, temperature, and their regional and temporal distribution (Mudbhatkal *et al.* 2017; Ramesh and Goswami 2007).

LULC and CC are two significant elements closely linked to the hydrologic cycle and are expected to influence regional water resources. Over the last few decades in Karnataka, an extensive urbanization, increased agriculture area, and deforestation led to changes in the surface flow, soil erosion, and Evapotranspiration (ET), which ultimately caused flood or drought-like situations in the basins. The increase in soil erosion leads to the deposition of silt in the river bed, which decreases the water holding capacity of river flow and increases outflow, causing floods in the river basin. Thus, it is critical to investigate probable reasons, such as the effects of changes in LULC and climate on future hydrological parameters in river basins. As a result, this research aims to evaluate the impacts of LULC and CC on water resources in different time periods from 1981 (historical) to 2100 (future), using Representative Concentration Pathway (RCP) 4.5 and 8.5 emission scenarios. Though many hydrological models are available, the Soil and Water Assessment Tool (SWAT) is recommended for hydrological modeling to determine the impact on streamflow. It has been extensively used for different hydro-climatic conditions over the past two decades can accurately simulate river flows even in heterogeneous basins.

1.6 OBJECTIVES

Given the literature gap (section 2.8) and scope that exist for the west coast basin of India, the following objectives are proposed for the investigation:

1. Assessment of satellite and India Meteorological Department (IMD) rainfall products for streamflow simulation in the study area.
2. To investigate long-term changes in current LULC and model predicted future LULC scenarios on streamflow.
3. To evaluate the impact of long-term climate change on regional hydrology using SWAT and to assess the catchment responses.

4. To assess the combined impact of land use land cover change and climate change over the study area.
5. Scenario analysis of the combined effect of land use change and climate change on blue water and green water availability.

1.7 ORGANIZATION OF THE THESIS

The thesis report comprises of seven chapters as listed below:

• Chapter 1 (Introduction) presents the overview of climate change, land use change, satellite based rainfall data and the basis for the research.

• Chapter 2 (Literature Review) deals with a critical review of current understanding of work related to climate change, landuse change and its hydrological impacts.

In chapter 2, a brief review of the literature on importance of hydrological models, studies on different land use land cover models, studies performed on land change modelling using CLUE model and literature on streamflow, sediment yield and satellite precipitation datasets are mentioned. Each of the study is discussed based on the past work that has performed by various researchers and the need of the present study has been identified.

• Chapter 3 (Study Area) presents the details of the study area and the rivers considered.

• Chapter 4 (Evaluation of satellite precipitation products in simulating streamflow) deals with different types of satellite precipitation products and its capability to simulate the steamflow.

• Chapter 5 (River basin response on effects of land use and climate change) describes the impact of landuse change, climate change and the combined effect of both on the water availability in rivers of west coast of Karnataka.

• Chapter 6 (Basin-scale water availability and vulnerability assessment) deals with water availability in future scenarios in terms of Blue Water Flow (BWF), Green Water Flow (GWF) and Green Water Storage (GWS).

• Chapter 7 (Summary and Conclusions) presents the summary and conclusions, and other related information of the research.

CHAPTER 2

LITERATURE REVIEW

2.1 GENERAL

The hydrology of the river basin is significantly affected due to changes in both natural and anthropogenic activities. Thus, it is a challenging but achievable task to evaluate the effect of these alterations in the watershed. The hydrological modeling offers a solution to analyze these impacts and understand the regime changes in the river basin. Various investigations have been carried out to understand the individual and the combined effects of these alterations on surface water in India and worldwide.

2.2 ADEQUACY OF SATELLITE RAINFALL DATA FOR STREAMFLOW PREDICTION

Precipitation is the critical element of the hydrological cycle responsible for replenishing the fresh water on the planet. It is an essential input for hydrologic modeling and forms the basis of hydrological, agricultural research applications, environment studies, and climate change studies (Gao *et al.* 2018; Stagl *et al.* 2013). It is seen that areas of high rain gauge density give more reliable precipitation estimates than low-density areas (Chappell *et al*. 2013; Su *et al.* 2020). But due to economic constraints and infeasibility due to natural conditions, such as in the Arctic (Zhao and Garrett 2008) and in the Tibetan Plateau, ground-based observations are usually sparse, especially in several developing countries where the ground-based rainfall observation networks have always been relatively sparse (Sharannya *et al*. 2020). As a result, precipitation data retrieved from satellite sensors is an excellent resource for various research projects (Huang *et al*. 2020; Schuster *et al*. 2011). Recently, many satellite rainfall estimates were made available free of cost from different sources having high temporal and spatial resolutions providing global coverage at sub-daily, daily, and monthly time steps (Funk *et al*. 2015). Various rainfall satellite products are available worldwide which could categorized into satellite only (Soil Moisture to Rain - SM2

RAIN product), satellite adjusted (Precipitation Estimation from Remotely Sensed Information using Artificial Neural Networks- Climate Data Record - PERSIANN CDR, Global Precipitation Climatology Centre - GPCC), reanalysis category (Climate Hazards Group Infrared Precipitation - CHIRP, European Centre for Medium-Range Weather Forecasts ReAnalysis - ERA and Multi-Source Weighted-Ensemble Precipitation - MSWEP), and near real-time products (TRMM-RT) (Ashouri *et al.* 2015; Beck *et al*. 2017; Ochoa *et al.* 2014; Pakoksung and Takagi 2016). The advancement in blending infrared, microwave and gauge datasets, and the availability of spatial and global coverages, and multi-temporal resolutions have increased the applicability of satellite rainfall datasets over a wide range of applications even though signal calibration and corrections for beam filling, bright band, attenuation, etc. could be considered as their limitations (Kerle and Oppenheimer 2002; Seyyedi 2010). These satellite data could be validated either by comparing them to station data and ground-based radar estimates or by confirming their predictive ability and effectiveness through a hydrological modeling framework (Satge *et al.* 2019; Tuo *et al.* 2016).

A comparative analysis of various satellite-derived datasets with gauge datasets is available elsewhere (Islam 2018; Li *et al*. 2018; Shrestha *et al*. 2017; Xue *et al.* 2013). The statistical evaluation displays the inherent data consistency of the satellite precipitation data. In contrast, the hydrological simulation of these data gives an insight into the utility of the datasets within the given application. Many investigators addressed the assessment and evaluation of satellite precipitation products efficiency for the statistical and hydrological analysis (Kolluru *et al.* 2020; Tarek *et al*. 2020). Only a few were conducted over the Indian basins (Himanshu *et al*. 2018; Kumar and Lakshmi 2018). Several investigations (Li *et al*. 2018; Kolluru *et al*. 2020) have reported that better statistical analysis for the precipitation have not yielded reliable hydrological analysis. This mandates the testing of each precipitation data using hydrological models for different applications.

2.3 LAND USE LAND COVER STUDIES

A study by Ghaffari *et al*. (2010) in Northwest Iran reported a significant association between changes in LU and its effect on hydrology. They reported a fall in grasslands

by 34.5% and an increase in rain-fed agriculture by 13.9%, resulting in a 33% increase in surface runoff and a 22% decline in groundwater recharge. Garg *et al*. (2019) studied the risks of anthropogenic (human-induced) LU changes on hydrology over Indian basins and revealed an increase in the runoff by ~0.14%. These changes were triggered by a 0.14% rise in the urban landscape and a reduction in natural forests by 0.7%. It may be noted from earlier studies that most of the research is carried out on past changes to LULC and very few researches studied future/projected LULC changes (Chen *et al*. 2020; Roy and Inamdar 2019). A perspective toward future LULC is essential for developing 'what-if' scenarios and can support LU planning and policy. Therefore, this study presents a scenario analysis of impacts on water scarcity due to future/projected LU and climate change during the near (T1) (2006-2040), mid (T2) (2041-2070) and long term (T3) (2071-2100).

Numerous studies are carried out on LU prediction, and several models have been proposed for projecting future LU (Marquez *et al*. 2019; Verburg and Overmars 2009). Most of the models are Geographic Information System (GIS)-based models, machine learning models, and a combination of GIS and machine learning models known as hybrid models (Gaur *et al*. 2020; Kolluru *et al*. 2020; Shrestha *et al*. 2018; Verburg and Overmars 2009). From the review of theoretical and practical attributes of LU change modeling, a vast assortment of methods and approaches exist to model LU and more importantly, these approaches are rooted in a multitude of disciplinary backgrounds. The selection of a LU prediction model thus needs to be based upon achieving a balance between integrating the disciplinary approaches, earning a high degree of Spatio-temporal dynamics, and multi-scale features of LU.

Data availability at the requisite resolution in both time and space is another significant consideration for selecting a model. Essentially, LU change models are constructed hierarchically that consider several layers of input data. The overall change volume is commonly computed by assigning the individual grid cells and applying cut-down values to the probability surface for the research region as a whole (Bryan *et al*. 2002). Actual LU change allocations are established by regional and local parameters and are assigned at aggregate levels to drivers such as the population. Conversion of Land Use and its Effects (CLUE) is a multi-scale model based on this approach that

generates spatial interactions through feedback over a large scale (Veldkamp and Fresco 1996). An improvement of CLUE is the Dyna-CLUE model (Dynamic Conversion of Land Use and its Effects), a more widely used Spatio-temporal model to test LU conversions and their effect. Dyna-CLUE has a flexible and generic framework that promotes scale and specific contexts for regional applications. One of the significant strengths of the Dyna-CLUE model is the elasticity allotted to each LU type. The model allows certain land uses (such as permanent crops) to be reluctant to change and other land uses (such as shifting cultivation, locally known as Jhum in India) to change easily. Several case studies in India have employed the Dyna-CLUE model justifying its suitability of the model (Behera and Behera 2020; Shrestha *et al*. 2020; Sinha and Eldho 2018; Venkatesh *et al*. 2020a).

2.4 CLIMATE CHANGE STUDIES

General models of circulation (GCMs) enable three-dimensional simulations under rising greenhouse gas concentration scenarios of the earth's climate system and are excellent tools for quantitative comprehension of climate dynamics (Raneesh and Santosh 2011; Xu *et al.* 2020). Evaluation of the hydrological effects of CC includes merging hydrological models with GCM outputs (Pechlivanidis *et al*. 2011; Wang *et al*. 2020). Pre-processing in terms of bias correction is required to ensure that GCMs are reasonably accurate and reproduce the future climate to remove the biases in the data (Kolluru *et al*. 2020b; Mudbhatkal and Mahesha 2018a). Various studies assessed the efficiency of bias correction methods and addressed the capability of the methods to fairly represent regional climate (Bennett *et al*. 2011; Iizumi *et al*. 2017; Teutschbein and Seibert 2012). Regarding the statistical properties of reanalysis and the time series simulated by GCM, quantile-based remapping yields satisfactory results (Bennett *et al*. 2011; Mudbhatkal and Mahesha 2018b; Salvi *et al*. 2013). Numerous studies reported the effects of climate change on streamflow (Pervez and Henebry 2015; Phung *et al*. 2019; Zhang *et al*. 2016) and it may be noted that these studies lack the use of multiple GCMs in their evaluations. Using multiple GCMs instead of single GCM for impact studies overcomes the limitations of imperfect parameterization of climate processes and uncertainties that may arise due to inappropriate boundary conditions (Phung *et al*. 2019; Pierce *et al*. 2009; Raju and Kumar 2020; Teutschbein and Seibert 2012). The

GCMs developed by Beijing Normal University (BNU-ESM), second-generation Canadian Earth System Model (CanESM2), CNRM-CM5 (developed by French National Centre for Meteorological Research), MPI-ESM-LR and MPI-ESM-MR (both developed by Max Planck Institute for Meteorology) are reasonable over South Asian catchments (Salvi *et al*. 2013; Singh *et al*. 2017; Sinha *et al*. 2020). Therefore, this study employs outputs from five bias-corrected GCMs for carrying out a scenario analysis of water scarcity in the Western Ghats of India.

2.5 RELATED STUDIES IN THE WESTERN GHATS

Babar and Ramesh (2014) and Sinha and Eldho (2018) identified the response of streamflow due to LULC change over the Netravati River basin of Western Ghats. They found that the significant LULC changes have a substantial impact on the surface runoff and sediment yield in the past as well as near future. Hence, they might be considered for water resource management plan in the study area. They also recommend that the methods used in their study can be used to assess changes in surface runoff and sediment yield due to LULC changes in other river basins where remotely sensed LULC data are available. Also, a longer-term analysis of future changes in climate and LULC is recommended to compare possible changes in streamflow and sediment yield beyond 2030.

Mudhbhatkal *et al*. (2017, 2018a) confirmed spatiotemporal variation of rainfall and increasing temperatures in the Western Ghats region's sub-humid and per-humid river regimes due to climate change. They examined bias correction for the Regional Climate Model (RCM) data set for the Western Ghats of India and found southern rivers as extremely sensitive to changing climate, followed by the middle portion. Sharannya *et al*. (2018) assessed the hydrological consequences of climate change on rainfall, temperature, and streamflow in a west-flowing river originating in the Western Ghats of India and found a declining trend at a rate of 2.63mm per year for historical and 8.85mm per year for RCP 4.5 future scenarios with 0.10˚C increase in average temperature in every decade.

2.6 THE RAINFALL-RUNOFF MODELS

Model selection demands a deep understanding of the model's complexity and functioning. Analytical models solve the governing equations that define energy, mass, and momentum conservation, whereas experimental data is used to build empirical models. The climatic (rainfall, temperature, and other water balance components) and spatial variability (land use and land cover, soil, slope, and terrain) of watershed processes are fairly well represented by distributed models based on physicality (Niehoff *et al.* 2002; Sharannya *et al*. 2016). Infiltration excess, subsurface runoff, infiltration, canopy interception, soil moisture storage, and groundwater flow are all represented using hydrologic models.

Soil and Water Assessment Tool (SWAT) (Arnold *et al.* 1998), a physically-based semi-distributed model, has been widely utilized in analysing the impact of climate change on hydrology in the last two decades (Raneesh and Santosh 2011; Mudbhatkal *et al*. 2017). The applications of the SWAT model include: impacts of climate change on hydrology and water resources (Mudbhatkal *et al*. 2017), impacts of land management on water resources (Venkatesh *et al*. 2020b), assessment of watershed response to land use cover changes on the annual water balance and temporal runoff dynamics and streamflow prediction for a variety of watersheds (Kim *et al*. 2013; Shrestha and Htut 2016).

2.7 WATER SCARCITY AND VULNERABILITY ANALYSIS

The consumption and availability of blue water (i.e., fresh surface water and groundwater) are good indicators for assessing water scarcity. Several studies have assessed water scarcity in different parts of the world and most of the studies adopt an annual scale for their assessments. The principal driving forces for global growing water demands are rapid urbanization, higher living standards, deforestation, and the proliferation of irrigated croplands. In addition to these driving forces, there are auxiliary causes such as altered weather patterns, droughts, increased greenhouse gases, and variations to streamflow as a result of CC (Mukherjee *et al*. 2018; Papalexiou *et al*. 2020; Rajulapati *et al*. 2020; Swain *et al.* 2020). Recent research on water availability

in the basin-scale has focused on quantifying Blue Water Flow (BWF), crop evapotranspiration concerning Green Water Flow (GWF), and soil moisture storage portion as Green Water Storage (GWS) (Swain *et al.* 2020; Vanham 2016). As per the global water cycle perspective, approximately 65% of the total precipitation is returned into the atmosphere in terms of ET from forests and croplands, constituting GWF (Gerten *et al*. 2005). The surface and groundwater runoff and the mid-soil flow are integrated into the BWF (Schuol *et al*. 2008; Zang and Mao 2019). Increased blue water significantly decreases green water when CC is induced (Zang & Mao, 2019). Much of the blue water is turned into green water by physical and anthropogenic activities to satisfy the water requirement (Mao *et al.* 2018). Numerous studies also emphasize changes in the streamflow pattern due to changes in climate and/or LU, along with the alterations in various water balance components such as base flow, soil and basin-scale evapotranspiration (Swain *et al.* 2020; Visakh *et al.* 2019). However, the research does not highlight the underlying risk of water scarcity for basin hydrology in historical and future periods.

2.8 LITERATURE GAP

Even though in-situ ground-based precipitation datasets provide highly accurate results, the non-availability of datasets, uneven distribution of gauges over unpopulated areas, makes it difficult to use for global applications. On the other hand, many satellite rainfall estimates were made available free of cost from different sources having high temporal and spatial resolutions providing global coverage at sub-daily, daily and monthly time steps. Several investigations have reported that better statistical analysis for the precipitation have not yielded reliable hydrological analysis. This mandates the testing of each precipitation data using hydrological models for different applications. Although studies on satellite-based rainfall on the Western Ghats have been carried out, none of those studies have evaluated it for simulating the streamflow in the study area. Considering this, the precipitation products that are produced from satellite sensors are used for hydrological modeling for simulating streamflow because of its competitive ability to establish when compared to gauge measured datasets in terms of availability and accuracy standards.

From the literature review, it is evident that several studies have been undertaken using SWAT model for assessing the impact of CC and LULC on streamflow in many parts of the world and proved to be effective. There are fewer studies where discrete and combined effects of both CC and LULC on hydrological impacts of west coast of Karnataka. Several studies have been undertaken using Dyna CLUE model for understanding and assessing the future impacts on land use land cover change due to external drivers and impacts of land use land cover change on various climatic and hydrological parameters in many parts of the world. There are fewer studies where Dyna CLUE has been applied for Indian basins for studying the dynamics of land use change which is of utmost necessary for land use management and policy studies. A perspective toward future LULC is essential for developing 'what-if' scenarios and can support LU planning and policy. Using multiple GCMs instead of single GCM for impact studies overcomes the limitations of imperfect parameterization of climate processes and uncertainties that may arise due to inappropriate boundary conditions. Numerous studies also emphasize changes in the streamflow pattern due to changes in climate and/or LU, along with the alterations in various water balance components such as base flow, soil and basin-scale evapotranspiration. However, the research does not highlight the underlying risk of water scarcity for basin hydrology in historical and future periods. Therefore, this study presents a scenario analysis of impacts on water scarcity due to future/projected LU and climate change using 5 GCM's during the T1 (2006-2040), T2 (2041-2070) and T3 (2071-2100).

CHAPTER 3

STUDY AREA

3.1 GENERAL

The study area stretches from 12˚ 40' N to 14˚ 40' N latitude and 74˚ 20' E to 75˚ 20' E longitude and covers the west coast of Karnataka. Three west-flowing rivers of the Western Ghats representing different levels of anthropogenic influence were chosen for this study to understand the combined effect of LU and CC on water scarcity which spreads over the northern, middle and southern portions of the west coast of Karnataka. They are Aghanashini River Basin (ARB) (north part of the study area), Varahi River Basin (VRB) (mid-central part of the study area) and Gurupura River Basin (GRB) (south part of the study area) (Fig.3.1). The basic information is presented in Table 3.1.

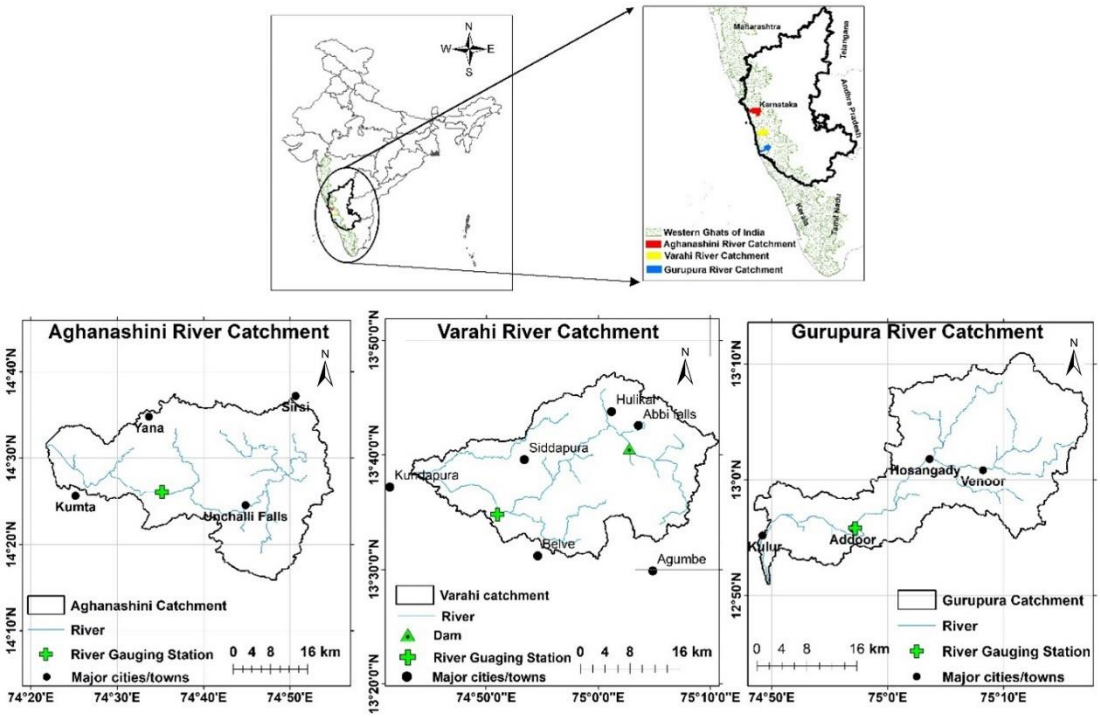

Fig. 3.1. Study area

3.1.1 Aghanashini River Basin (ARB)

In the Western Ghats region, the ARB has an elevation in the range of 0 – 700 m (Fig. 3.2. (b)), a total river length of approximately 117 km and a catchment area of about 1333 km^2 (Fig. 3.2). It extends between 14º15' – 14º37' N and 74º 21, - 74º 56' E. As per the 2016 land cover analysis, the basin is mainly covered by forests (58.57%), barren (25.93%) and plantations (12.74%) (Fig. 3.2 d). The monthly precipitation variation over the last 40 years (1981-2020) is plotted in Fig 3.2 e. The average annual rainfall is 3987 mm (based on 1981 to 2020 data), with most of the precipitation falling between June to September during the southwest monsoon season.

Table 3.1. Salient characteristics of the study area

Sl. No	Feature	ARB	VRB	GRB
1	Basin Extent	14º15'-14º37' N and 74º 21' - 74º 56' E	13º31'-13º47' N and 74º 43' - 75º 11' E	12º 50' - 13º 11' N and 74º 45' - 75º 18' E
2	Area (Sq.km)	1333	813	839
3	Mean Annual Rainfall (mm)	3980	3753	3812
4	Mean Minimum/ Maximum Temperature (ºC)	21 / 31	19 / 30	20 / 35
5	Numbers of gauging stations	1 (Santeguli)	1 (Haladi)	1 (Addoor)

The minimum and maximum temperature of the basins are 21°C and 31°C, respectively. According to the soil map procured from the National Bureau of Soil Survey & Land Use Planning (NBSS & LUP) Nagpur India of the ARB, sandy clay loam and silty clay are predominant (Fig. 3.2 c). The land cover classes include forest, plantation, barren, water, and wetland. The river basin is divided into 23 sub-basins for hydrological parameter studies (Fig. 3.2). In this research, the digital elevation model (Cartosat, 30m), land cover (Landsat, 30m), soil (NBSS), and meteorological data (IMD - 0.25°) such as rainfall and temperature were employed as model inputs. Climate

Forecast System Reanalysis data on relative humidity, solar radiation, and wind velocity were interpolated at 0.25° as the same grid points to precipitation data for all three river basins. The hydrological data such as observed runoff is collected from a gauging location at Santeguli from 1989–2010 at a daily time scale from the Central Water Commission of India. Table 3.2 lists the necessary information on the input data, resolutions, and sources.

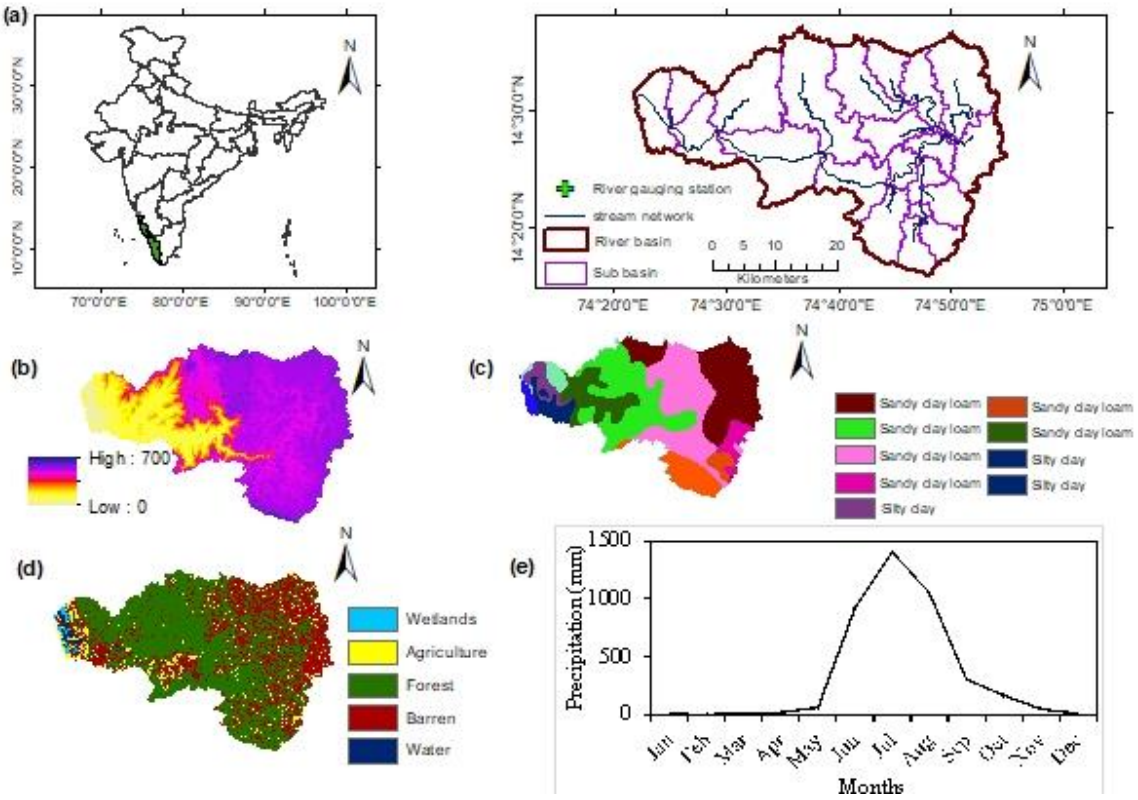

Fig. 3.2. (a) Location map and sub-basins of the study area, (b) DEM (c) Soil data, (d) LULC categories, and (e) monthly average precipitation of ARB.

3.1.2 Varahi River Basin (VRB)

The VRB has an elevation in the range of 0 − 879 m (Fig. 3.3b), a total river length of approximately 66 km and a catchment area of about 813 km^2 (Fig. 3.3). It extends between 13º31’ – 13º47’ N and 74º 43’ - 75º 11’ E. As per the 2016 land cover analysis, the basin is mainly covered by forests (61.78%), agriculture (23.55%) and barren (10.63%) (Fig. 3.3d). The monthly variation of precipitation over the last 40 years (1981-2020) is plotted in Fig. 3.3e. The average annual rainfall is 3850 mm (based on

1981 to 2020 data) and most of the precipitation occurs from June to September monsoon months. The minimum and maximum temperature of the basins are 19°C and 30°C, respectively. As per the soil map procured from NBSS & LUP Nagpur India of the VRB, sandy clay loam and silty clay are predominant (Fig. 3.3c). The land cover classes include forest, agriculture, barren, water, and urban. The hydrological data such as observed runoff is collected from a gauging location at Haladi from 1986 to 2015 at a daily time scale from the Central Water Commission of India. The reservoir inflow data for Mani dam (Latitude=13˚ 40’ 34.68’’ and Longitude=75˚ 2’ 46.39’’) is collected from Karnataka Power Corporation Limited for 2009-2015. The reservoir area at Full Reservoir Level (FRL) is 56 km^2 with a storage capacity of 883.8 Million Cubic Meters. The relevant details of the input data, resolutions, and sources are listed in Table 3.2.

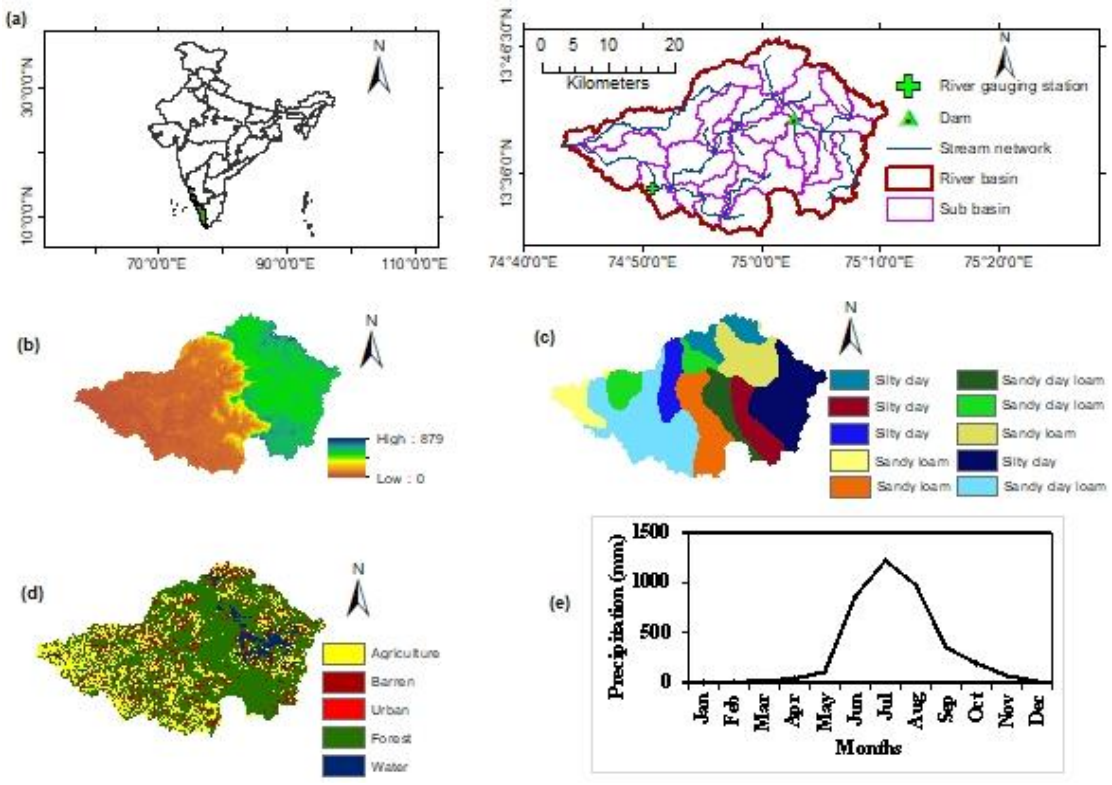

Fig. 3.3. (a) Location map and sub-basins of the study area, (b) DEM (c) Soil data, (d) LULC categories, and (e) monthly average precipitation of VRB.

3.1.3 Gurupura River Basin (GRB)

The GRB has an elevation in the range of 0 − 1886 m (Fig. 3.4b), a total river length of approximately 85 km, and a catchment area of about 839 km^2 (Fig. 3.4). It extends between 12º 50' - 13º 11' N and 74º 45' - 75º 18' E. As per the 2016 land cover analysis, the basin is mainly covered by agriculture (37.88%), forests (29.53%), and barren (13.35%) (Fig. 3.4d). The monthly variation of precipitation over the last 40 years (1981-2020) is plotted in Fig 3.4e. The average annual rainfall is 3902 mm (based on 1981 to 2020 data), and most of the precipitation occurs from June to September monsoon months. The average minimum and maximum temperatures are 20°C and 35°C, respectively. As per the soil map procured from NBSS & LUP Nagpur India of the GRB, sandy clay loam is predominant (Fig. 3.4c). The land cover classes include forest, agriculture, plantation, barren, water, and urban. The hydrological data such as observed runoff is collected from a gauging location at Addoor for 2006–2012 at a daily scale from the Central Water Commission of India. The relevant information of the input data, resolutions, and sources are listed in Table 3.2.

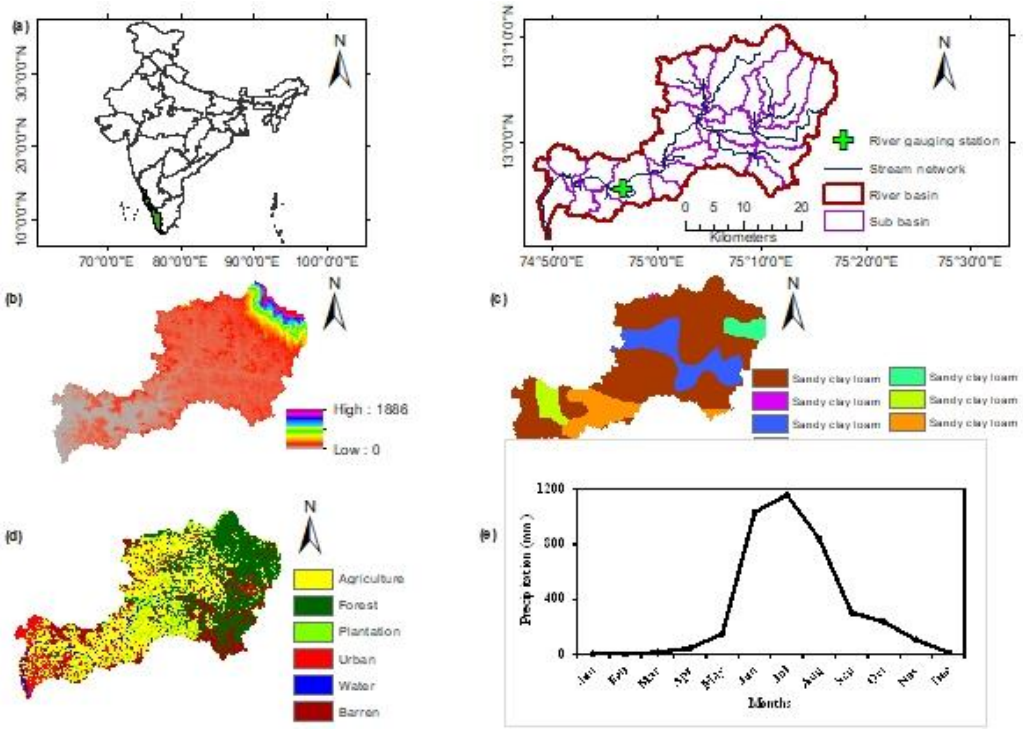

Fig. 3.4. (a) Location map and sub-basins of the study area, (b) DEM (c) Soil data, (d) LULC categories, and (e) monthly average precipitation of GRB.

Table 3.2 Input data used in the study.

Input data	Resolution	Source
Cartosat Digital Elevation Model (DEM)	30 m	National Remote Sensing Centre (http://www.nrsc.gov.in/)
Land use map	30 m	Landsat-imageries (http://earthexplorer.usgs.gov/)
Soil data	Toposheet	National Bureau of Soil Survey & Land Use Planning (NBSS&LUP)
Meteorological data (rainfall and min-max temperature)	0.25º (daily)	India Meteorological Department (IMD)
TRMM rainfall data	0.25º /daily	https://disc.gsfc.nasa.gov
CHIRPS rainfall data	0.05º and 0.25º /daily	ftp://ftp.chg.ucsb.edu/pub/org/chg/products/CHIRPS-2.0/global_daily/netcdf/p25
Meteorological data (solar radiation, relative humidity, and wind velocity)	0.25º (daily)	Climate Forecast System Reanalysis (CFSR)
Observed Hydrological data (streamflow)	Daily	Central Water Commission (http://www.indiawris.nrsc.gov.in/)

CHAPTER 4

EVALUATION OF SATELLITE PRECIPITATION PRODUCTS IN SIMULATING STREAMFLOW

4.1 GENERAL

In this study, an attempt was made to evaluate the performance of Tropical Rainfall Measuring Mission (TRMM) and Climate Hazards Group InfraRed Precipitation with Station data (CHIRPS), employing a semi-distributed hydrological model, i.e., Soil and Water Assessment Tool (SWAT). This is used for simulating streamflow and validating them against the flows generated by the IMD rainfall dataset in the Gurupura river basin of India. Various testing scenarios for simulating streamflow were attempted to examine the suitability of these satellite precipitation datasets.

4.2 SATELLITE PRECIPITATION DATASETS

4.2.1 Gauge-Based Meteorological Data

Since the study area is poorly gauged, daily precipitation data for 1998 – 2013 were collected from 0.25˚x 0.25˚ grid points from the India Meteorological Department (IMD), Government of India (Pai *et al*. 2014). Similarly, daily maximum and minimum temperature, relative humidity, wind speed and solar radiation for the same period were obtained from the IMD (1˚x 1˚) (Srivastava 2009) and Climate Forecast System Re-analysis (CFSR, 0.25˚x 0.25˚) for calculating the potential evapotranspiration (PET) which are required for the SWAT model. Even though CFSR data is not up to the mark compared to such as ERA in terms of resolution and real time availability, ERA was proved to give poor streamflow simulation for Indian basins in the study by *(Kolluru et al*. 2020). Also, studies have proved that CFSR data suits watershed modeling to meet the challenges of modelling un-gauged watersheds and real-time hydrological modelling (Fuka *et al*. 2014; Tomy and Sumam 2016). Hence in the present study CFSR data is used for hydrological modelling. The daily discharge data for 2006-2012 at the Addoor gauging station is collected from the Central Water Commission (CWC) via India Water Resources Information System (IWRIS) platform.

4.2.2 TRMM Rainfall Data

The Tropical Rainfall Measuring Mission (TRMM) Multi-Satellite Precipitation Analysis (TMPA) 3B42 version 7 algorithm is the post real-time version which is a gauge–adjusted product superseding all the previous versions of TRMM launched by NASA and the Japanese Aerospace Exploration Agency (JAXA) to monitor precipitation in the tropical and subtropical areas of 50˚S – 50˚N with near-global coverage (Huffman *et al*. 2007). Its spatial and temporal resolutions are 0.25˚x 0.25˚ and 3-hourly, respectively spanning from 1998 to the present. Daily TRMM 3B42 v7 is obtained by summing 3-hourly precipitation, obtained as a combination of microwave-IR-gauge precipitation estimates from multiple independent satellites. The daily rainfall data obtained from https://disc.gsfc.nasa.gov during from 1998-2013 is being used to drive the SWAT model.

4.2.3 CHIRPS Rainfall Data

The CHIRPS rainfall data Climate Hazards Group InfraRed Precipitation with Station data version 2 (CHIRPS-2.0) is a 30+ year quasi-global rainfall dataset to analyze the precipitation at different scales. The CHIRPS was created in collaboration with scientists at the United States Geological Survey (USGS) and Earth Resources Observation and Science (EROS) Centre (Funk *et al*. 2015) to deliver reliable up-to-date , and more complete datasets for several early warning objectives. Spanning 50˚S-50˚N (and all longitudes), starting from 1981 to the present, CHIRPS incorporates 0.05˚ x 0.05˚ and 0.25˚ x 0.25˚resolution satellite imagery with in-situ station data to create gridded rainfall time series for trend analysis and seasonal drought monitoring. The CHIRPS is a gridded land-only precipitation dataset developed by synergistic satellite infrared cold cloud duration measurements and ground-based rain gauge observations (Funk *et al.* 2015). The daily rainfall data were extracted for 1998 – 2013 and were added as an input for the rainfall-runoff model (ftp://ftp.chg.ucsb.edu/). The main difference between climate hazard group climatology and other precipitation climatology is that, it uses longer period satellite rainfall for deriving climatological surfaces, which improves its performance in mountainous terrain (Funk *et al.* 2015).

4.3 METHODOLOGY

4.3.1 Statistical Evaluation of the Satellite Precipitation Data

In the present work, categorical and continuous statistics were computed between the satellite precipitation data and the gauge-based products (IMD gridded data) to understand these datasets error characteristics and estimation capabilities. The categorical statistics included Probability of Detection (POD), False Alarm Ratio (FAR), and Critical Success Index/Threat score (CSI/TS) metrics. In contrast, continuous statistical indices included Correlation Coefficient (r), Root Mean Square Error (RMSE), and Percentage Bias (PBIAS). The categorical statistics are the number of rainfall events detected or missed by the satellite rainfall data with respect to gauge data. The continuous statistics signify the efficiency of satellite datasets in estimating the amount of precipitation. The POD refers to the ratio of hits (successful detection of rainfall as reference data) to the actual number of rainfall events recorded according to base datasets (sum of hits and misses), whereas FAR represents the ratio of false alarms (satellite precipitation products detecting the rainfall during non-occurrence of precipitation in the base dataset) to the events that are not diagnosed by reference dataset (Jiang and Wang 2019; Li *et al*. 2018). R represents the degree of significance or the synchronicity of precipitation differences between satellite precipitation products and gauge or gridded data. The RMSE measures the precision of data or the average error magnitude between the gauge and satellite data, while PBIAS shows the likelihood of overestimation and underestimation. Lower bias and RMSE and higher R-value reflect higher accuracy of satellite datasets with respect to reference datasets (Bitew and Gebremichael 2011; Jiang *et al*. 2018). The POD and CSI/TS values close to one, and FAR values close to zero reflect a satellite precipitation dataset's better capacity to detect rainfall events.

4.3.2 Hydrologic Model

The Soil and Water Assessment Tool (SWAT) is a physically-based semi-distributed model intended to compute and route water, sediments and contaminants from the individual drainage units (sub-basins) to their outlets throughout the river basin (Arnold

et al. 1998). The SWAT is widely used for simulating the hydrological process ie. erosion, vegetative growth, water quality, streamflow and pollutant concentration for quite a long period (Liew *et al*. 2003; Mudbhatkal *et al*. 2017; Venkatesh *et al*. 2020b). It segments the river basin into a number of sub-basins leading to Hydrologic Response Units (HRUs), defined by various combinations of land use, soil characteristics, topography and management systems.

The hydrological cycle is determined based on water balance, which is regulated by climate inputs such as daily precipitation and maximum/minimum air temperature. The SWAT simulates the daily, monthly and annual water fluxes and solutes in river basins using daily input time series. The simulations begin by calculating the amount of water, sediment, and pollutants loading into the main channel each sub-basin's land. These loads are conveyed and routed through the streams and reservoirs within the basin. The Shuttle Radar Topography Mission (SRTM), Digital Elevation Model (DEM), Land use land cover map (LULC) obtained from the supervised classification technique (maximum likelihood algorithm) for the year 2003 and the soil map were the input to the SWAT model. The spatial/temporal resolution and source of data obtained are listed in table 3.2. After providing the land use and soil maps as input, 27 sub-basins and 266 Hydrologic Response Units (HRU) were generated. The user-defined weather generator could supply the residual climate data such as solar radiation, relative humidity, and wind speed (Table 3.2).

4.3.3 Model Calibration, Validation and Uncertainty Analysis

The first five years (2001-2005) were used as a warm-up period to denote the initial conditions in the model. The model was calibrated against the daily runoff from 2006-to 2009 and was validated for 2010-to 2012 for the Gurupura river. The calibration and validation of the model were performed using the Sequential Uncertainty Fitting version 2 (SUFI2) (Abbaspour *et al*. 2007) in the SWAT Calibration and Uncertainty Program (SWAT-CUP) tool developed for SWAT as an interface. The SUFI2 program parameter uncertainty accounts for all the sources of uncertainties such as, uncertainty in driving variables (e.g., rainfall), conceptual model, parameters, and measured data. Initially, the models were calibrated using the initial ranges of parameters listed in table

4.2. According to the new parameters suggested by the program (Abbaspour *et al.* 2007) and their physical limitations, the ranges of each parameter are modified after each iteration. The sensitivity analysis before calibration helps to reduce the number of parameters and reduces the computational time. Many iterations were carried out to obtain an optimized parameter value. In each step, previous parameter ranges are updated to a new value-based sensitivity matrix calculation sets. The parameters are then updated way so that the new ranges are always smaller than the previous ranges and centered around the best simulation. SUFI-2 methodology could be found elsewhere (Khoi and Thom 2015; Me *et al*. 2015).

4.3.4 Performance Indices for Examining Streamflow Simulation

The ability of a hydrological model to reproduce observed streamflow could be expressed through various output measurement indices. A variety of performance indices usually evaluates the streamflow simulations. These evaluations include statistical performance measurements, e.g. Pearson correlation coefficient; weighted R^2, and hydrological performance measurements (e.g. Nash and Sutcliffe Efficiency (NSE). The performance evaluation of hydrological models is commonly made by comparing the simulated and observed values. The statistical coefficients used for assessing the model performance were the percent bias (PBIAS), coefficient of determination (R^2), and the Nash-Sutcliffe efficiency (NSE). The criteria *(Moriasi et al.* 2007) were used to evaluate the model performance. The statistical indices were determined as follows:

The percent bias (PBIAS) measures the tendency of simulation compared to the observed streamflow (Mudbhatkal and Amai 2018a). The optimal value of percent bias is zero. A negative value indicates that the model is overestimating and a positive value suggests that the model is underestimating (Musie *et al.* 2019).

$$PBIAS = 100 * \frac{\sum_{i=1}^{n}(O_i - P_i)}{\sum_{i=1}^{n}(O_i)} \quad (4.1)$$

where O is the observed value, P is the predicted value, n is the number of samples, and $\overline{\boldsymbol{O}}$ and $\overline{\boldsymbol{P}}$ denote the average observed and predicted values.

The coefficient of determination (R^2) is the proportion of the variation which can be explained by fitting a regression line. This is a crucial output of regression analysis. The coefficient of determination is a number that shows how well the data fit a statistical model. R^2 is the squared value of the correlation coefficient (r). Its value ranges from 0 to 1, with higher values indicating lesser error variance.

$$R^2 = \frac{\sum_{i=1}^{n}(O_i-\bar{O})(P_i-\bar{P})}{\sqrt{\sum_{i=1}^{n}(O_i-\bar{O})}\sqrt{\sum_{i=1}^{n}(P_i-\bar{P})}} \quad (4.2)$$

The Nash-Sutcliffe Efficiency (NSE) is a statistical criterion used to assess the predictive power of hydrological models. This normalized statistic determines the relative magnitude of the residual variance compared to the measured data variance (Musie *et al*. 2019).

$$NSE = 1 - \frac{\sum_{i=1}^{n}(O_i-P_i)^2}{\sum_{i=1}^{n}(O_i-\bar{O})^2} \quad (4.3)$$

4.3.5 Streamflow Simulations Using Satellite Precipitation Datasets in SWAT

Four calibration scenarios were considered using gauge and satellite precipitation datasets to simulate streamflow using the SWAT model. (a) The IMD rainfall data were first used to drive the model and optimise the parameter values, and (b) the daily TRMM, CHIRPS-0.25, and CHIRPS-0.05 rainfall data were subsequently used to run the model with the same optimal parameter values, and (c) the simulated runoffs for the three model runs were compared with IMD rainfall-driven results.

Scenario 2 (S2): the daily TRMM rainfall was used to drive the SWAT model and optimise the parameter values, and then, the IMD, CHIRPS-0.25, and CHIRPS-0.05 rainfall were taken to drive the model.

Scenario 3 (S3): CHIRPS-0.25 rainfall data were used to obtain the optimal parameter values, and the IMD, TRMM, and CHIRPS-0.05 rainfall data were used to drive the model.

Scenario 4 (S4): CHIRPS-0.05 was used to run the model and obtain the optimal parameter value, and the other three rainfall datasets viz. IMD, TRMM, and CHIRPS-0.25 were utilized to run the model for comparison.

4.4 RESULTS AND DISCUSSION

4.4.1 Performance of Satellite Precipitation Datasets

In the present study, three categorical statistical metrics (POD, FAR and CSI/TS) were used to understand the capability of satellite precipitation products to detect rainfall events (Table 4.1). The TRMM exhibited higher POD value (0.74) than CHIRPS-0.25 (0.71) and CHIRPS-0.05 (0.58). The TRMM also exhibited a lower FAR value of 0.11 than CHIRPS-0.25 and CHIRPS-0.05 (0.18 and 0.16 respectively). The FAR value near zero represents the capability of a satellite rainfall product to detect rainfall events accurately. The critical success index that measures the satellite precipitation products event was correctly predicted should have values closer to 1. CHIRPS-0.25 exhibited excellent value for CSI which has better rainfall detection capabilities than TRMM.

Continuous statistics such as CC, PBIAS and RMSE were obtained for the satellite datasets with respect to IMD data. The correlation between TRMM and IMD data was better than the correlation between CHIRPS and IMD data. Among the satellite data, TRMM exhibited lower bias than IMD data and a similar pattern was observed in the case of RMSE also. From the overall statistical analysis of rainfall, TRMM produced better results than CHIRPS-0.25 followed by CHIRPS 0.05.

Table 4.1. Categorical and continuous statistical values of precipitation datasets.

	TRMM	CHIRPS 0.25	CHIRPS 0.05
POD	0.74	0.71	0.58
FAR	0.11	0.18	0.16
CSI/TS	0.67	0.85	0.52
CC	0.56	0.47	0.47
Bias	0.91	1.02	1.02
RMSE	19.44	22.78	23.74

4.4.2 Evaluation of Streamflow Generation

A large number of parameters are available, sensitive parameters are identified based on the previous literature (Sinha and Eldho 2018) and are used for calibration and validation of streamflow. The calibration of the SWAT model was carried out by comparing the observed and simulated streamflow on the daily scale at the outlet of the basin i.e. Addoor. Around 14 parameters with varying ranges were used for different sets of iterations required for different input product calibrations. The various parameters used in the present study are CN2 (Initial Soil Conservation Service Curve Number - SCS CN II Value), GW_Delay (Groundwater delay (days)), CH_K2 (Effective hydraulic conductivity in main channel alluvium (mm/h)), ALPHA_BNK (Baseflow alpha factor for bank storage (days)), SOL_AWC (Available water capacity of the soil layer), Alpha_BF (Base flow alpha-factor (day)), GWQMN (Threshold depth of water in the shallow aquifer required for return flow to occur (mm)), ESCO (Soil evaporation compensation factors), GW_REVAP (Groundwater "revap" coefficient) , CH_N2 (Manning 'n' coefficient for the main channel), SOL_K (Saturated hydraulic conductivity of soil), REVAPMN (Depth of water required for revap to occur in the shallow aquifer), SLSUBBSN (Average slope length) and SLSOIL (Slope length for lateral subsurface flow). Out of the above parameters, global sensitivity analysis was performed using the SUFI-2 algorithm of SWAT-CUP and the nine most sensitive parameters were selected for simulating the flow using the model. The allowable ranges and fitted values for each dataset are represented in Table 4.2.

The daily simulation of streamflow using the four datasets is represented in Fig 4.1. It is noticed that the IMD gridded data which was derived from the observed gauged data is the best simulating the observed flow compared with other datasets. In the daily time scale, the TRMM underestimates the flow whereas it tries to match the peak flow. This may be mainly because of orographic precipitation during the monsoon season resulting from the Western Ghats mountainous region in the study area. The orographic lifting of moist air leads to cloud formation, and even when the cloud top is relatively warm the rainfall will occur. The deep convection of this cloud system is due to latent heat release. The infrared satellite sensors may not detect precipitation from warm clouds and may lose the capture of ice loft, thereby seeing only a portion of rain from

deep convection (Funk *et al*. 2015; Sharannya *et al*. 2018). This process may be the reason for the lower performance of the satellite data-driven model than the IMD data-driven model. Even though the spatial resolution of both CHIRPS datasets (0.25˚ and 0.05˚) is different, it was found that the finer resolution does not make much improvement in the flow simulation.

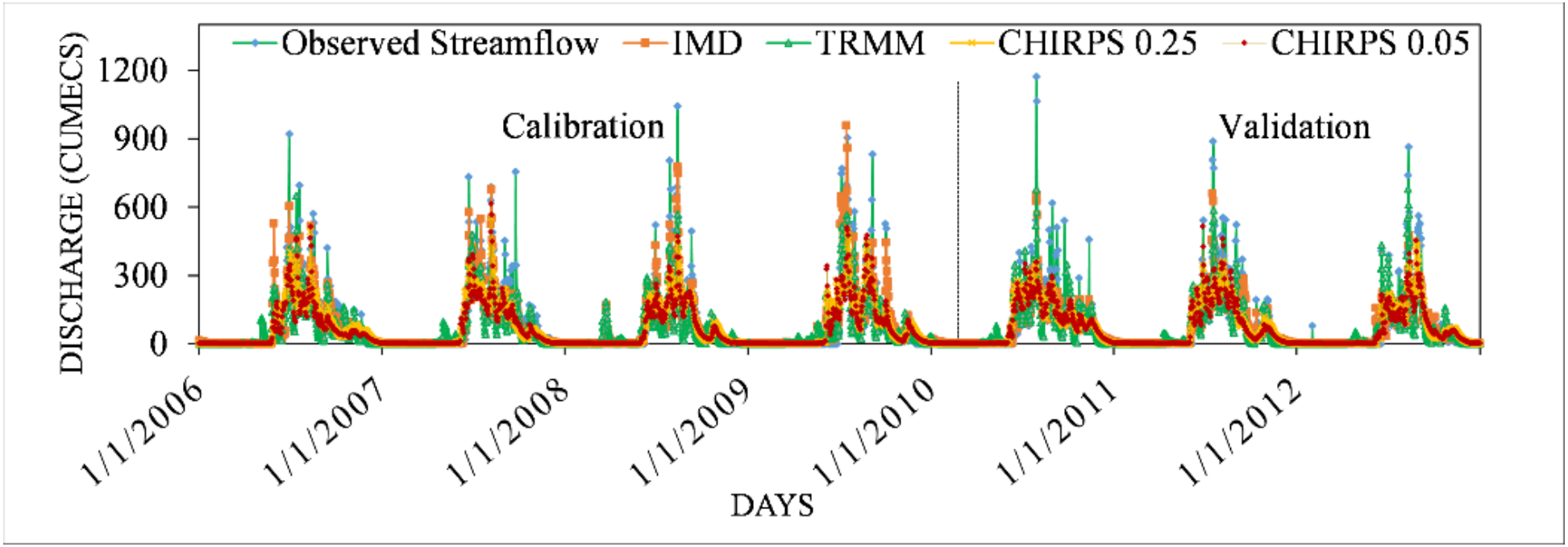

Fig. 4.1. Daily simulation of streamflow for different precipitation datasets.

Table 4.2. The optimized value of each sensitive parameter for the four scenarios ("v_" and "r_" stand for replacement and a relative change to the initial parameter values, respectively).

Parameter	**Description**	**Lower limit**	**Upper limit**	Optimal value				Process
				S1	S2	S3	S4	
r_CN2	Initial SCS CN II Value	-0.20	0.20	-0.08(2)	0.18(7)	-0.18(1)	-0.12(4)	Runoff
v_GW_DELAY	Groundwater delay (days)	10	350	22.09(9)	309.25(8)	9.56(4)	14.61(3)	Groundwater
v_CH_K2	Effective hydraulic conductivity in main channel alluvium (mm/h)	0	500	291.50(7)	483.44(5)	422.13(8)	487.19(9)	Channel
v_Alpha_Bnk	Baseflow alpha factor for bank storage (days)	0.5	1	0.79(1)	0.70(6)	0.54(9)	0.89(8)	Channel
r_SOL_AWC	Available water capacity of the soil layer	0	1	0.31(3)	0.79(2)	0.24(2)	0.73(2)	Soil
v_ALPHA_BF	Baseflow alpha-factor (day)	0	1	0.89(6)	0.42(9)	0.43(7)	0.86(5)	Groundwater
v_GWQMN	Threshold depth of water in the shallow aquifer required for return flow to occur (mm)	0	5000	4100.8(8)	1391.14(4)	1706.12(6)	3742.63(7)	Groundwater
v_ESCO	Soil evaporation compensation factors	0	1	0.88(4)	0.45(3)	0.41(5)	0.36(6)	Evaporation
v_GW_REVAP	Groundwater "revap" coefficient	0.02	0.2	0.17(5)	0.02(1)	0.11(3)	0.19(1)	Groundwater

Note: Numbers in the parenthesis represent the rank of sensitive parameters.

4.4.3 Hydrologic Process Simulation

To assess runoff predictions obtained from the IMD and satellite rainfall datasets, specific analysis were performed by applying the SWAT model with inputs from both datasets over the Gurupura river basin. The SWAT model includes the parameters that need calibration for reasonable flow simulation. Nonetheless, calibrated values were swayed due to the correlation between model parameters and the observed data *(Li et al.* 2018). The NSE is the objective function for testing the hydrological processes for four scenarios. Each scenarios is explained below to eliminate the calibration effects of different datasets that are important (Li *et al.* 2018) but not adequately discussed in the relevant literature:

Scenario 1 (S1) is used to check the capacity of IMD gridded data and to assess the other datasets in the simulation process. In the first phase of S1, the daily IMD rainfall data is used to calibrate the model and obtain the optimized value for each sensitive parameter. In the second phase of S1, the daily TRMM, CHIRPS 0.25 and CHIRPS 0.05 rainfall data were used to drive the model with the same optimized parameter values of phase S1. The rationale behind implementing this second phase is to understand the effect of satellite precipitation products on the variations in streamflow simulations under a set of normal calibration sensitive parameters (Bitew and Gebremichael 2011). The last phase of S1 is to compare the simulated runoff of satellite datasets with the IMD rainfall-driven results.

In Scenarios 2, 3 and 4 (S2, S3, S4), the daily TRMM, CHIRPS 0.25 and CHIRPS 0.05 rainfall were used to drive the SWAT model and optimize the parameter values respectively. The corresponding phases used in the case of S1 are performed. The rationale behind this scenario is that (i) Calibrating the model with different satellite precipitation products collected from various sources reveals the impact of the rainfall data source on calibration performance and discharge simulations and (ii) understanding the hydrological usability of these data products, which significantly helps in data-scarce basins and ungauged basin where there are only satellite precipitation products.

Based on the SUFI-2 algorithm of SWAT-CUP, the sensitivity analysis was performed prior to calibration to identify before calibration the most sensitive parameters (Table 4.2). In general, in subtropical and tropical regions, the SUFI-2 approach is a promising technique in the calibration and uncertainty analysis *(Uniyal et al.* 2015) and was adopted for the present study. It may be noted that, each parameter exhibits different optimized values for different scenarios. The curve number, which is the most sensitive parameter, showed different optimized values for all the datasets. The value of CN2 for S1, S2, S3 and S4 are -0.8, 0.18, -0.18 and -0.12, respectively. These values correspond to the relative values of the parameter in the SWAT model.

The shallow aquifer transit parameter GW_DELAY (Malagò *et al.* 2015) showed a higher value of 309. Twenty-five days for TRMM rainfall whereas IMD and CHIRPS datasets had lower values as the value is higher, the lag between the entry of water into shallow aquifer to release increases. Other groundwater parameters such as ALPHA_BF, a direct index for altering the recharge of groundwater response, GWQMN the measure of capillary rise, and GW_REVAP the indicator of water removed from the aquifer correspond to different optimized values for meeting up with the observed streamflow. It could be observed that the pair of IMD and CHIRPS-0.05 & TRMM and CHIRPS-0.25 datasets represented an optimized value closer to each other for groundwater parameters. It may be presumed that the spatial resolution in the CHIRPS datasets and their optimized parameter values are significantly different which shows a variation in resolution and parameter value.

The parameter ESCO is directly related to the evapotranspiration process (Malagò *et al.* 2015). As the value of ESCO decreases, it makes the lower layer to compensate for the water deficit in the upper layer such that the soil evapotranspiration increases. The satellite-based rainfall datasets depicted an opposite trend to IMD with a lower value of ESCO corresponding to higher soil evapotranspiration. Similar patterns were expressed by the channel parameter CH_K2 used to estimate the peak runoff. The sensitive parameter values of SOL_AWC which influence the streamflow and base flow having a range of 0-1 are given in table 4.2. As the value increases, the ability of soil to hold water also increases which leads to decreased streamflow.

The details of the model performance under all four scenarios are presented in table 4.3. In Scenario 1, the IMD rainfall model generated a strong overall fit for hydrological processes. The NSE, PBIAS and R^2 for Gurupura river using IMD data are 0.86, 0.87, 0.86 during calibration and 0.76, -13.5, and 0.81 for the validation period respectively. This exhibits an excellent performance rating (Moriasi *et al*. 2007), indicating that IMD rainfall data leads to a robust and reliable testing model for applicability and precision that could be used to validate and compares the results obtained from TRMM and CHIRPS rainfall (phase one in S1). Nevertheless, the subsequent performances using TRMM and CHIPRS data exhibited relatively lower agreements (see phase two above).

The NSE, R^2 and PBIAS were in the range of 0.57 to 0.7, 0.57 to 0.74, and -21.69 to 0.44 respectively which are in the range of satisfactory and good performance ratings as per (Moriasi *et al*. 2007). The TRMM results showed better agreement than CHIPRS-0.05 spatial resolution, which is better than the coarser-resolution product of CHIRPS with 0.25 spatial resolutions.

For scenario 2, the model performance using TRMM also produced a good score with NSE, PBIAS and R^2 of 0.71, -14.98, 0.75 and 0.71, -8.18, 0.72 during calibration and validation respectively. The performance of IMD data with TRMM optimized parameter showed a higher value than the parent model (TRMM model) which is interesting. The CHIRPS data under S2 is also in the acceptable range. In the case of S3 and S4 it was found that, as spatial resolution increases, there is an improvement in the model's performance. This indicates that the resolution of datasets also has a vital role in model performance and hydrologic processes.

It showed higher performance for the IMD gridded data irrespective of the parameters of the models which are used for calibrating. While comparing the performance of model simulations, the IMD rainfall-driven streamflow emerged as the best followed by the TRMM, CHIRPS 0.05 and CHIRPS 0.25. Since the TRMM and CHIRPS rain driven model results are in the acceptable range. They could be utilized for similar basins to analyze hydrologic responses since these datasets are available free of cost with different spatial and temporal resolutions. This result and the performance of satellite precipitation products are particularly desirable for data-scarce and

ungauged river basins. As the performance of the satellite precipitation data-driven model reduces by using the calibrated parameters of the other datasets, it may be better for each dataset should be calibrated and validated separately when using satellite rainfall products in hydrological modeling, rather than using gauge-calibrated sensitive parameters to calibrate other data sets. Such findings are consistent with the results of Kolluru *et al* (2020), Xue *et al*. (2013) and Yuan *et al*. (2018).

It is noteworthy that the parameters of a dataset which provided better results during calibration of the model, served similar or higher performance for the other datasets by transferring the same parameters in the model. For example, IMD rainfall-driven model outperformed both TRMM and CHIRPS models which were forced with calibrated parameters using TRMM and CHIRPS. When TRMM data was used to simulate using the calibrated parameters of the CHIRPS-0.05 model, products yielded better or higher results than when forced with CHIRPS-0.05 parameters. Therefore, it is inferred from these results that the parameters from a dataset that prove efficient when calibrated and could be transferred to calibrate the model with other datasets. Nonetheless, applying satellite precipitation products specific sensitive parameters for calibration is recommended because it often leads to substantially improved hydrological simulations compared to a model calibrated with other sensitive parameters of the satellite dataset or gage dataset (Bitew and Gebremichael 2011; Thiemig *et al*. 2013).

Table 4.3. Statistical indexes for Gurupura streamflow using different rainfall data.

Scenario	Period of model run	IMD Rainfall based model			TRMM Rainfall based model			CHIRPS-0.25 Rainfall based model			CHIRPS-0.05 Rainfall based model		
		NSE	PBIAS	R^2	NSE	PBIAS	R^2	NSE	PBIAS	R^2	NSE	PBIAS	R^2
1	Calibration	**0.86**	**0.87**	**0.86**	0.66	-21.69	0.74	0.61	-7.21	0.61	0.65	-2.32	0.66
	Validation	**0.76**	**-13.50**	**0.81**	0.70	-12.92	0.73	0.57	-7.03	0.57	0.63	0.44	0.64
2	Calibration	0.75	10.71	0.77	**0.71**	**-14.98**	**0.75**	0.55	4.90	0.56	0.54	-1.85	0.58
	Validation	0.72	-5.52	0.73	**0.71**	**-8.18**	**0.72**	0.55	3.98	0.56	0.55	2.40	0.59
3	Calibration	0.73	2.08	0.73	0.63	-27.25	0.74	**0.64**	**-6.20**	**0.65**	0.63	-0.70	0.64
	Validation	0.67	-13.19	0.70	0.67	-19.22	0.73	**0.62**	**-7.41**	**0.63**	0.61	1.66	0.62
4	Calibration	0.75	-0.91	0.75	0.60	-30.8	0.74	0.67	-9.67	0.65	**0.66**	**-13.76**	**0.69**
	Validation	0.70	-16.09	0.65	0.66	-22.60	0.75	0.62	-10.71	0.65	**0.65**	**-11.01**	**0.67**

Note: Values in bold represent the statistical index values obtained when a particular set of precipitation data is used to calibrate the model.

4.5 CLOSURE

An attempt was made to evaluate the Tropical Rainfall Measuring Mission (TRMM) and Climate Hazards Group InfraRed Precipitation with Station data (CHIRPS) employing a semi-distributed hydrological model i.e. Soil and Water Assessment Tool (SWAT) for simulating streamflow and validating them against the flows generated by driving India Meteorological Department (IMD) rainfall dataset in the Gurupura river basin of India. Distinct testing scenarios for simulating streamflow were made to check the suitability of these satellite precipitation data. The TRMM was able to estimate better rainfall than CHIRPS after performing categorical and continuous statistical results concerning IMD rainfall data. While comparing the performance of model simulations, the IMD rainfall-driven streamflow emerged as the best followed by the TRMM, CHIRPS-0.05 and CHIRPS-0.25. The coefficient of determination (R^2), Nash-Sutcliffe efficiency (NSE) and percent bias (PBIAS) were in the range of 0.56 to 0.86, 0.54 to 0.86 and -14.98 to 10.71 respectively.

CHAPTER 5

RIVER BASIN RESPONSE ON EFFECTS OF LAND USE AND CLIMATE CHANGE

5.1 METHODOLOGY

5.1.1 Historical and predicted climate database

Two sets of meteorological data (historical and predicted) were used in the present study to investigate the long-term climate variation in the ARB, VRB and GRB. All the datasets were consistent on a daily time step with a spatial resolution of 0.25° × 0.25°. Historical rainfall and temperature data from 1981 to 2010 were collected from the IMD. For evaluating future/forecasted climate in the river basins, precipitation and temperature data from five downscaled GCMs was employed. The five GCMs used in this investigation were carefully selected based on the review of earlier studies (Kannan and Ghosh 2013; Salvi *et al.* 2018*;* Sinha *et al*. 2020). The direct use of climate variables simulated by GCMs might be acceptable over a large scale. However, at a local scale, the data may demonstrate considerable bias compared with the measured data (Salvi et al. 2013). For better accuracy and representation of rainfall characteristics, the climate variables must be bias corrected. In this study, the daily GCM data which is bias corrected using the quantile-based method proposed by Li et al. (2010) against the India Meteorological Department (IMD) gridded data were obtained from www.regclimindia.in. The quantile-based remapping approach provides accurate results until the statistical properties of the observed and simulated (GCM) time series are concerned (Salvi et al. 2013). A detailed description of the methodology is provided by Li et al. (2010). The obtained bias corrected GCM data are segregated into the three climate windows viz; near-future (T1) (20011–2040), mid-future (T2) (2041–2070), and far-future (T3) (2071–2099). The output from the five GCMs including CCCMA CanESM2; CNRM CM5; MPI ESM MR; MPI ESM LR, and BNU ESM respectively are the source of predictor data used for precipitation downscaling for future RCP scenarios. A brief description of the GCM datasets is given in Table 5.1 below.

Table 5.1 The GCM input data used for the future period in the present study for RCP 4.5 and 8.5 emission scenarios.

Model	Institution	Spatial Resolution
CanESM2	Canadian Centre for Climate Modelling and Analysis	2.8˚x2.8˚
BNU-ESM	Beijing Climate Center, China Meteorological Administration"	2.8˚ x2.8˚
CNRM-CM5	Centre National de Recherches Meteorologiques/Centre Europeen de Recherche et Formation Avancees en Calcul Scientifique	1.4˚x1.4˚
MPI-ESM-LR	Max Planck Institute for Meteorology (MPI-M)	1.8˚x1.8˚
MPI-ESM-MR	Max-Planck-Inst. for Meteorology	1.87˚x1.87˚

5.1.2 Pre-processing of Landsat data

The Landsat images were procured for 1988, 1995, 2003 and 2016 to determine to determine land cover changes. All of the images in this research were obtained during the post-monsoon season (October to January) and were clear of clouds. Because of its effectiveness, the supervised maximum likelihood approach was employed to classify images (Wagle *et al*. 2020). The overall accuracy and kappa coefficient (κ) in 76%–83% and 0.75–0.83 respectively for ARB, 82%–89% and 0.79–0.86 for VRB and 79%– respectively 85% and 0.78–0.86 for GRB, are generally acceptable. Section 5.2.2 describes the details of classified images and their changes.

5.1.3 Principle of Dyna-CLUE and its structure for projection of future LULC

To determine the effects of future changes in land cover on runoff, the future land cover for 2030, 2050, 2075, and 2100 were projected. The Dyna-CLUE model was used for obtaining future land use in the river basin. The Dyna-CLUE has a flexible and generic framework that promotes scale and specific contexts for regional applications. One of the significant strengths of the Dyna-CLUE model is the elasticity allotted to

each LU type. The model allows certain land uses (such as permanent crops) to be reluctant to change and other land uses (such as shifting cultivation, locally known as Jhum in India) to change easily (Venkatesh *et al*. 2020b). Dyna-CLUE model is categorized into two modules: the non-spatial and the spatial.

In the non-spatial module, demands of different land use classes are calculated, while the spatial module transforms the yearly demands into possible land use changes at different spatial locations within the given time frame in the study area.

The second module is a spatially explicit allocation module, which uses a raster-based system to estimate land use demands and to convert into land use changes at different locations within the study region. Spatial module again has two parts. The first part aims at establishing relations between land use and its driving factors, explicitly considering scale dependencies. The second part aims at dynamically allocating demanded land use through an iterative procedure to ensure that a location gets the most suitable land class.

Model Parameters

Land use demand: Land use demand estimation cannot be done using the Dyna-CLUE model user interface as it only has the ability to spatial allocate land use change. For estimation of land use demand, different models are adopted. Such a model could be as simple as trend extrapolations to complex economic models. Demand estimation model should be chosen based on the nature of land use conversions taking place and the scenarios to be simulated.

Spatial policies and restrictions: Land use policies and land tenure can influence the outline of land use conversions. For the simulation of land use maps, areas with policy implementation and the restriction must be indicated. An area for which the policy is implemented is supplied as restriction layer.

Land use type specific conversion settings: Each land use class changes its states differently. The temporal characteristics of land use and their specific conversion settings are specified in a conversion matrix. This matrix defines the possible and not possible interchangeability among different land use types and approximate time required for each change process.

Conversion elasticity: Conversion elasticity defines the flexibility of a land use types towards change. Land use class with high capital investment is less prone for conversion to other land uses as long as there is ample demand. Examples are urban areas, plantations with permanent crops (e.g., fruit trees), etc. Value needs to be specified for each land use class that represents the relative elasticity to change. Elasticity co-efficient ranges from 0 (easy conversion) to 1 (irreversible change) and defined by the user based on experience or observed behaviour in the recent past.

Time steps: Defines the time of a land use class in a location should remain the same before it can change into another class. This can be relevant in the case of regrowth of the forest.

Location Characteristics: Finally, a location most suitable for a specific type of land use at that moment gets converted. Suitability embodies the result of interaction between different actors and decision-making processes that have resulted in a spatial land use pattern. The preference is calculated using Equation (5.1).

$$R_{ki}=a_k X_{1i}+b_k X_{2i}+\ldots\ldots \quad (5.1)$$

Where R is the preference to devote location *i* to land use type *k*, $X_{1,2}$,... are biophysical or socio-economical characteristics of location *i* and a_k and b_k the relative impact of these characteristics on the preference for land use type *k*. R_{ki} is estimated as a probability because it cannot be observed or measured directly. A logit model is defined (Equation 5.2) to relate these probabilities with biophysical and socioeconomic location characteristics.

$$\text{logit}(P_i) = \ln\left(\frac{P_i}{1-P_i}\right) = \beta_o + \sum_{j=0}^{n} \beta_j X_{j,i} \quad (5.2)$$

Where P_i : probability of a grid cell to be allocated with a specific land-use class in a specific location;

β_0 *:* constant obtained from the BLR model;

β_j : driving factors coefficients estimated through the BLR model; and

$X_{j.i}$: the (j^{th}) location factor affecting the suitability of land-use (*i*).

Details of the Logistic regression model is presented below

5.1.4 Logistic Regression

To interpret the locational preferences of each land use class, the possible driving factors and each land use class are related by constructing a Binary Logistic Regression (BLR) model. BLR is a form of statistical regression, used when the dependent variable is dichotomous (0 or 1) and the independent variables are continuous or categorical. In logistic regression, the dependent variable follows Bernoulli distribution with an unknown probability *p*. Bernoulli distribution is a kind of Binomial distribution where *n* = 1. The occurrence of a variable is 1 and not occurrence is 0. So the probability of occurrence is *p* and not occurrence is $q = 1 - p$. In logistic regression, unknown p is estimated for any given linear combination of independent variables. Here a function is required to essentially link independent variables with the probability of occurrences of dependent variables which follow Bernoulli distribution. The natural log of the odds ratio (ratio between the probability of occurrence and not occurrence) is that link function.

If p = 0, then $\ln\left(\frac{P_i}{1-P_i}\right) = \ln\left(\frac{0}{1-0}\right) = \ln 0 = undefined.$ Similarly, if p = 1, then $\ln\left(\frac{P_i}{1-P_i}\right) = \ln\left(\frac{1}{1-1}\right) = In\ undefined = undefined.$ Interestingly, when p = 0.5, then $\ln\left(\frac{P_i}{1-P_i}\right) = \ln\left(\frac{0.5}{1-0.5}\right) = \ln 1 = 0$. Thus, when the odds ratio is even the logit is 0. If it is plotted on a graph, 0 to 1 run along the x axis. However, it should be along the y axis to fulfil our objective. Inverse of the logit function can be used to achieve that. Part of Equation 5.1 is represented here again for better clarity, here P is between 0 and 1.

$$\text{logit}(P_i) = \ln\left(\frac{P_i}{1-P_i}\right) \tag{5.3}$$

Then inverse of the logit is

$$\log^{-1}(\alpha) = \frac{1}{1+e^{-\alpha}} = \frac{e^{\alpha}}{1+e^{\alpha}} \tag{5.4}$$

Here α is some number

For the present study, "some number" will be the linear combination of the driving factors (independent variables) and their coefficients. The Inverse-logit will return the probability of being a '1' or the probability of occurrence of a particular land use class.

In the case of land use maps, land use classes act as the dependent variables and the absence or presence of a particular land use class in a specific grid cell is indicated by the value 0 or 1 (Overmars and Verburg 2005).

The driving factors are independent variables in the equation. In SPSS® software package, an estimation model is developed that fits the Inverse logit model. The analysis gives the coefficients that can be input into the model.

The estimation of regression coefficients is a Maximum Likelihood Estimation or MLE. In this study, the main goal is to estimate the probability of each cell to be allocated to a land use class. The natural logarithm of the odds ratio is equivalent to a linear function of the independent variables. The antilog of the logit function allows to find the estimated probability. The binary logistic regression model of Equation 5.2 is represented here again for better clarity,

$$\text{logit}(P_i) = \ln\left(\frac{P_i}{1-P_i}\right) = \beta_o + \sum_{j=0}^{n} \beta_j X_{j,i} \qquad (5.5)$$

Now a method is essential to solve the *P*. Using antilog this can be done. Hence,

$$\frac{P_i}{1-P_i} = e^{\beta_0+\beta_j X_{j,i}} \qquad (5.6)$$

Or,

$$P_i = e^{\beta_0+\beta_j X_{j,i}}(1-P) \qquad (5.7)$$

Or,

$$P_i = e^{\beta_0+\beta_j X_{j,i}} - e^{\beta_0+\beta_j X_{j,i}} * P_i \qquad (5.8)$$

Or,

$$P_i + e^{\beta_0+\beta_j X_{j,i}*} P_i = e^{\beta_0+\beta_j X_{j,i}} \qquad (5.9)$$

Or,

$$P_i\left(1 + e^{\beta_0+\beta_j X_{j,i}}\right) = e^{\beta_0+\beta_j X_{j,i}} \qquad (5.10)$$

Or,

$$P_i = \frac{\left(1+e^{\beta_0+\beta_j X_{j,i}}\right)}{e^{\beta_0+\beta_j X_{j,i}}} \qquad (5.11)$$

Then Known β is used to estimate the probability of a cell to change its state.

5.1.5 Allocation Procedure

The spatial allocation module iteratively compares the allocated area of individual land use types to grids with the land use demand. The iterative process continues until the demand has been satisfied.

The allocation procedure allocates at the time (*t*) for each location (*i*) the land use type (*lu*) with the highest total probability ($Ptot_{i,t,lu}$). The total probability is defined as the sum of the location suitability (*Ploci,t,lu*), neighbourhood suitability ($Pnbh_{i,t,lu}$), conversion elasticity ($ELAS_{lu}$) and competitive advantage ($COMP_{t,lu}$) in Equation (5.12).

$$Ptot_{i,t,lu} = Ploc_{i,t,lu} + Pnbh_{i,t,lu} + ELAS_{lu} + COMP_{t,lu}, \quad (5.12)$$

Among the model parameters, land use demand is very crucial. Accuracy of model output largely depends on this. Biophysical characterization of study area is usually carried out to generate land use time series data. Land use time series data could be extrapolated or interpolated to fill missing time step and could be used as a land use demand parameter. Land use demands, as well as spatial land use configuration, are outcomes of interactions between different factors and decision making processes in the study area. Different factors are spatially mapped as driving factors and used in statistical models as independent variables.

5.1.6 Mapping of Input Drivers

Thematic maps of three categories of drivers are prepared by integrating data from several sources using GIS platform. The three categories of drivers are broadly classified as Bio-physical, proximity, and socio-economic drivers (Fig. 5.1, Fig 5.2 and Fig. 5.3). Socio-economic and biophysical driving factors of land use change are location specific and scale dependent. They are selected based on experts' knowledge of study area and factors frequently identified in land-change studies (Geist and Lambin 2006; Hersperger *et al*. 2010). A list of proximate land use change drivers are identified from literature and existing case studies (Lin *et al*. 2011). Distance to cities, distance to road and distance to railway are grouped under proximity drivers.

Lack of theoretical understanding of land use system is the first roadblock to identify land use change drivers in India. Land use change is locally influential and scale-

dependent mechanism. Due to that, having a guideline or a handbook for listing up the proximate drivers of land use change is not possible. Some studies have used household survey to list up the proximate land use change drivers (Overmars and Verburg 2005; Kindu *et al*. 2015). Several other related literatures such as district handbooks, planning report could also be assimilated to gain an insight into the proximate causes of land use change. In order to identify proximate land use change driving factors in present study area, a number of existing literature on land use change modeling are reviewed (Koch et al. 2012; Zheng *et al*. 2012; Li and Wu 2013; Venkatesh *et al*. 2020b).

The land use database for the Dyna-CLUE model was constructed with the data retrieved from the supervised maximum likelihood classification technique for 1988, 1995, 2003 and 2016 as described earlier. The land use map corresponding between 1995 and 2003 was used to predict the land use of 2016. The overall accuracy of 76% (ARB), 79% (VRB), and 76% (GRB) was achieved when compared to the historical land use map of 2016. A total of 12 drivers categorized under bio-physical, proximity and socio-economic were implemented in this study. The bio-physical drivers examined were the Digital Elevation Model (DEM), lineament density, average annual precipitation, slope, average annual solar radiation, average annual temperature, and average annual wind speed. The proximity drivers were distance to cities, roads and water bodies and population density obtained from open-source spatial data provided by DIVA-GIS (https://www.diva-gis.org/). The data on socio-economic drivers such as population was obtained from WorldPop (https://www.worldpop.org/).

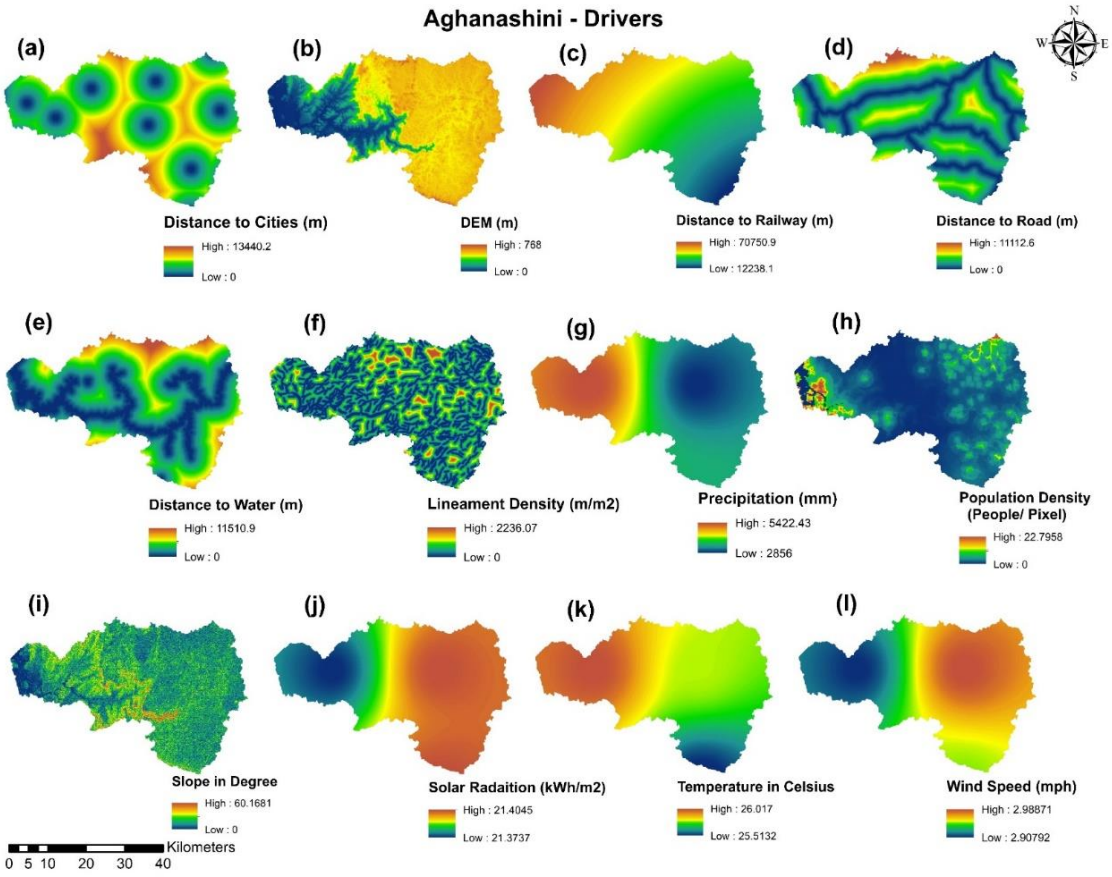

Fig. 5.1. Input drivers used for predicting land use in ARB

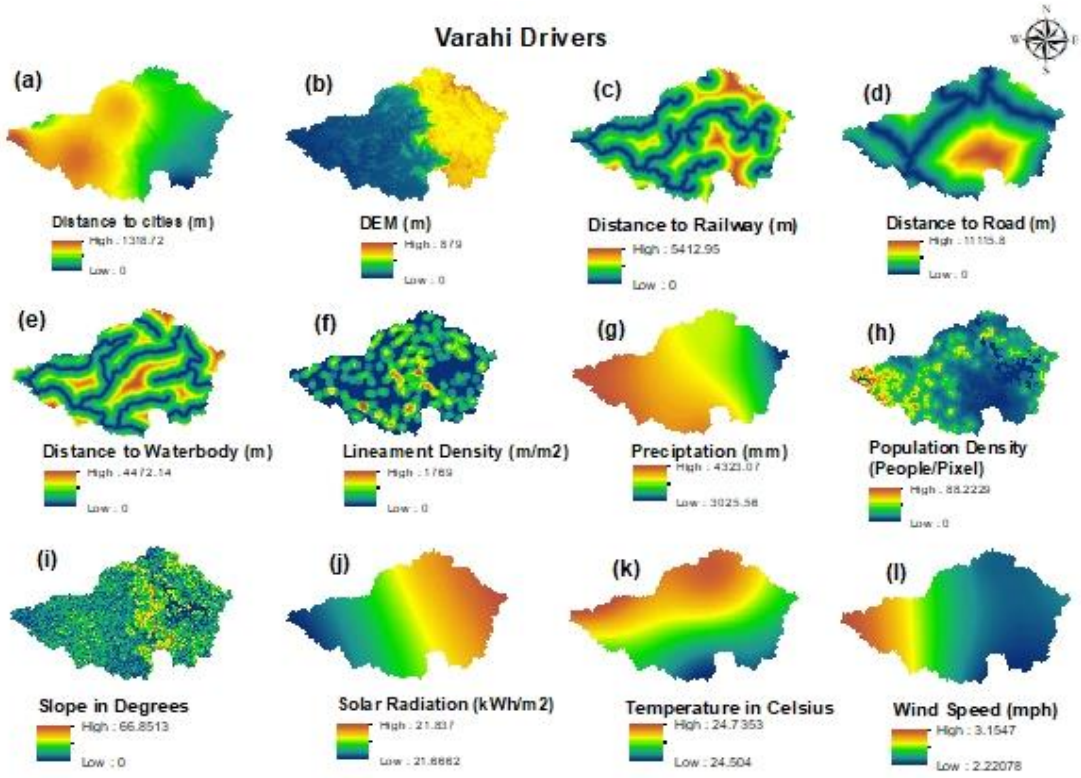

Fig. 5.2. Input drivers used for predicting land use in VRB

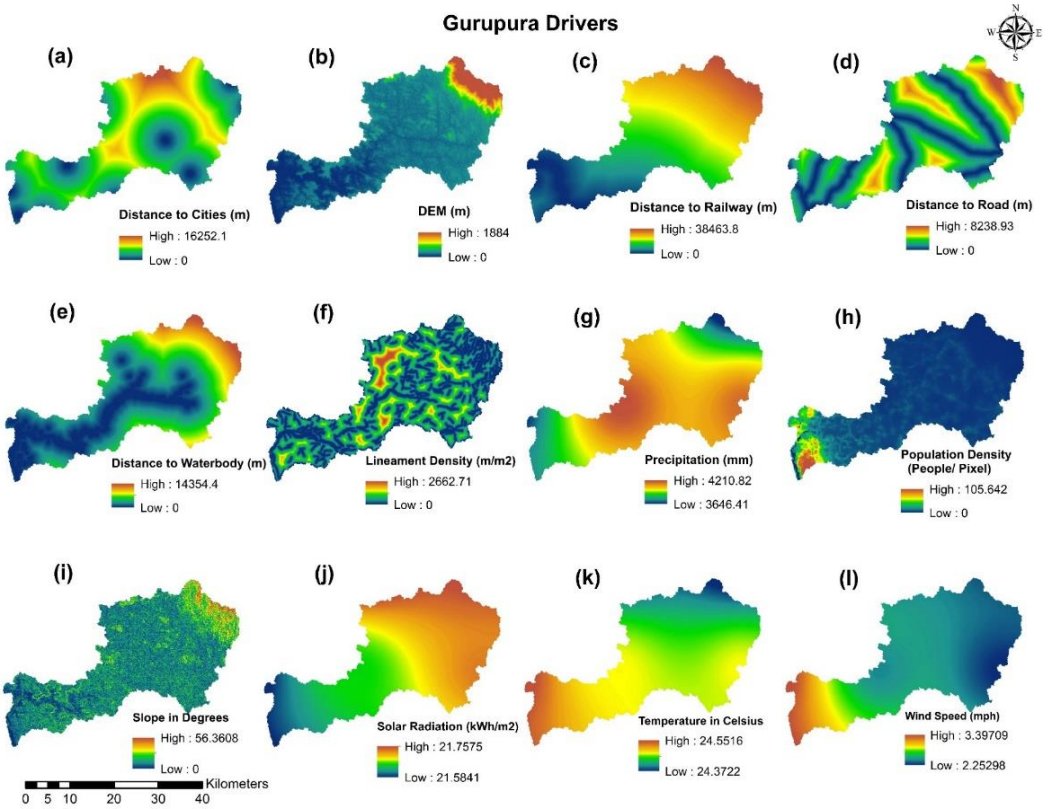

Fig. 5.3. Input drivers used for predicting land use in GRB

The drivers adopted for LU forecasting in the ARB, VRB and GRB are presented in Fig. 5.1, Fig 5.2 and Fig. 5.3 respectively. As the effect of independent variables (drivers) on dependent variables (LU classes) cannot be directly established, Binary Logistic Regression (BLR) (Behera *et al*. 2018; Khoury 2012; Trisurat *et al*. 2010; Zheng *et al*. 2012) was performed and the influence of each of the drivers for a particular LU was evaluated.

5.1.7 Scenario Analysis

Impacts of LULC changes on streamflow are carried out by holding the climatology constant understanding the hydrological effects of man-made LULC variations. Simulations are performed to examine the impact of climate change on streamflow. To explore the impact of climate change on streamflow, simulations are carried out with LULC fixed for 2016 and the changing climate during the baseline period (1981 to 2010) and future periods (2011-2099). GCM results for future periods are divided into three-time slices for both emission scenarios (RCP 4.5 and 8.5): T1 (2011-2040), T2 (2041-2070), and T3 (2071-2099). The SWAT was performed using five downscaled, bias-corrected GCM ensemble outputs (RCP 4.5 and 8.5) to quantify the change in streamflow. The simulation results were compared with simulated results from the baseline period (1981 to 2010). The results obtained during simulations are referred to as Qclim hereon. To carry out the analysis of both LULC and climate change, three different scenarios were set up: (i) near (2011-2040) – baseline (T1); (ii) mid (2041-2070) – baseline (T2); and (iii) far (2071-2100) – baseline (T3). In this study the strategy developed is the baseline as climate 1981-2010 by using 2016 LULC (near to present), and for the future period, it is near, mid and far scenarios are considered like the climate of 2011-2040 by using 2030 LULC (for the T1 scenario), climate 2041-2070 by using 2050 LULC (for the T2 scenario), climate 2071-2100 by using 2075 LULC (for T3 scenario) respectively.

5.2 RESULTS AND DISCUSSION

5.2.1 GCM climate data analysis

The statistics of the observed and the GCM-simulated climate variables (after bias correction) for the ARB, VRB and GRB are illustrated in a Taylor diagram in Fig. 5.4. As GCM outputs came from the same modeling centre, all GCM models may have been clustered together. The model cluster for precipitation (Fig. 5.4 (i, ii, iii) a) was slightly away from the observed point for all river basins. However, perfect correlation (> 0.90) for ARB and (>0.95) for VRB and GRB were noted between the observed and GCM precipitation.

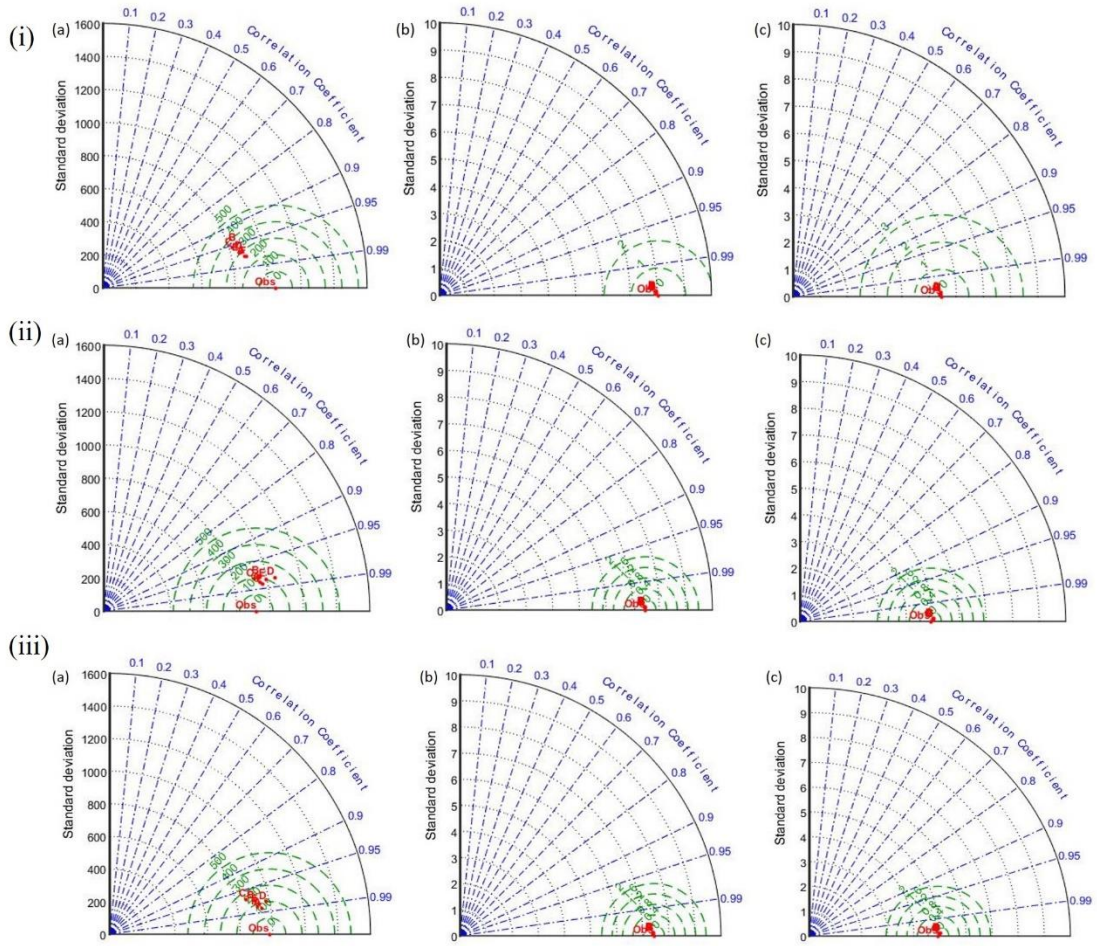

Fig. 5.4 Taylor diagram for: a) rainfall (mm/month), b) Tmax (°C), and c) Tmin (°C) for (i) ARB, (ii) VRB, (iii) GRB

Furthermore, from 1981 to 2005, the long-term average daily data of observed and GCM-simulated variables were compared for an average of all grids inside the basins daily (Fig. 5.5- ARB, Fig. 5.6- VRB, Fig. 5.7- GRB). The figure illustrates the rainfall, maximum and minimum temperature comparisons of all 5 GCMs and ensemble data after bias adjustments with IMD data. From fig.5.5a, it could be observed that, BNU, CNRM, MPIL and MPIM represents average daily rainfall better when compared with CCMA for ARB. The ensemble of all five GCM show poor peak rainfall estimation. Therefore the outputs of CCMA is excluded in ensemble of rainfall for streamflow simulation in ARB. For VRB, MPIM is removed for ensemble calculation of GCM as it shows poor simulation in rainfall (Fig 5.6a). Whereas CNRM is eliminated for GRB ensemble rainfall for streamflow simulations as it represented poor trend with IMD when compared with other GCMs (Fig 5.7a). In the case of maximum and minimum temperature, all GCM could generate better simulation. Thus GCMs were able to correctly depict the trend of rainfall and temperature climatology, as seen in the figures. As a result, downscaled variables accurately reflected the climatic conditions in the research region and were utilized in SWAT model simulations.

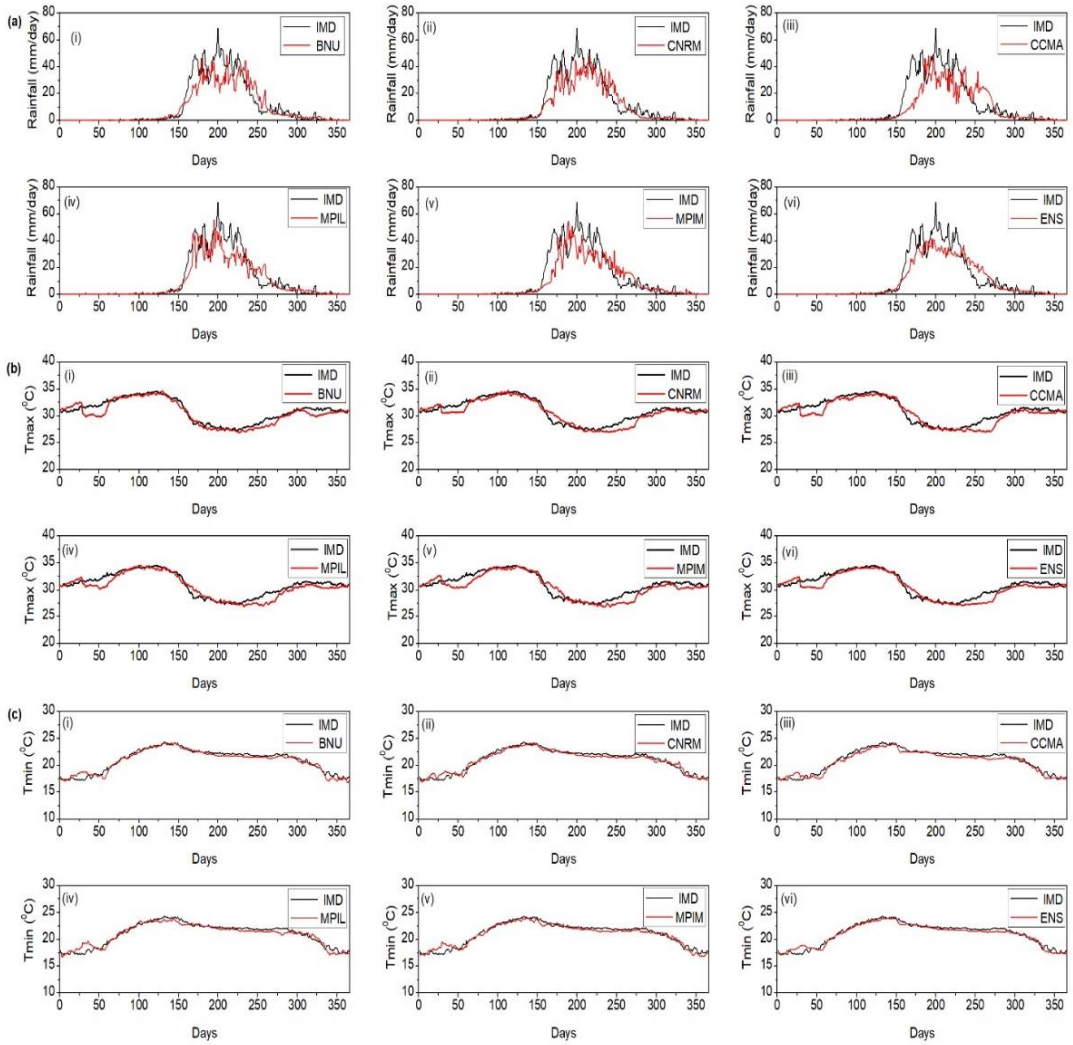

Fig. 5.5 GCM variables (red) compared with observed variables (black) for daily: a) rainfall; b) maximum temperature, and c) minimum temperature from 1981 to 2005 in ARB.

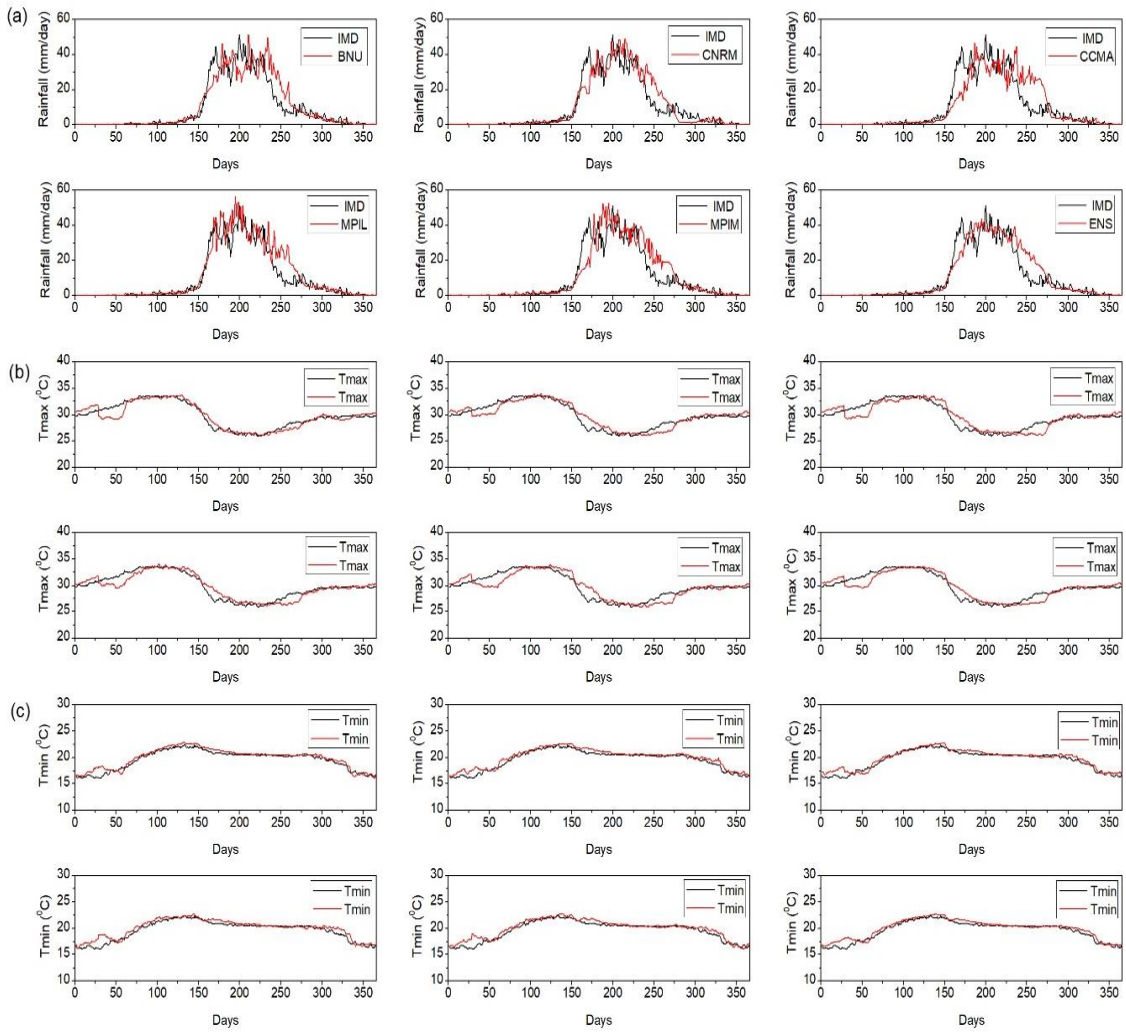

Fig. 5.6 GCMs variables (red) compared with observed variables (black) for daily: a) rainfall; b) maximum temperature, and c) minimum temperature from 1981 to 2005 in VRB.

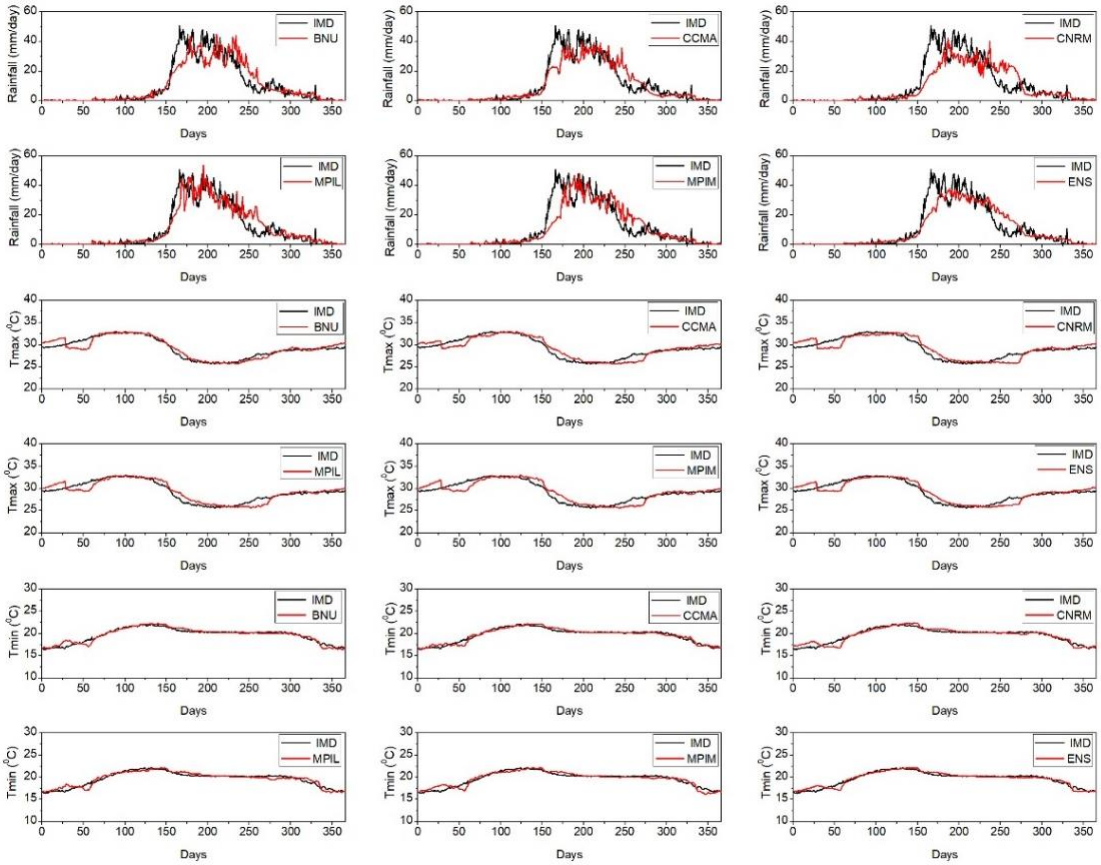

Fig. 5.7 GCMs variables (red) compared with observed variables (black) for daily: a) rainfall; b) maximum temperature, and c) minimum temperature from 1981 to 2005 in GRB.

Fig. 5.8, Fig 5.9, and Fig 5.10 shows the time series plots of historical IMD rainfall with historical GCMs rainfall from 1981 to 2005 and future GCMs from 2006 to 2100 for both RCP 4.5 and RCP 8.5 scenarios for ARB, VRB and GRB respectively. The trend of ensemble GCM (ENS) is showing a decreasing trend in the historic period and an increasing trend in the projected period for both RCP 4.5 and 8.5 emission scenarios in ARB. However in the overall time period it depicts an increasing trend (Fig 5.8) in ARB. It could be observed that, the GCMs underestimates the rainfall when comparing with IMD in the historic period for ARB (Fig 5.8). Also from the figure 5.8, it could be noticed that MPIL shows comparatively better results in ARB. In the case of VRB, CNRM is the best rainfall predicted GCM (Fig 5.9). The trends of GCMs are good for VRB when compared it with ARB trends. The trend of all GCMs and as well ensembled

(ENS) are showing slightly decreasing trend in VRB (Fig 5.9) for projected period for both RCP 4.5 and 8.5 emission scenarios. In the case of GRB, BNU depicted matching trend with IMD (Fig 5.10). The trend of ENS is showing a slight decreasing trend in the historic period and an increasing trend in the projected period for both RCP 4.5 and 8.5 emission scenarios in GRB. However in the overall time period it potrays an increasing trend (Fig 5.10) in VRB. However, the variations for ensembled scenarios (ENS) are reasonably matching giving good correlations (Fig. 5.4) for the all the three river basins.

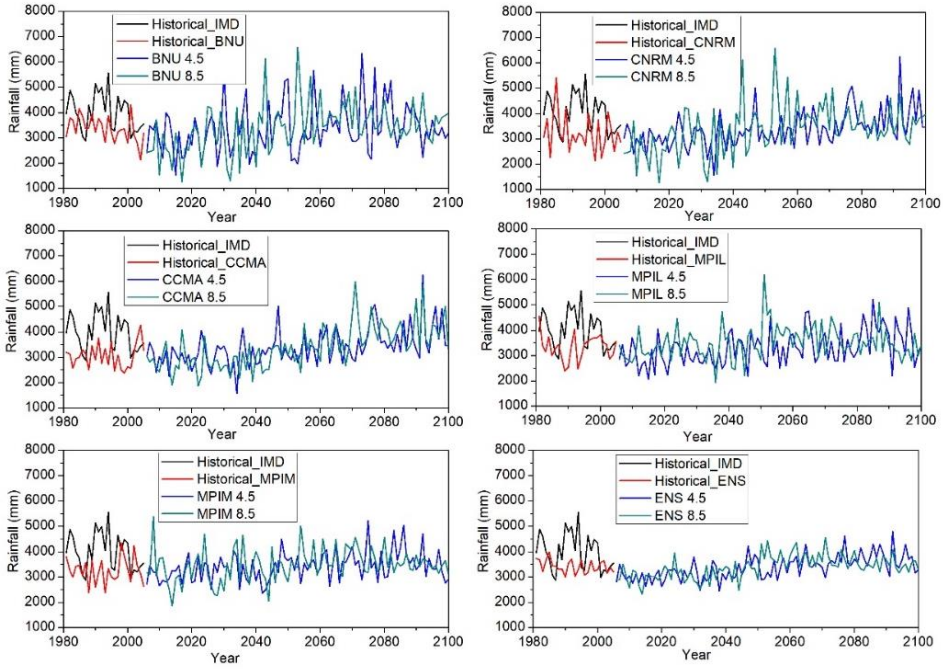

Fig. 5.8 Comparison of historical observed and GCMs simulated rainfall (1981 to 2005) and projection of future rainfall (2006 to 2100) of RCP emission scenarios in ARB

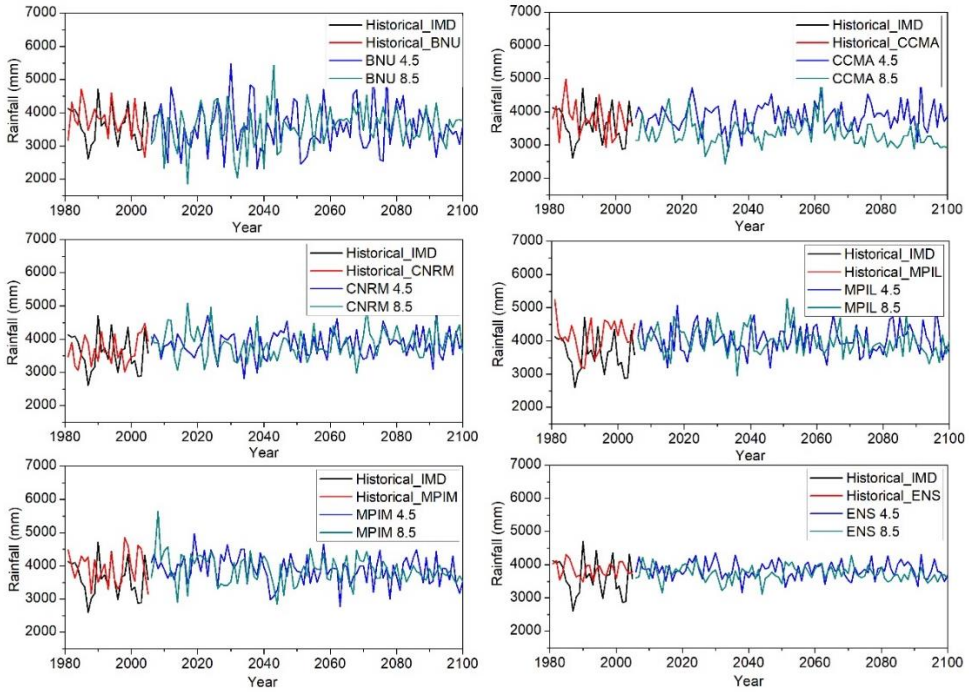

Fig. 5.9 Comparison of historical observed and GCMs simulated rainfall (1981 to 2005) and projection of future rainfall (2006 to 2100) of RCP emission scenarios in VRB

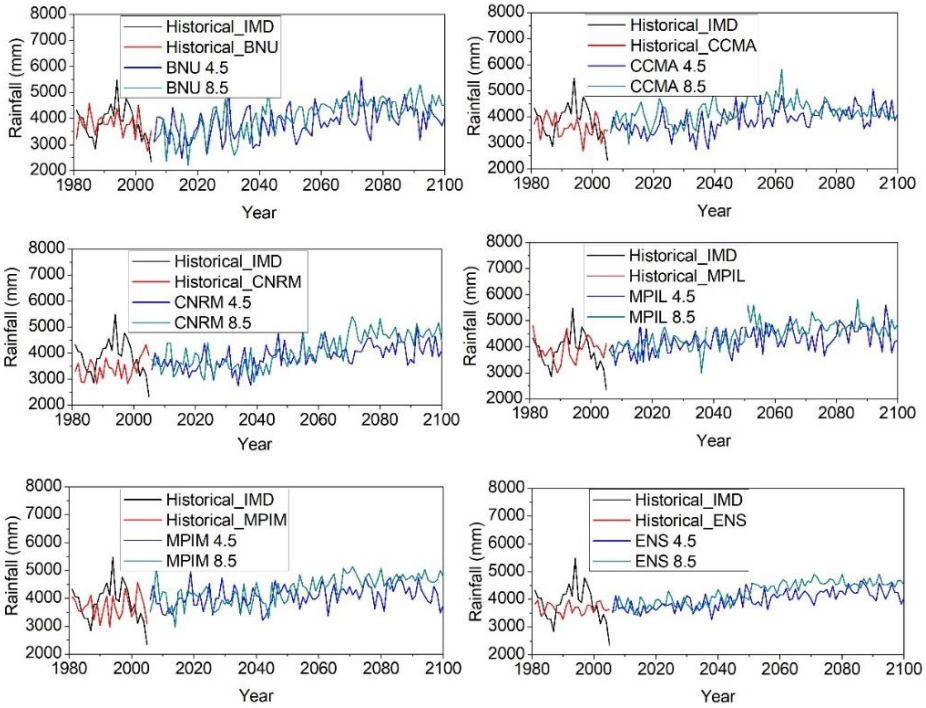

Fig.5.10 Comparison of historical observed and GCMs simulated rainfall (1981 to 2005) and projection of future rainfall (2006 to 2100) of RCP emission scenarios in GRB

Fig. 5.11, Fig. 5.12, Fig. 5.13 gives comparison of historical maximum temperature (Tmax.) from the IMD and historical maximum temperature of different GCMs including ensemble (ENS) which shows the good correlation for ARB, VRB and GRB respectively. The future maximum temperature of RCP 4.5 and 8.5 for all the 5 GCMs as well as ensembled one (ENS) indicated that the RCP 8.5 scenario would have higher maximum temperature in comparison to RCP 4.5 by 2 degrees Celsius for ARB (Fig 5.11), by 1 to 2 degree Celsius for VRB (Fig 5.12) and by 1 to 2 degrees Celsius for GRB (Fig 5.13). The trend for RCP 4.5 and 8.5 for maximum temperature is acceptable for future time periods. CCMA and MPIM depicts the best trends when compared with other GCMs in the ARB (Fig 5.11) and VRB (Fig 5.12). Whereas in the case of GRB, all the five GCM represented a matching trend with IMD maximum temperature (Fig 5.13). Similarly, the minimum temperature (Tmin.) time series plot for the historical and future period is plotted in Fig.14 for ARB, Fig 15 for VRB and Fig 16 for GRB. It is also showing a good correlation with the IMD observed data. The comparison of the future minimum temperatures for RCP 4.5 and 8.5 using all five GCMs and the ensemble model (ENS) revealed that the RCP 8.5 scenario would have higher minimum temperatures than RCP 4.5 by 3 degrees Celsius for ARB (Fig 5.14) and VRB (Fig 5.15), and 2 degrees Celsius for GRB (Fig 5.16). After the bias correction, the figures show acceptable range for future maximum and minimum temperature for these river basins the temperatures. Hence, these data are used to estimate hydrological simulations in the basin.

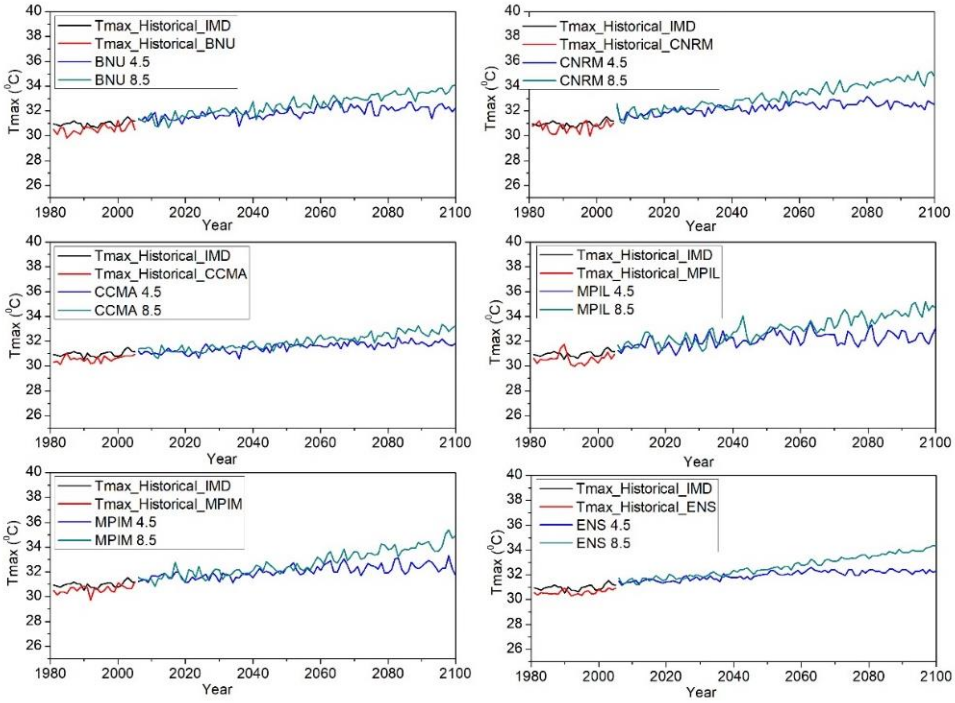

Fig. 5.11 Comparison of historical observed and GCMs simulated maximum temperature (1981 to 2005) and projection of future maximum temperature (2006 to 2100) of RCP 4.5 and RCP 8.5 emission scenarios (ENS- Ensembled) for ARB.

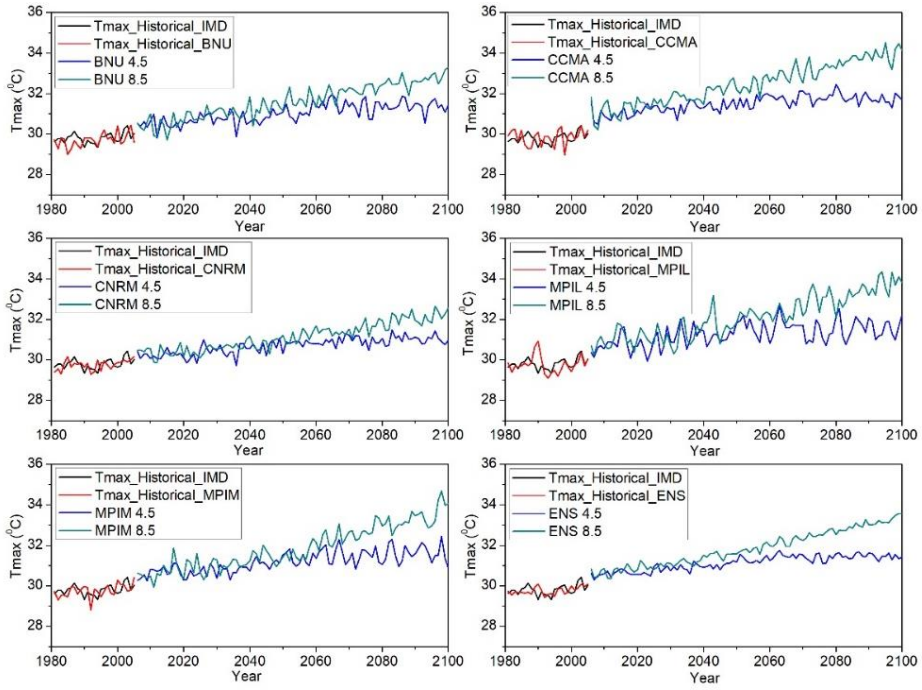

Fig. 5.12 Comparison of historical observed and GCMs simulated maximum temperature (1981 to 2005) and projection of future maximum temperature (2006 to 2100) of RCP 4.5 and RCP 8.5emission scenarios (ENS- Ensembled) for VRB.

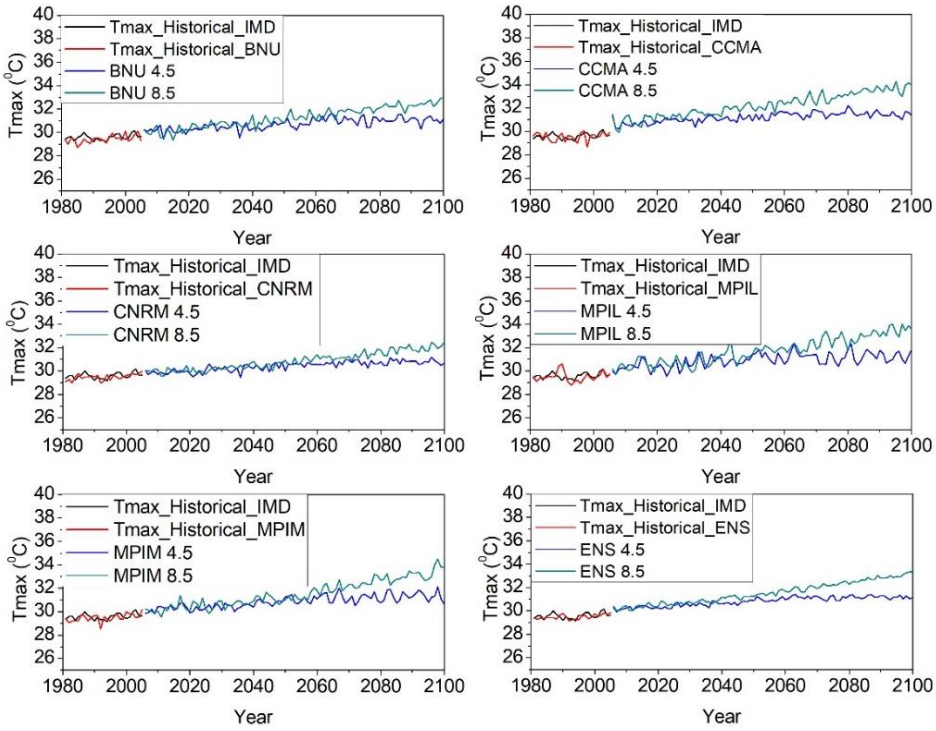

Fig. 5.13 Comparison of historical observed and GCMs simulated maximum temperature (1981 to 2005) and projection of future maximum temperature (2006 to 2100) of RCP 4.5 and RCP 8.5 emission scenarios (ENS- Ensembled) for GRB.

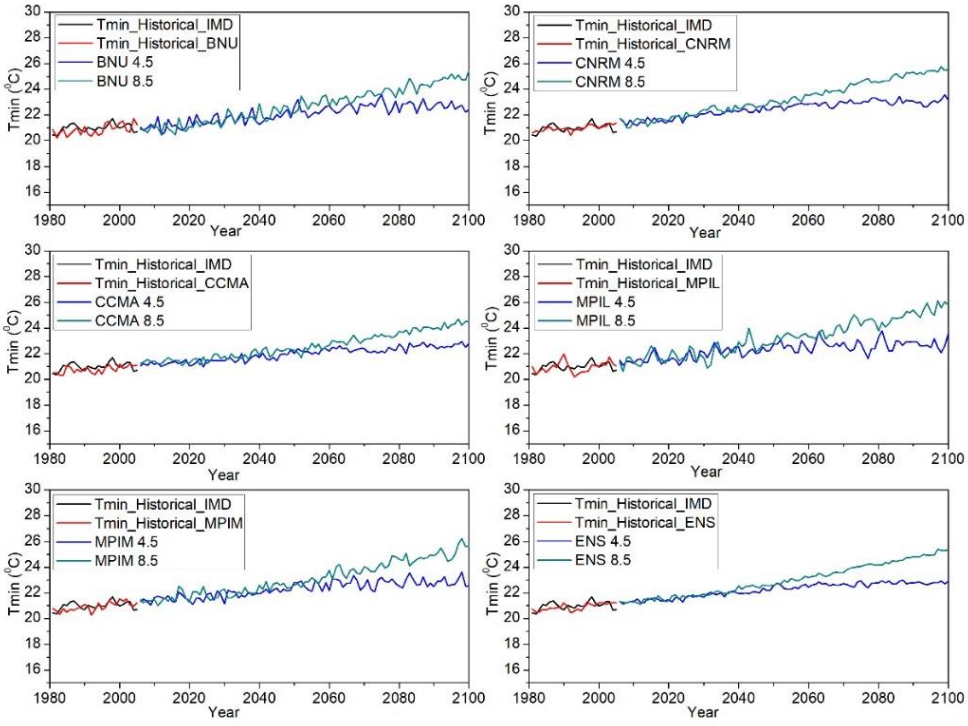

Fig. 5.14 Comparison of historical observed and GCMs simulated minimum temperature (1981 to 2005) and projection of future minimum temperature (2006 to 2100) of RCP 4.5 and RCP 8.5 emission scenarios (ENS- Ensembled) for ARB.

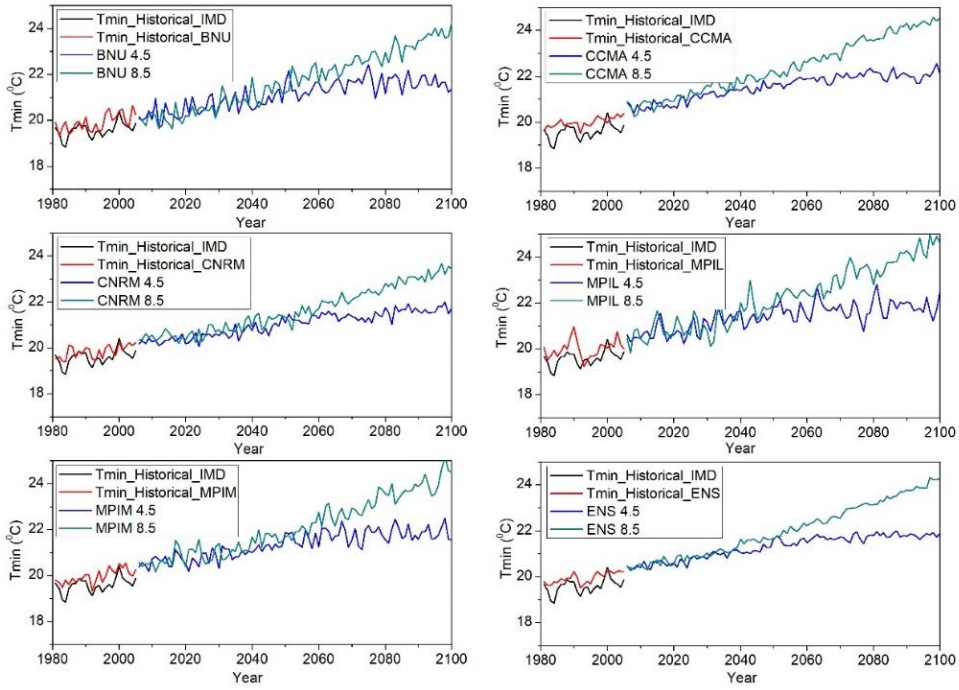

Fig. 5.15 Comparison of historical observed and GCMs simulated minimum temperature (1981 to 2005) and projection of future minimum temperature (2006 to 2100) of RCP 4.5 and RCP 8.5 emission scenarios (ENS- Ensembled) for VRB.

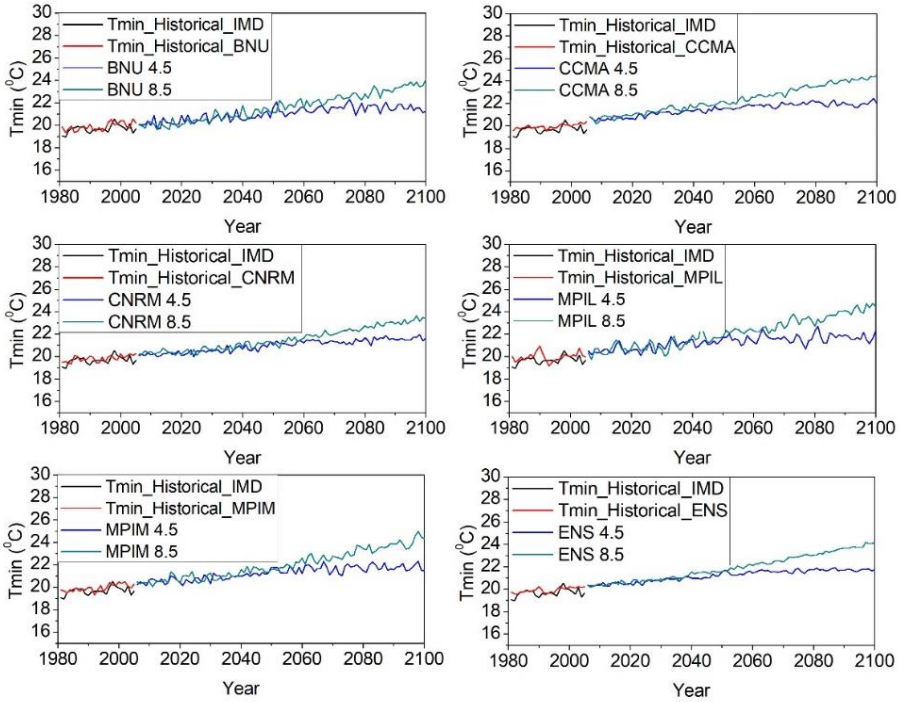

Fig. 5.16 Comparison of historical observed and GCMs simulated minimum temperature (1981 to 2005) and projection of future minimum temperature (2006 to 2100) of RCP 4.5 and RCP 8.5 emission scenarios (ENS- Ensembled) for GRB.

5.2.2 LULC Change Analysis from 1988 to 2100

The different temporal LULC maps for 1988, 1995, 2003 (historical), 2016 (present), 2030, 2050, 2075 and 2100 (future) are presented in Fig. 5.17 for ARB, Fig. 5.18 for VRB and Fig. 5.19 for GRB. The major assumptions considered in the prediction of LULC are (i) the Dyna Clue is a linear model, and hence it is assumed that the trend in LULC demand is also linear and (ii) the drivers are maintained as static variable and an average of the input is used for the prediction of LULC. The changes in various LULC types of the river basins are calculated and presented in Table 5.2. In the case of ARB the forest and barren were the most dominant land use in 1988 (87.43% collectively). The barren area decreased throughout the period. The wetland area is showing an increasing trend (0.81% to 7.53%) from 1988 to 2100. It could be due to the conversion of forests and barren into plantations and water bodies into wetlands. So, the sequence of transformation of land use is from forest to the plantation, water to wetlands and barren to the plantation. For VRB, forest and agriculture were the most prevalent land use in 1988 (85.59%). The barren area decreased throughout the period. The urban area is showing an increasing trend (0.01% to 0.54%) from 1988 to 2100. It could be due to the conversion of forests and barren into agriculture and urban areas. So, the sequence of conversion of land use is from forest and barren into agriculture and the urban regions. The results indicate that in the future, the expansion of plantations and wetlands in the ARB may lead to changes in the streamflow. On the other hand, the increase of plantation from 1988 to 2100 which are converted from forest land produces huge foliage and behaves like forested land use. Whereas in VRB, the increase of agriculture converted from forest land produces agricultural runoff that are known to be associated with higher transport of nutrient-rich sediments.

For GRB, the forest and agriculture were the most dominant land use in 1988 (80.48%). From 1988, the evergreen forest decreased and continued throughout though the % decrease was reduced. The agriculture area decreased throughout the period. The amount of plantation showed an increasing trend in 2003 but decreased by 2016 and then further a rising trend throughout the period (this may be due to the similarities in few crops and growing stages of plantation and related classification issues). The land used by forest, agriculture, and water are dynamically changed throughout the study

period (1988 to 2100). The urban area shows an increasing trend (1.70% to 24.25%) from 1988 to 2100. It could be due to the highest deforestation after 1988 and converted into plantation and urban. So, the sequence of land-use conversion is from forest to plantation, to agriculture to urban in GRB. The results indicate that the expansion of mainly plantation and urbanization in GRB leads to land degradation/ desertification in the future, significantly affecting the streamflow. On the other hand, the increase of urban and plantations together from 1988 to 2100 indicates that previous desertification may lead the local people to further farm/ plant trees to cope with the scarcity of fuel-wood and other uses. Soil stabilization, stopping wind and water erosion, and maintaining the soil nutrients cycle are the better appropriate ways to protect land deterioration and desertification in the GRB. The most affected LULC between 2050 to 2100 could be the forest and agriculture, which is likely to decrease. However, on the other hand, plantation and urban areas are supposed to increase simultaneously. The increase in plantations such as Coconut and Arracunut in coastal areas through a decrease in agriculture may be due to the availability of seawater for the plantation to cope with the water required for agriculture.

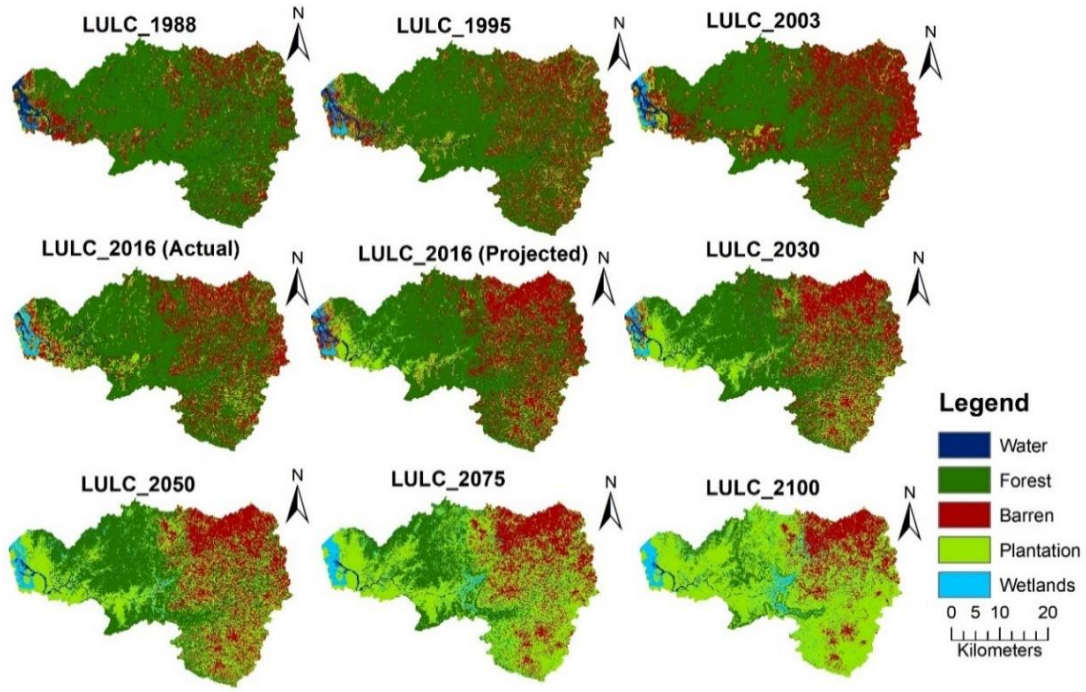

Fig. 5.17 LULC maps for 1988, 1995, 2003, 2016 (actual), 2016 (projected), 2030, 2050, 2075 and 2100 for ARB

Table 5.2 LULC changes analysis between 1988 to 2100

LULC Types	**ARB Area (% of the total area of 1333 km^2)**							
	1988	1995	2003	2016	2030	2050	2075	2100
Plantation	9.93	12.75	13.80	15.74	22.12	34.19	49.40	64.46
Barren	22.88	25.93	26.54	27.93	26.98	24.22	20.77	17.30
Forest	64.55	58.57	56.89	53.57	46.93	36.32	23.03	9.89
Wetlands	0.81	1.46	1.48	1.47	2.71	4.12	5.87	7.53
Water	1.83	1.29	1.29	1.29	1.26	1.15	0.93	0.81
LULC Types	**VRB Area (% of the total area of 813 km^2)**							
Agriculture	19.34	21.39	21.34	23.55	25.91	29.26	33.34	37.63
Barren	11.88	10.78	11.98	10.63	9.57	7.77	3.86	1.74
urban	0.01	0.03	0.03	0.05	0.20	0.29	0.44	0.54
Forest	64.25	63.67	62.49	61.78	60.66	59.36	59.36	57.51
Water	4.51	4.13	4.16	3.99	3.65	3.32	3.00	2.58
LULC Types	**GRB Area (% of the total area of 839 km^2)**							
Agriculture	42.80	40.01685	37.52	37.88	31.26	21.55	12.66	11.68
Forest	37.69	34.40872	33.03	29.53	20.86	17.26	12.08	11.21
Plantation	3.44	5.665367	9.82	6.97	14.07	16.54	21.43	21.65
Urban	1.70	1.88592	2.06	9.44	10.11	18.23	23.9	24.25
Water	5.15	4.069955	2.91	2.83	3.45	3.26	3.04	3.01
Barren	9.23	13.95319	14.66	13.35	20.25	23.16	26.89	28.20

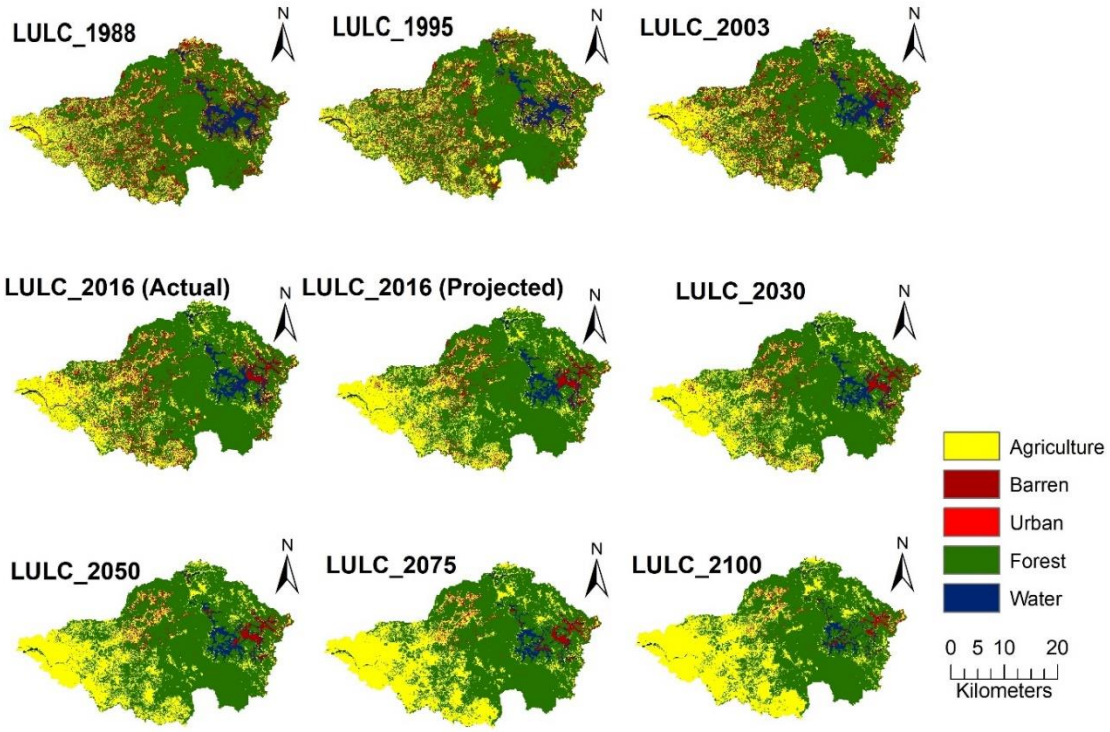

Fig. 5.18 LULC maps for 1988, 1995, 2003, 2016 (actual), 2016 (projected), 2030, 2050, 2075 and 2100 for VRB.

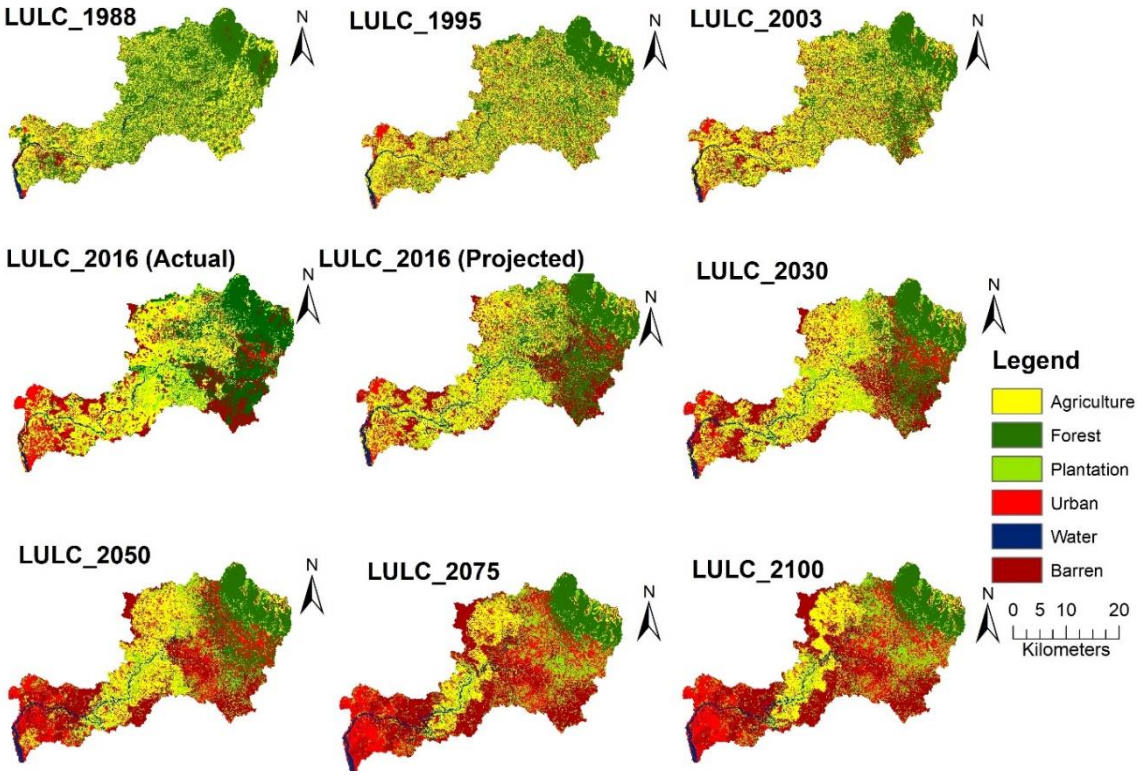

Fig. 5.19 LULC maps for 1988, 1995, 2003, 2016 (actual), 2016 (projected), 2030, 2050, 2075 and 2100 for GRB.

5.2.3 Calibration and Validation of the SWAT Model

The Soil and Water Assessment Tool (SWAT) is a physically-based semi-distributed model intended to compute and route water, sediments, and contaminants from the individual drainage units (sub-basins) to their outlets throughout the river basin (Sinha and Eldho 2018). The model calibration and validation goal are to improve the SWAT model's performance for streamflow on a monthly time scale. In the present study, it is hypothesised that there won't be significant change in the sensitive parameters with change in LULCs. Similar result was obtained by Sinha and Eldho (2018) in which they ccompared the fitted value of sensitive parameters in calibration for different LULC scenarios, which were found to be exactly similar. Therefore the three river basins were calibrated and validated using a single LULC map from 2003. ARB, VRB, and GRB have calibration periods of 1989-2003, 1986-2005, and 2006-2009, respectively, and validation periods of 2004-2010, 2006-2015, and 2010-2012. The model was run using the three-year warm-up period for the basins. The figure 5.20 shows the time series hydrograph of the monthly values of the discharge variation between observed and the simulated for calibration period of 15 years, i.e. 1989 to 2003 and validation period of 7 years (2004-2010) for ARB. The graph clearly indicatbes that the peak occurs each year during the monsoon period. The graph shows the variation of discharge during the considered time period. It can be noticed that, the SWAT model for calibration period underestimated the peak flow and for validation period SWAT model overestimated the peak flow for the year 2004, 2006 and 2009 (Fig 5.20). Overestimation may be attributed to the fact that, water percolates to the deep aquifer considered lost and is not included in the simulation process in SWAT. However, the SWAT model shows good performance in simulating monthly streamflow in the ARB with acceptable range of performance indices (Table 5.3).

The monthly discharge deviation between actual and simulated values for a 20-year calibration period, from 1986 to 2005, and a 10-year validation period (2006-2015) are depicted in the time series hydrograph in figure 5.21 for VRB. Here also the graph makes it abundantly evident that during the monsoon season, the peak happens annually. It can be noticed that, the SWAT model for calibration period underestimated the peak flow and for validation period SWAT model overestimated the peak flow (Fig

5.21). However, the SWAT model exhibits adequate range of performance indices and good performance in modelling monthly streamflow in the VRB (Table 5.3). The time series hydrograph in figure 5.22 for GRB shows the monthly discharge variation between actual and simulated values over a 4-year calibration period, from 2006 to 2009, and a 3-year validation period (2010-2012). As the data available for GRB was only for a short period, the calibration and validation period was divided as above said. In this case as well, the graph makes it plainly clear that the peak occurs every year during the monsoon season. The SWAT model underestimated peak flow during the calibration and validation period for GRB (Fig 5.22) and performed good in simulating the monthly streamflow.

Table 5.3 shows the values of statistical indicators for calibration and validation periods. According to Moriasi *et al*. 2007, the statistical metrics R^2 and NSE for streamflow are more than 0.75, and the PBIAS ranges within 20% for both calibration and validation, indicating satisfactory model performance (Table 5.3).

Table 5.3 The model performance during the calibration and validation

Items	ARB		VRB		GRB	
	Calibration (1989-2003)	Validation (2004-2010)	Calibration (1986-2005)	Validation (2006-2015)	Calibration (2006-2009)	Validation (2010-2012)
	Streamflow					
R^2	0.86	0.80	0.84	0.80	0.94	0.96
NSE	0.76	0.79	0.79	0.76	0.94	0.91
PBIAS	24.36	-4.83	9.36	15.89	2.94	-11.33

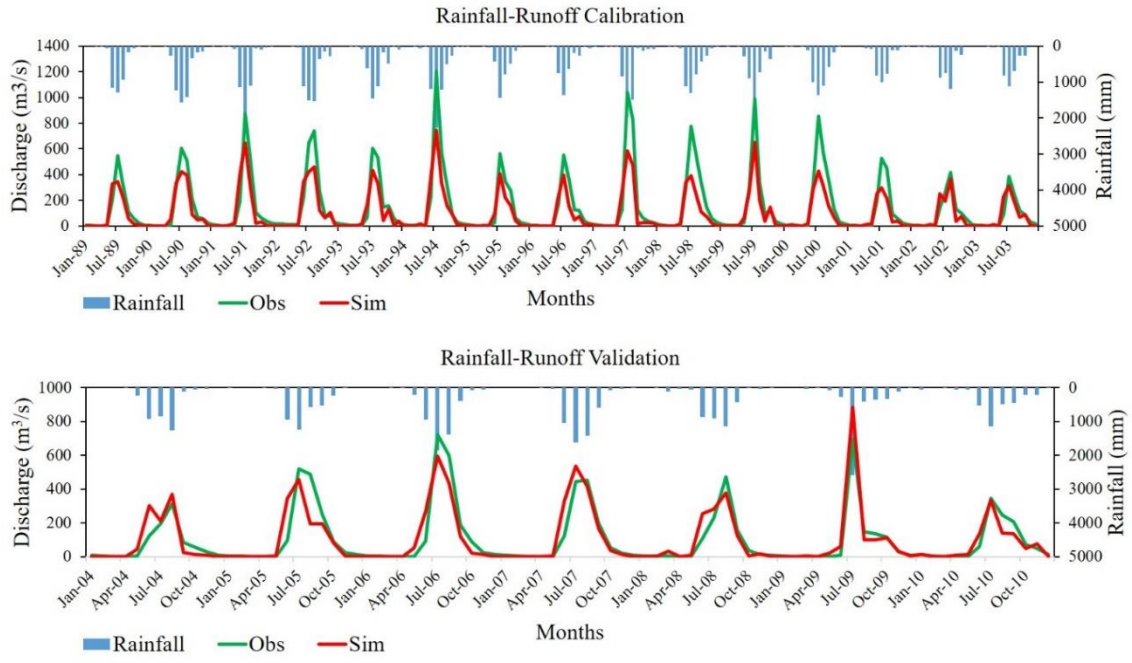

Fig. 5.20 Comparison between the observed and simulated monthly streamflow value for the calibration (a) and validation (b) for ARB

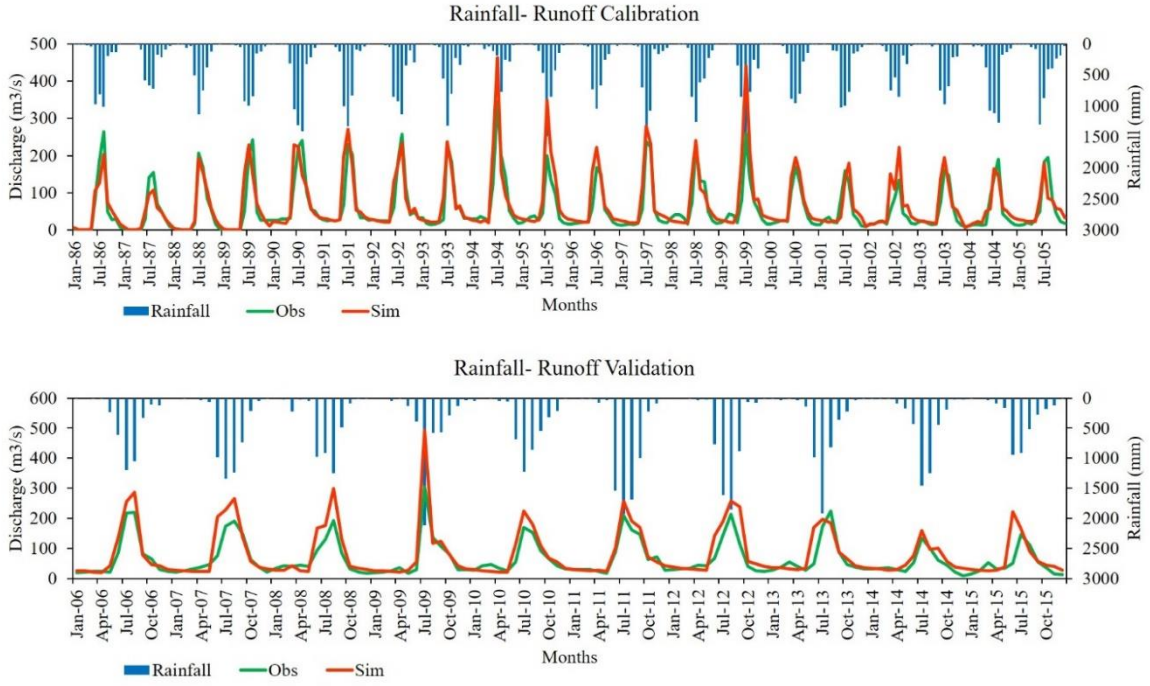

Fig. 5.21 Comparison between the observed and simulated monthly streamflow value for the calibration (a) and Validation (b) for VRB

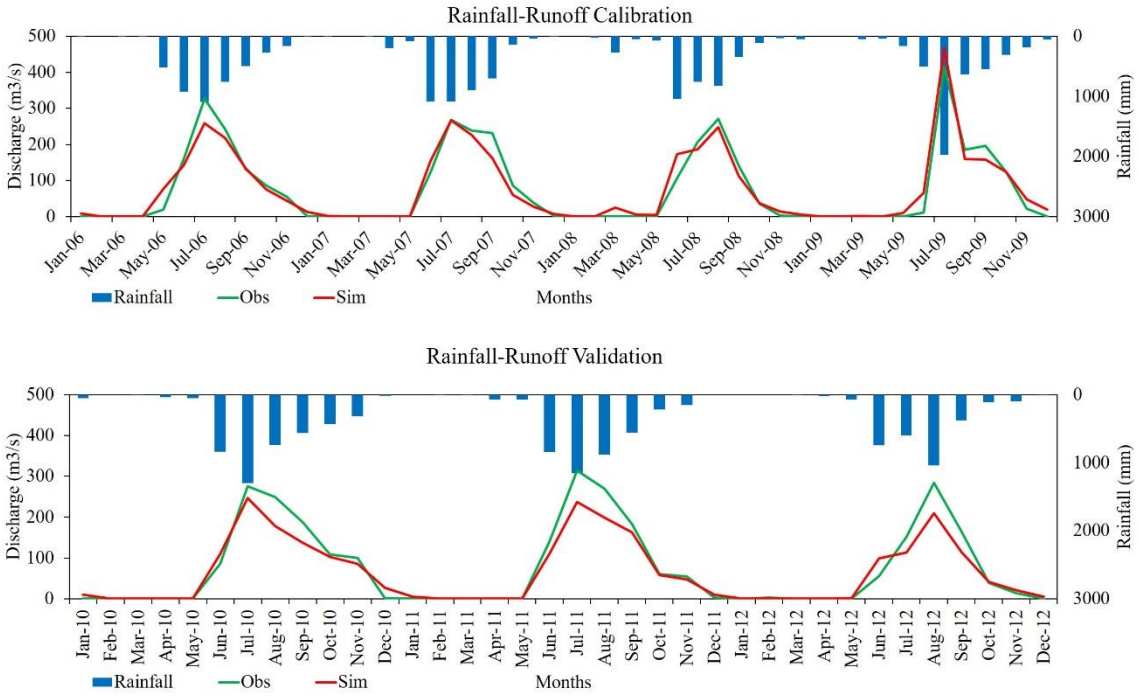

Fig. 5.22 Comparison between the observed and simulated monthly streamflow value for the calibration (a) and Validation (b) for GRB

5.2.4 Impacts of LULC changes on streamflow

As discussed earlier, it is vital to analyse the impacts of LULC changes by keeping the climate constant, to understand the hydrological effects of man-made LULC variations. In the ARB and VRB, the most substantial variations are noticed in the LULC classes for the forest and plantation, whereas in the GRB, it is seen for forest and agriculture. The effect of LULC changes on the ET and surface runoff is analyzed by considering the average climatology (including rainfall, temperature, solar radiations etc.) from 1981 to 2010. The spatial distribution of historical mean rainfall at sub-basin scale is presented in Fig. 5.23. It indicates high rainfall (more than 4000 mm) in the downstream of the basin, medium rainfall (2500 mm to 4000 mm) in the middle part and upstream of the basin while less rainfall (less than 2500 mm) in the south-east part of the ARB. The VRB indicates high rainfall (more than 4500 mm) distribution in downstream of the basin, medium rainfall (3500 mm to 4500 mm) in the middle part and less rainfall (less than 3500 mm) occurs in the areas around the medium rainfall. For GRB, it is with high rainfall (more than 4000 mm) distribution in the center of the basin, medium

rainfall (3700 mm to 4000 mm) in the upstream of the basin while less rainfall (less than 3700 mm) occurs in the downstream of the basin.

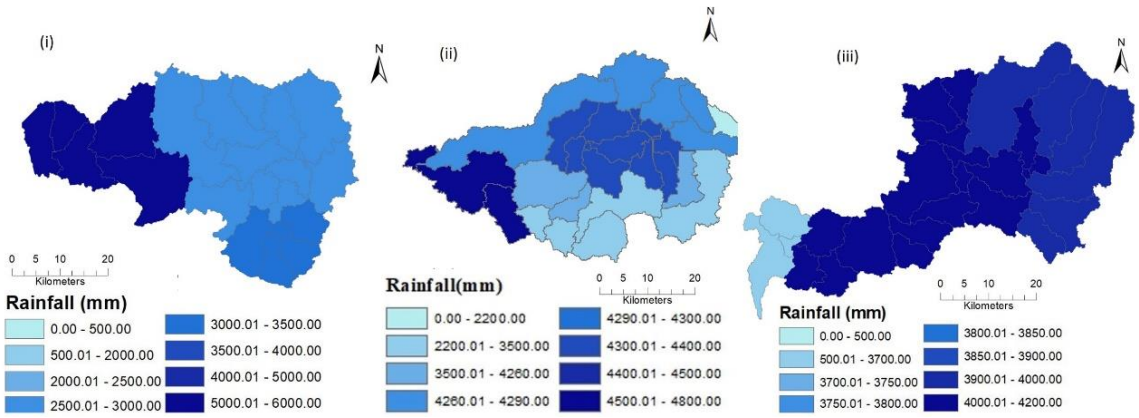

Fig: 5.23 Spatial distribution of historical mean rainfall at sub-basin scale used for simulation: (i) ARB, (ii) VRB, (iii) GRB.

Fig. 5.24 shows the comparison of the time series of runoff at the outlet for various LULC variations. It may be noted that the impacts on surface runoff are not significant as the LULC occurs gradually over substantial period time. Compared to ARB and VRB, the GRB exhibits slight variations in streamflow at the outlet. This may be due to expansion of urbanization over the basin.

The spatial distribution of surface runoff due to the LULC impacts on the historical and future are presented in Fig. 5.25 for ARB. The results show that, the change in surface runoff is very less in the historical and future period. This is mainly because the entire river basin is dominated by forest and plantations that exhibit the same vegetative characteristics with higher water percolation of water due to huge foliage (Ilstedt *et al.* 2016). Also, the increase in wetland compensated for the variation in inflow due to the deforestation. This makes the river basin pristine and resilient even though the forested area is converted into to plantation. The change in surface runoff in the historical period is with respect to the year 1988, whereas for future period it is with respect to the year 2016. It can be seen that in the historic period, surface runoff slightly increases from 1995 to 2016. Similarly in the case of future period also it is observed a slight increase in the streamflow (Fig 5.25).

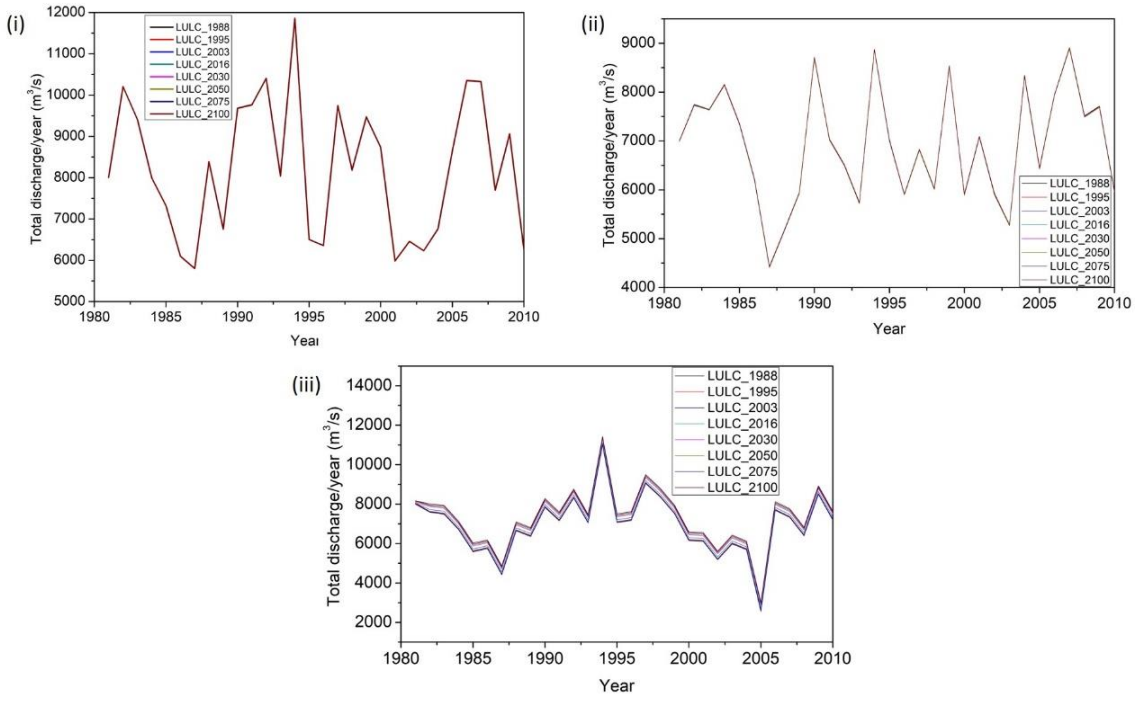

Fig. 5.24 Intercomparison of simulated streamflow at the watershed outlet for the LULC from 1988 to 2100: (i) ARB, (ii) VRB, (iii) GRB.

The LULC classification performed in this study is level 1 which considered all vegetation types except forest as agricultural land. It can be visualized that the streamflow variation over the T3 also exhibited a very minor change with respect to the baseline. The forest department has taken the initiative for development activity in this particular basin to convert all degraded land into either Acacia auriculiform or mixed forest which consumes more water and increases the percolation or groundwater recharge (Cover 1993). Large vegetated areas lead to greater water storage capacity of soil and thereby increase the increasing infiltration and groundwater recharge (Guevara-Escobar *et al.* 2007; Marhaento *et al.* 2018). This could be attributed to constant streamflow which makes it pristine. The decrease in surface runoff for historical period from 1988 to 1995, 1998-2003 and 2003-2016 are 0.002%, 0.023% and 0.002% respectively. Compared to the present LULC (2016), the average streamflow will be decreased by 0.017% by LULC 2030 and 0.01% by 2100. And decrement from 2016 to 2030 is by 0.017%, 2030 to 2050 by 0.0019%, 2050 to 2075 by 0.0017, and 2075 to 2100 by 0.01%. The maximum change in streamflow was found from 1988 to 2003 (0.02%) in historical and from 2016 to 2100 (0.01%) for the future.

Due to LULC change, the surface runoff will decrease in 2030, 2050, 2075, and 2100 by 0.017%, 0.018%, 0.02%, and 0.01% in comparison to baseline (2016) land use. The variation could be due to deforestation (mixed forest) and the conversion of other LULC into an unorganized plantation/ agriculture.

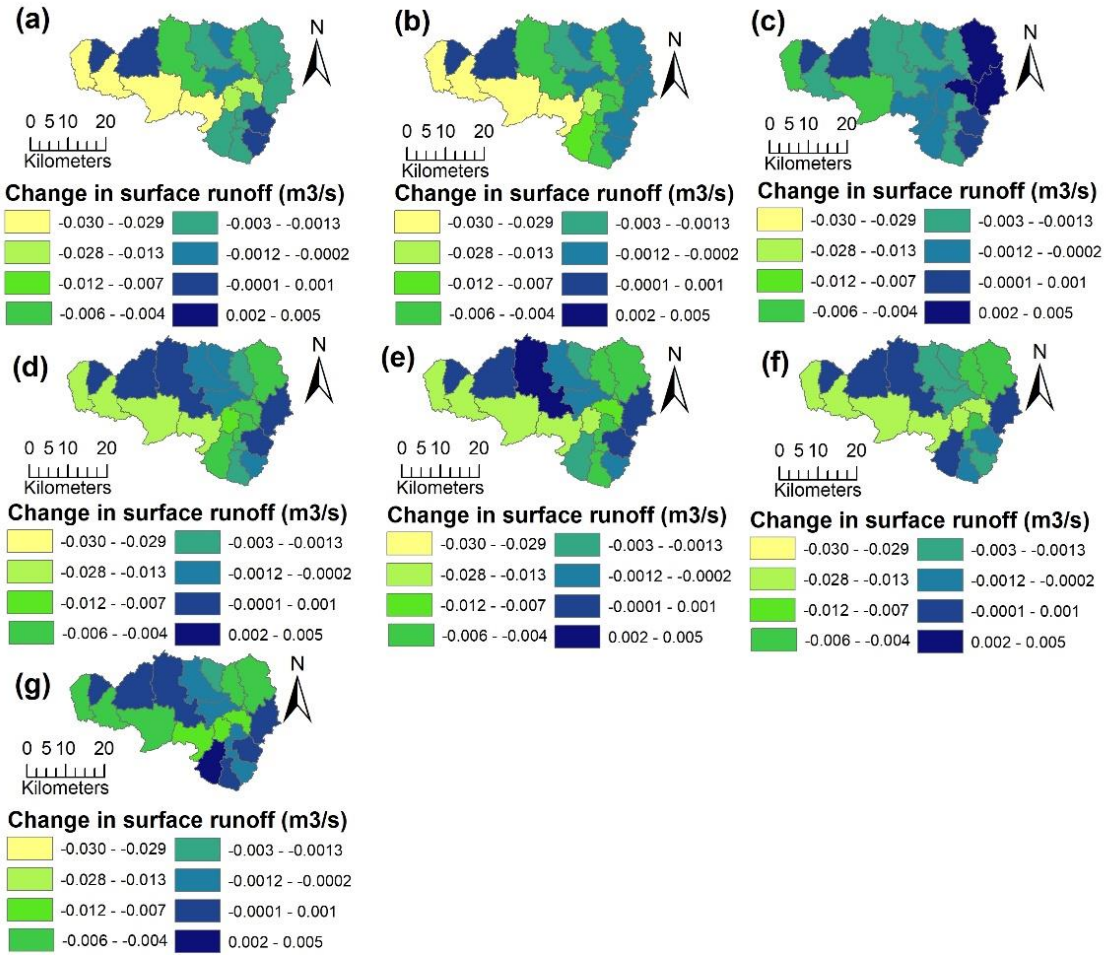

Fig. 5.25 Spatial distribution of change in the surface runoff (m3/s) for historical LULC 1988 to 2003 (a) 1988– 1995; (b) 1988– 2003; (c) 1988-2016; and for future (d) 2016 – 2030; (e) 2016 –2050; (f) 2016 – 2075; (g) 2016 – 2100 for the ARB.

The spatial distribution of surface runoff due to LULC impacts for historical and future are presented in Fig. 5.26 for VRB. The results show that, decrease in surface runoff for historical time period from 1988 to 1995 and till 2016 by 0.34%, from 1988 to 1995, 1995 to 2003 and 2003 to 2016 by 0.28%, 0.02% and 0.03%, and plausible increment from 2016 to 2030 by 0.09%, 2030 to 2050 by 0.03%, 2050 to 2075 by 0.16%, and 2075 to 2100 by 0.02% in comparison to LULC (2003). The maximum

change in streamflow was found from 1988 to 1995 (0.28%) in historical and from 2050 to 2075 (0.16%) for the future. The average streamflow will rise by 0.09% by LULC 2030 compared to the current LULC. However, the average annual streamflow increased by 0.318% from the current LULC (2016) to the projected LULC (2100) in the VRB. The variation in streamflow is more clearly observed in the lower part of the VRB (Fig 5.26) as more changes in LULC has occurred in the sub-basins these region.

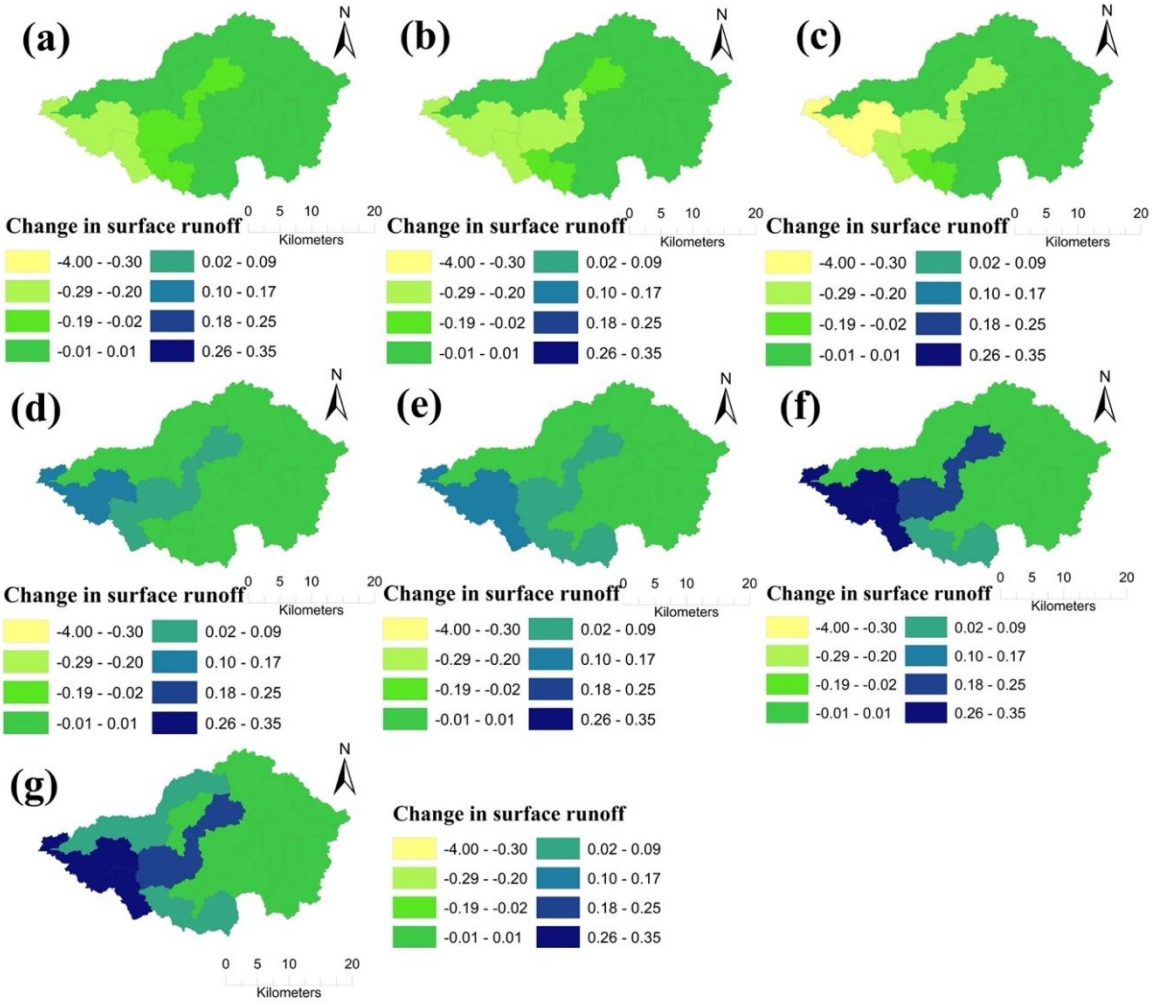

Fig. 5.26 Spatial distribution of change in the surface runoff (m3/s) for historical LULC 1988 to 2003 (a) 1988– 1995; (b) 1988– 2003; (c) 1988-2016; and for future (d) 2016 – 2030; (e) 2016 –2050; (f) 2016 – 2075; (g) 2016 – 2100 for the VRB.

The spatial distribution of surface runoff due to LULC impacts for historical and future are presented in Fig. 5.27 for GRB. Increase in surface runoff for historical time period from 1988 to 1995, 1998-2003 and 2003-2016 are 0.01%, 0.08% and 0.06% respectively. Compared to the present LULC (2016), the average streamflow will be increased by 0.06% by LULC 2030 and 0.14% by 2100. And increment from 2016 to 2030 is by 0.06%, 2030 to 2050 by 0.04%, 2050 to 2075 by 0.02, and 2075 to 2100 by 0.02%. The maximum change in streamflow was found from 1988 to 2003 (0.08%) in historical and from 2016 to 2030 (0.06%) for the future. Due to LULC change, the surface runoff will increase in 2030, 2050, 2075, and 2100 by 0.06%, 0.09%, 0.12%, and 0.14% in comparison to baseline (2016) land use. It could be due to deforestation (mixed forest) and the conversion of other LULC into an unorganized plantation/ agriculture. Furthermore, urban expansion may contribute to an increase in streamflow. Urban expansion is focussed in the downstream of the river basin in which the increased flow also is observed (Fig 5.27)

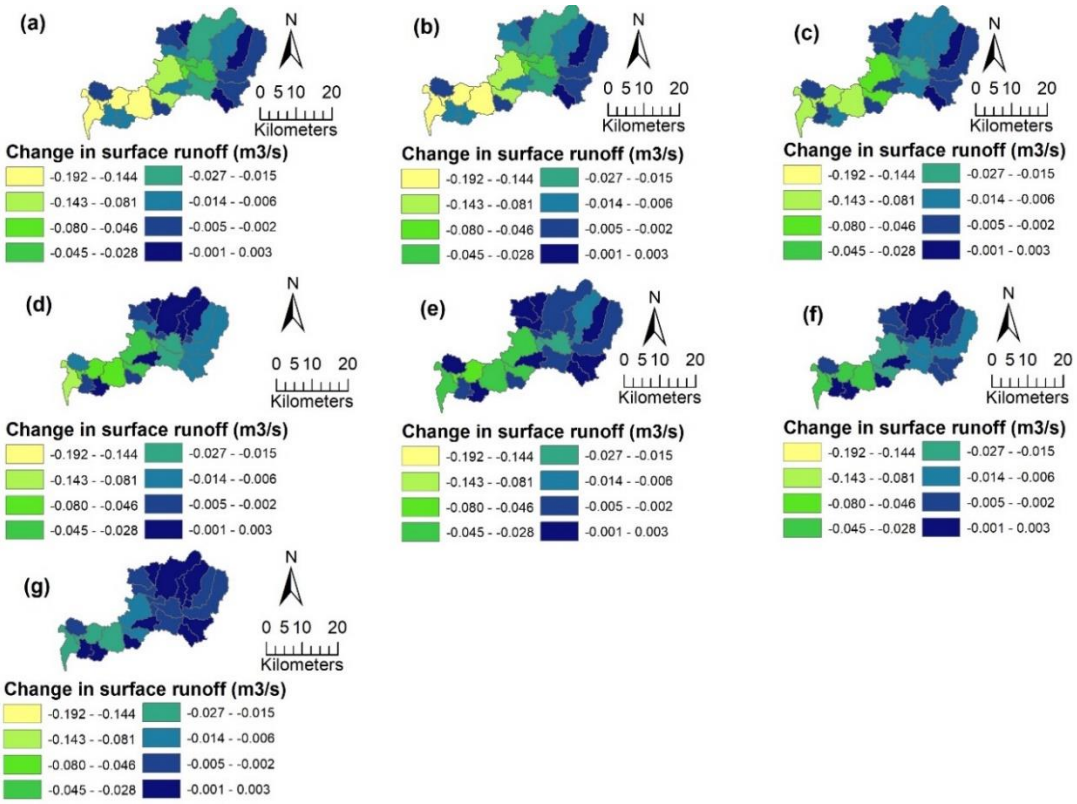

Fig. 5.27 Spatial distribution of change in the surface runoff (m3/s) for historical LULC (1988 to 2003 (a) 1988– 1995; (b) 1988– 2003; (c) 1988-2016; and for future (d) 2016 – 2030; (e) 2016 –2050; (f) 2016 – 2075; (g) 2016 – 2100 for the GRB.

Fig. 5.28, Fig 5.29 and Fig 5.30 show the variation in monthly, seasonally, and annual streamflow for the change in historical and future as per LULC changes for the river basins. It appears to be little change during the post-monsoon months such as September, October and November, and more in the pre-monsoon (summer) season (Fig. 5.28 a) for ARB and little change during monsoon months such as June, July, August, September, and more in the pre-monsoon season and post-monsoon season (Fig. 5.29 a) in VRB. Small changes during pre-monsoon months such as January, February, March and more in the monsoon and post-monsoon season (Fig. 5.30 a) are seen in GRB. However, it reveals that LULC changes have more significant impact on monthly, seasonal, and annual streamflow than on spatial distribution. In particular, in the pre-monsoon months such as January, February and March, streamflow is predicted to increase significantly except 2030 which reflects a decrease in flow for ARB and for VRB pre-monsoon months such as January, February and March, for future LULC such 2050, 2075, and 2100, streamflow is predicted to increase significantly. For GRB the post-monsoon months such as August to December, for all LULCs streamflow is predicted to decrease significantly and in monsoon months it is predicted to increase (Fig 5.30 a). The GRB exhibited increase in streamflow during summer and monsoon, and a decline in winter which contributed an annual decline in the streamflow (Fig 5.30 b)

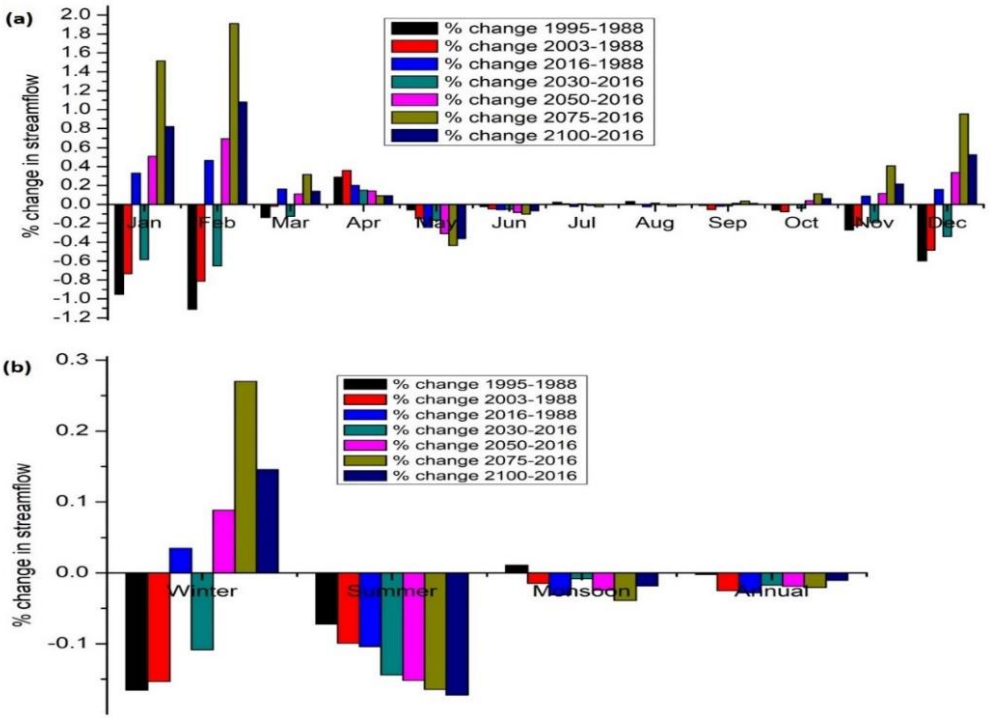

Fig. 5.28 Variation in streamflow owing to LULC change (a) mean monthly (b) mean seasonal and annual in the ARB.

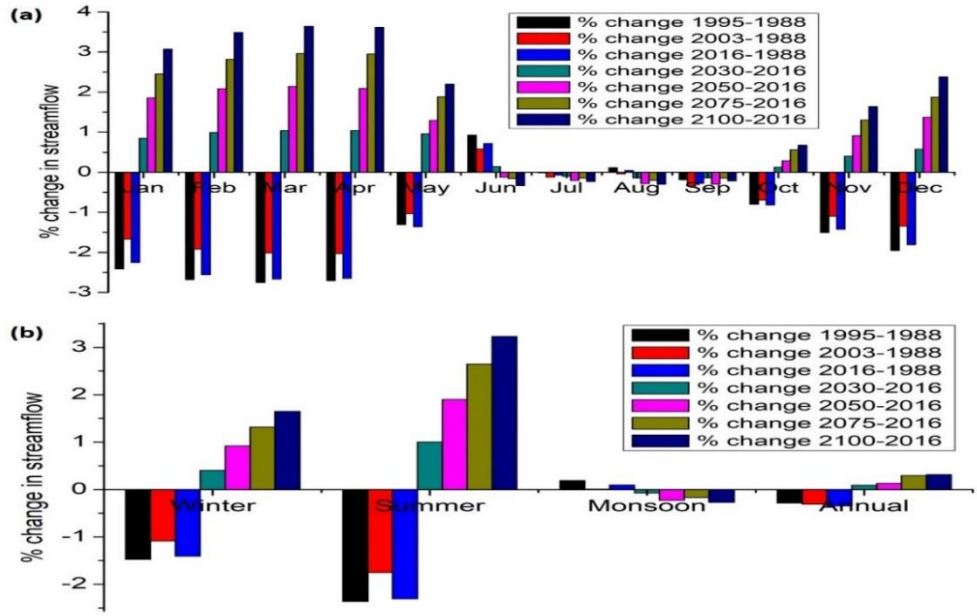

Fig. 5.29 Variation in streamflow owing to LULC change (a) mean monthly (b) mean seasonal and annual in the VRB.

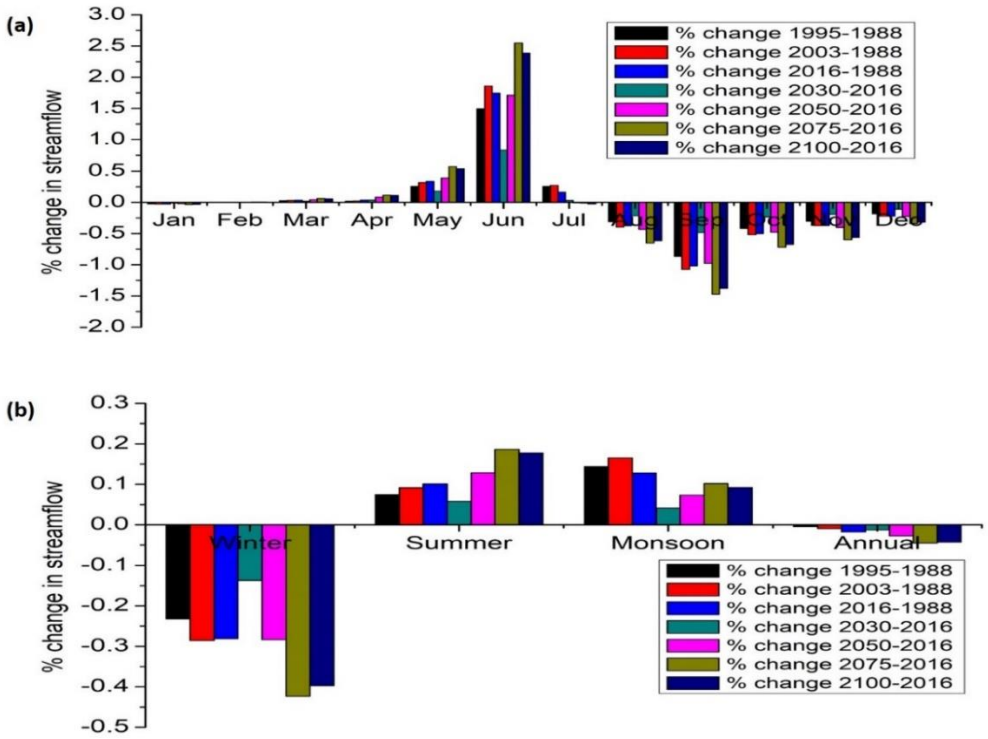

Fig. 5.30 Variation in streamflow owing to LULC change (a) mean monthly (b) mean seasonal and annual in the GRB.

As indicated in the findings, the seasonal and annual streamflows more clearly highlighted the unique impacts of both past and future LULC changes. The overall trend revealed a drop in historical and a rise in future ARB in the winter. The decline was predicted in the summer and the monsoon for future period. But winter and summer runoff shows more impact than during the monsoon. The VRB indicated a decrease in winter and summer for historical and an increase in the future and a decline in the monsoon for future period. But winter and summer show more impacts in comparison to monsoon. The GRB portrayed a decrease in winter for historical and future and an increase in the summer and monsoon for all time. But winter shows more impacts in comparison to summer and monsoon. The rise in average annual basin-scale surface runoff from 1988 to 2100 may be attributed mainly to the growth of agricultural and urban areas and the shrinkage of forests. Increased agricultural and urban development is generally linked with an increase in high flow, low flow decrease, more significant flow variability inflow (Dixon and Earls 2012; Kim *et al.* 2013). As impervious surface cover increases with urban expansion, impervious surface limits precipitation infiltration and increases runoff (Franczyk and Chang, 2009; Dixon and Earls, 2012).

5.2.5 Impact of climate change on streamflow

Simulations are performed to examine the effects of climate change on streamflow with LULC fixed for 2016 and the changing climate during the baseline period (1981 to 2010) and future periods (2011-2099). GCM results for future periods are divided into three-time slices for both emission scenarios (RCP 4.5 and 8.5) : T1 (2011-2040), T2 (2041-2070), and T3 (2071-2099). The SWAT was run using five downscaled, bias-corrected GCM ensemble outputs (RCP 4.5 and 8.5) to quantify the change in streamflow. The simulation results were compared to simulated results from the baseline period (1981 to 2010). The simulation results are referred to as Qclim from here on out.

Fig. 5.31, Fig 5.32, and Fig 5.33 depict the actual mean precipitation of all five GCMs ensembled for T1, T2 and T3 of RCP scenarios for ARB, VRB and GRB respectively. Rainfall will be more in downstream areas and less in upstream areas in ARB. The rainfall varies between 2000 to 5000 mm among the sub-basins level in the ARB but showed a slight increase compared to historical rainfall. More rainfall is received in the downstream of the river basin (Fig 5.31) in all scenarios for ARB. The amount of rainfall is increasing as it moves from T1 to T3 in RCP 4.5. Similarly an increase in rainfall is observed in the case of RCP 8.5 (Fig 5.31). In VRB, rainfall will be more in downstream areas and less in upstream regions and varies between mostly 2500 to 5400 mm among the sub-basins (Fig 5.32). The northern region of the catchment receives more rainfall than southern region of the basin. Both RCP 4.5 and RCP 8.5 depicts similar trend in the rainfall for VRB (Fig 5.32). In the case of GRB, the rainfall varied between 3000 to 5000 mm and showed a slight increase compared to historical rainfall (Fig 5.33). In the case of GRB the maximum rainfall is received in the middle part of the river basin (Fig 5.33). As the time slices move from T1 to T3, the amount of rainfall is observed to be increase in the GRB. Using these rainfall projections and other climatological paramaters such as temperature, solar radiation etc., the SWAT model was run for various scenarios and the results are presented here.

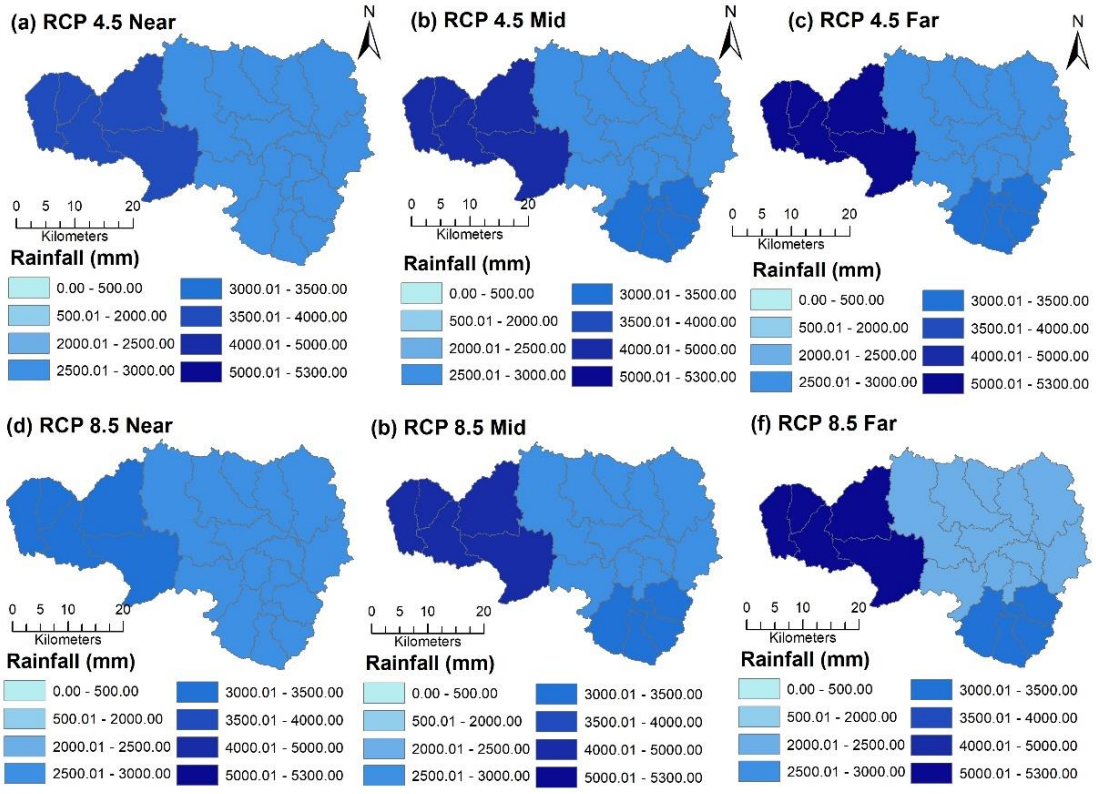

Fig: 5.31 Actual rainfall distribution in ARB for different scenarios

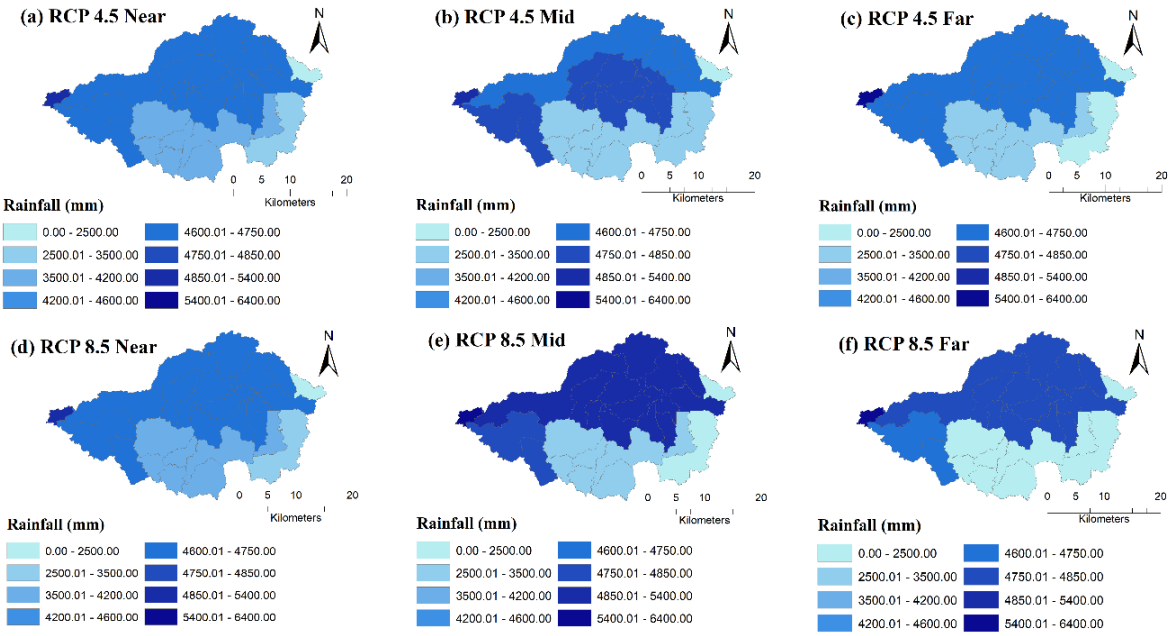

Fig: 5.32 Actual rainfall distribution in VRB for different scenarios

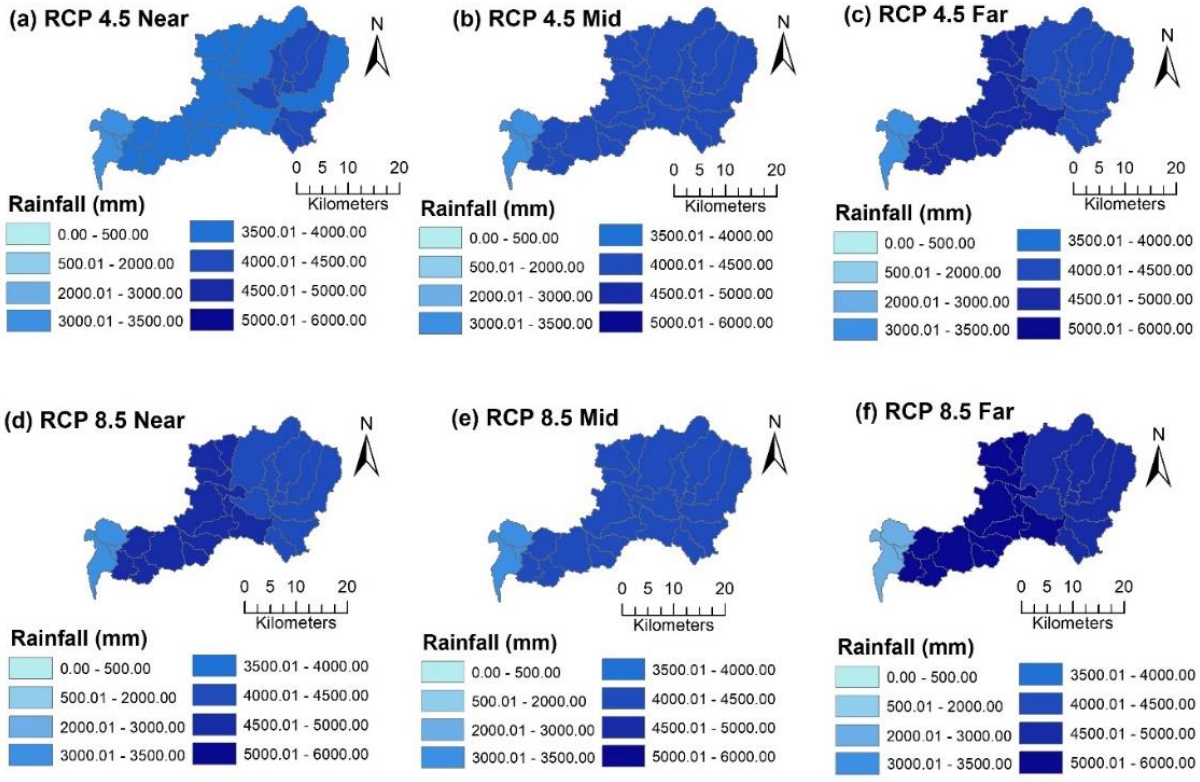

Fig: 5.33 Actual rainfall distribution in GRB for different scenarios

Fig. 5.34 depicts the simulated time series of runoff at the basin outlet for different scenarios and Fig. 5.35 portrays the intercomparison of runoff. It can be observed an increase in flow during T1, T2 and T3 of RCP 4.5 scenarios for ARB (Fig. 5.34i), whereas the flow decline in T1 and T3 for RCP 8.5 scenario with an increase in T2 8.5 scenario for ARB. In the case of VRB, annual discharge declines in all scenarios (Fig. 5.34ii). RCP 4.5 and RCP 8.5 scenarios for GRB show an increase in flow during T1, T2, and T3 except a decline in T3 of RCP 8.5 (Fig. 5.34iii).

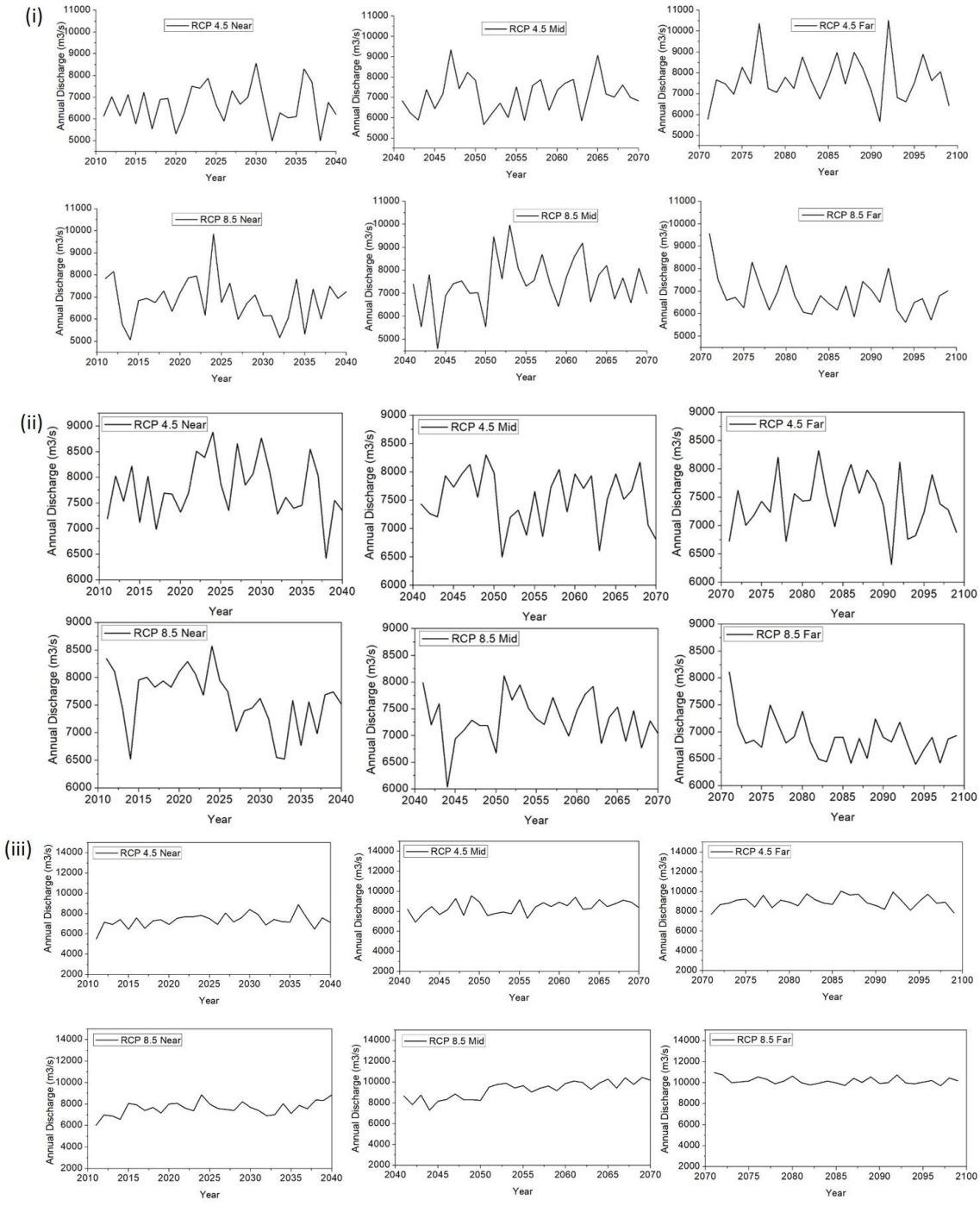

Fig. 5.34 Simulated runoff at the watershed outlet for various scenarios: (i) ARB, (ii) VRB, (iii) GRB

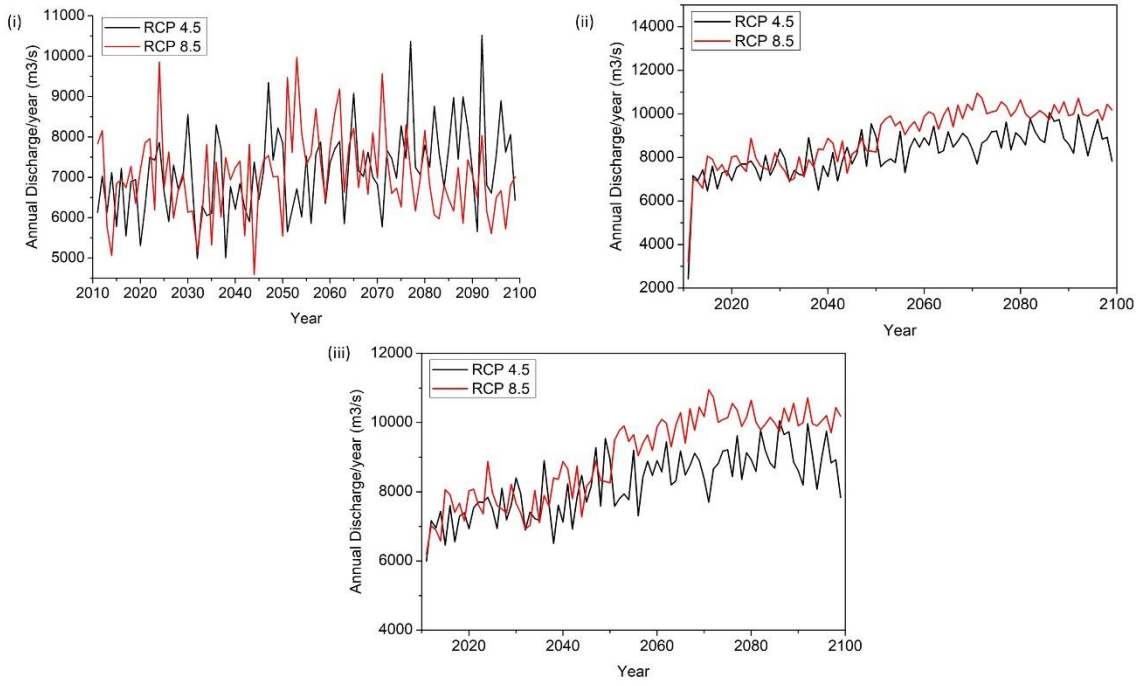

Fig. 5.35 Comparison of simulated runoff at the watershed outlet of RCP scenarios for 2010 to 2100 of (i) ARB, (ii) VRB, (iii) GRB.

The simulated Qclim (change in surface runoff due to CC) for the future period under both scenarios were compared to the corresponding values of all sub-basins from the baseline period (1981 to 2010), as given in Fig. 5.36 for ARB, Fig 5.37 for VRB and Fig 5.38 for GRB. It can be observed that change in annual Qclim for all the scenarios is moderate to extremely substantial for the future periods. In general, Qclim was predicted to increase in most subbasins while moving from T1 to T3 future mainly T1 to the main channel for ARB and GRB whereas in VRB it predicted to decrease in most subbasins while moving from T1 to T3 future mainly upstream.

In particular for ARB, the Qclim decreased from the baseline period by 19.09%, 13.35%, and 6.37% in RCP 4.5 from T1, T2, and T3 period respectively.In the case of RCP 8.5 there is an decrease in Qclim by 16.46% for T1 and decrease by 9.29% and 16.78% for T2 and T3 respectively (Fig. 5.36). For VRB, the Qclim increased from the baseline period by 12.7%, 9%, and 7.09% in RCP 4.5 from T1, T2, and T3 period respectively. Qclim increased from the baseline period by 10.01% and 5.81% in RCP 8.5 in T1 and T2 time scale and decreased by 0.27% in T3 time scale (Fig. 5.37). In the

case of GRB (Fig. 5.38), the Qclim increased from the baseline period by 6.11%, 23.24%, and 31.19% in RCP 4.5 from T1, T2, and T3 periods respectively. Under RCP 8.5 there is an rise in Qclim by 10.32% for T1, 35.77% for T2 and 49.18% for T3 respectively. In compared to the baseline period, Qclim's overall increases in all RCPs scenarios and all three-time slices suggested the necessity for involvement in water resource management.

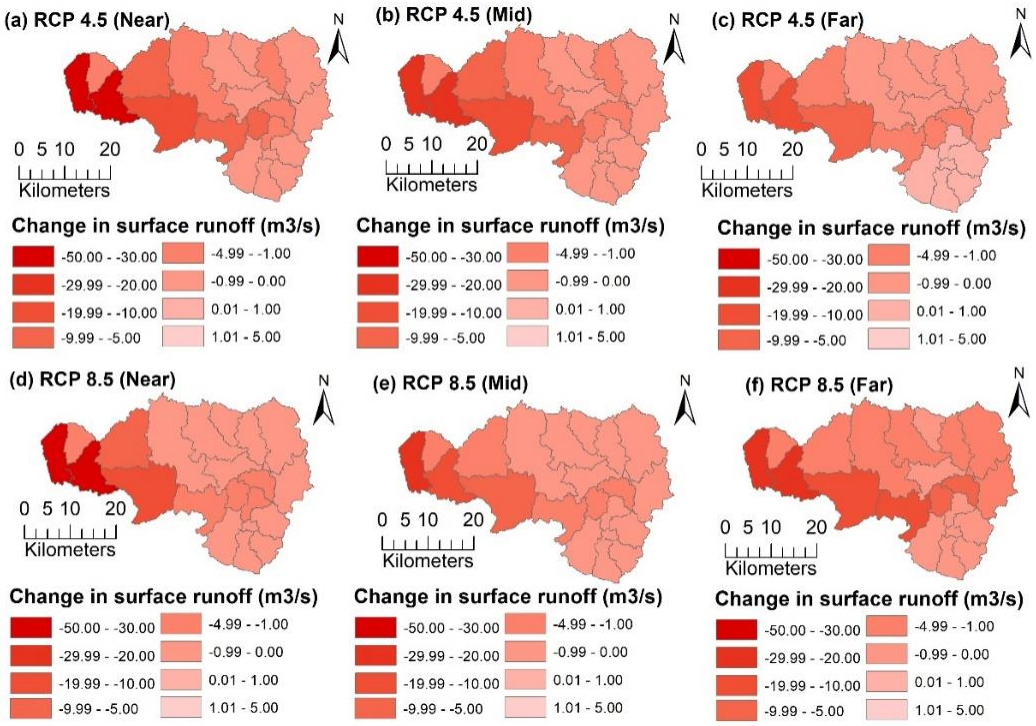

Fig. 5.36 Change in surface runoff for different scenarios in the ARB.

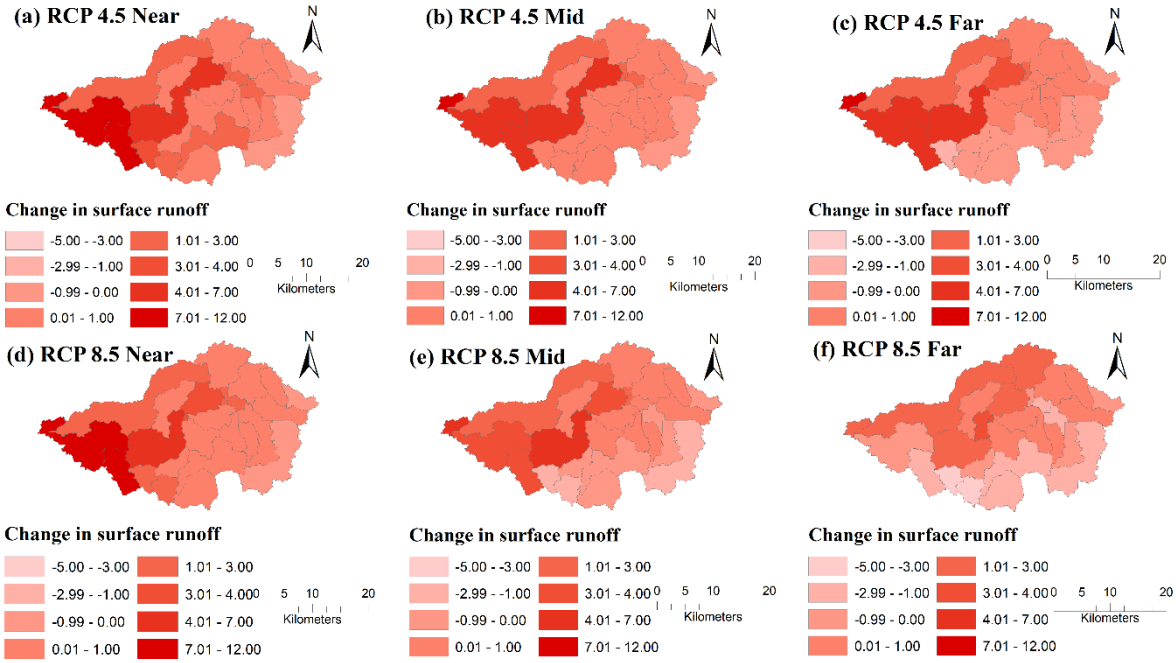

Fig. 5.37 Change in surface runoff for different scenarios in the VRB.

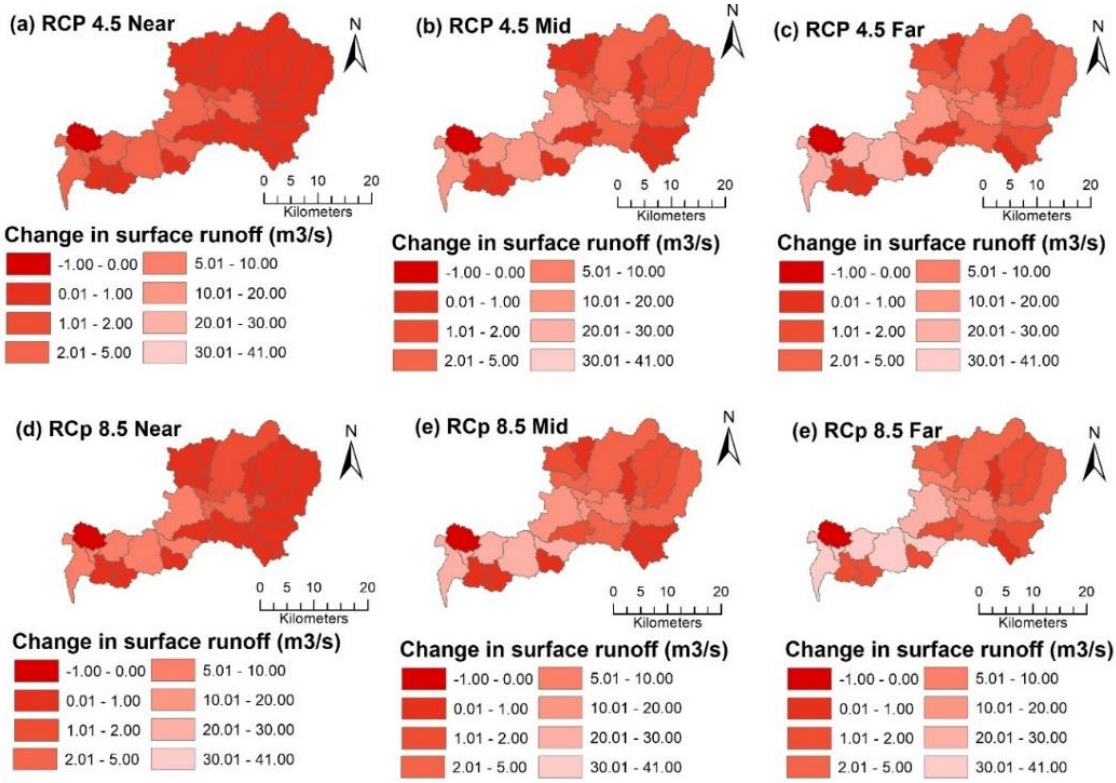

Fig. 5.38 Change in surface runoff for different scenarios in the GRB.

The increase in rainfall during the summer season induces the need for the study of seasonal variations of water resources in a basin for all future climate change studies. The seasonal flow reflects the effects of climate change more clearly than the other duration basis. The findings showed different seasonal climate patterns, with increased summer, monsoon and winter precipitation in future periods. The changes in monthly, seasonal, and annual streamflow are presented in Fig. 5.39 (ARB); Fig 5.40 (VRB); Fig 5.41 (GRB), due to climate change for the future period. There appeared to be a decrease in streamflow in May, June, July, August and October and an increase in streamflow for the other months (Fig. 5.39 a) in all scenarios under both emission scenarios for ARB. Fig. 5.39 b represents seasonal change and confirms more clearly change in the streamflow owing to climate change in the future. In compared to the baseline period, it clearly shows an increasing tendency in winter, summer, and monsoon season and a declining trend in winter and monsoon season in all T1 time slices for all RCP 8.5 scenarios.. Sinha *et al*., (2020) reported that streamflow is generally more sensitive towards precipitation change and temperature change. The increasing annual Qclim could be due to increasing precipitation in ARB. Because of the climate in the study area, the southwest monsoon significantly may decline (Krishnakumar *et al.* 2009), which has features of an altered marine climate and experiences a wet monsoon and dry, warm summer. The above results showed different annual Qclim patterns in all RCP scenarios because precipitation was reduced in the future period as compared to the baseline period in ARB.

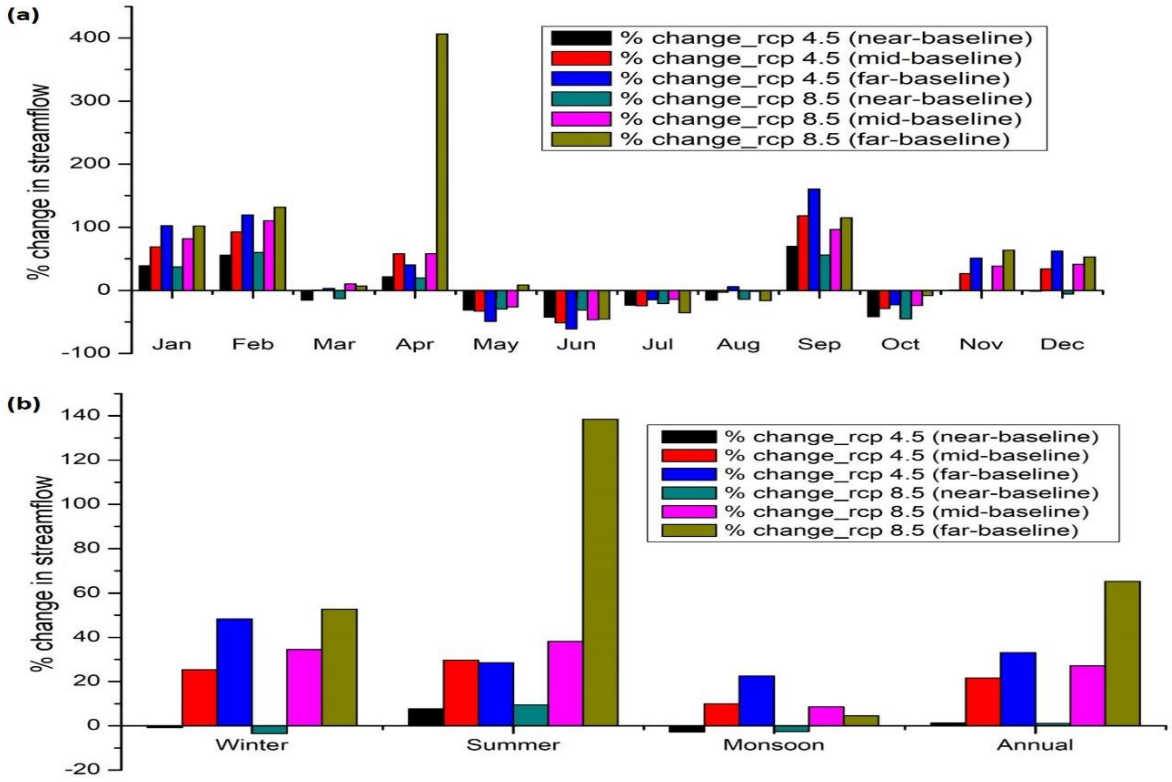

Fig. 5.39 Variation in streamflow owing to CC (a) mean monthly (b) mean seasonal and annual in the ARB.

The VRB portrayed a decrease in streamflow in June, July and an increase in streamflow for the other months (Fig. 5.40 a) in all scenarios under both emission scenarios except a decrease in August month during the T3 of RCP 8.5 emission scenario. Fig. 5.40 b clearly showing an increasing trend in winter, summer and monsoon season in all the time slices for both scenarios in comparison to the baseline period except a decrease in monsoon during T3 of RCP 8.5 emission scenario. The increasing annual Qclim could be due to increasing precipitation in VRB. The above results showed different annual Qclim patterns in all three-time slices because precipitation has increased in the future period as compared to the baseline period in VRB.

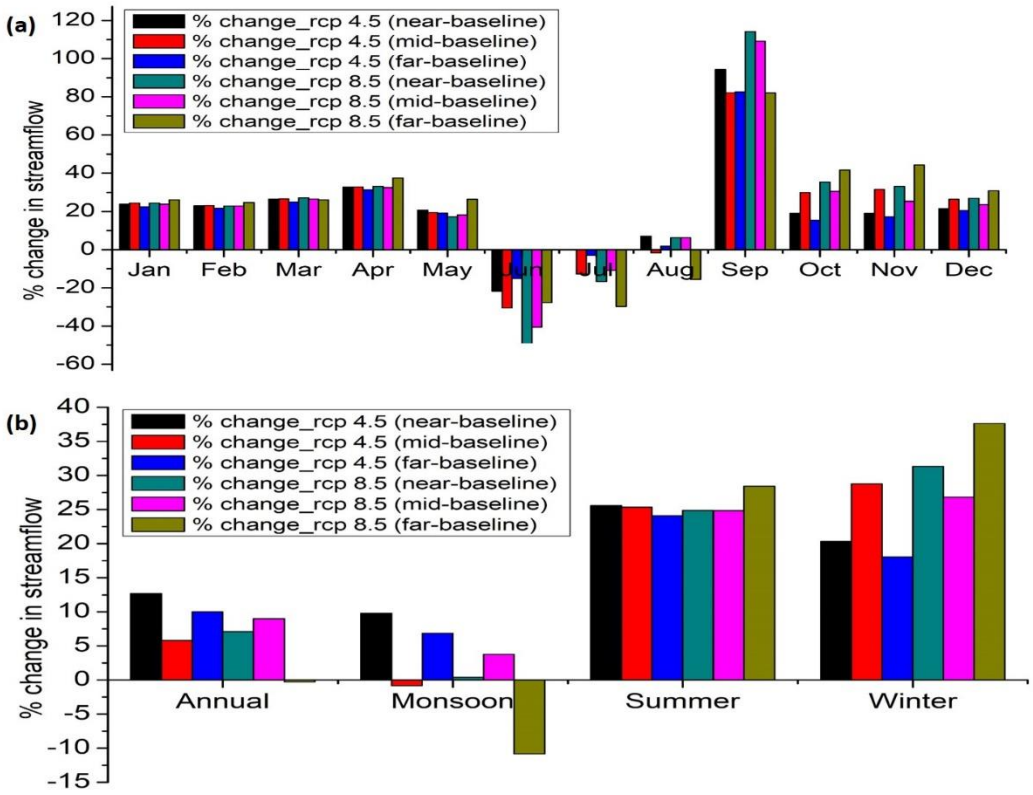

Fig. 5.40 Variation in streamflow owing to CC (a) mean monthly (b) mean seasonal and annual in the VRB.

A considerable increase in streamflow in January and February, with a slight increase from September to December (Fig. 5.41 a) in all scenarios is observed in GRB. A slight decline during March with negligible changes in the monsoon months can be observed. Seasonal change shows an increasing trend in winter and monsoon seasons in all the time slices for both scenarios compared to the baseline period (Fig 5.41 b). There is a decline in the summer season of T1 future in the case of both RCP emission scenarios. The increasing annual Qclim could be due to increased precipitation in GRB. The above results showed different annual Qclim patterns in RCP 4.5 and 8.5 in all three-time slices because rainfall increased in the future period compared to the baseline period in GRB. Besides, Qclim in this region is closely related to ecosystem health. A new strategy for water resource management is required, one that considers future climate change and the risk of decreased streamflow.

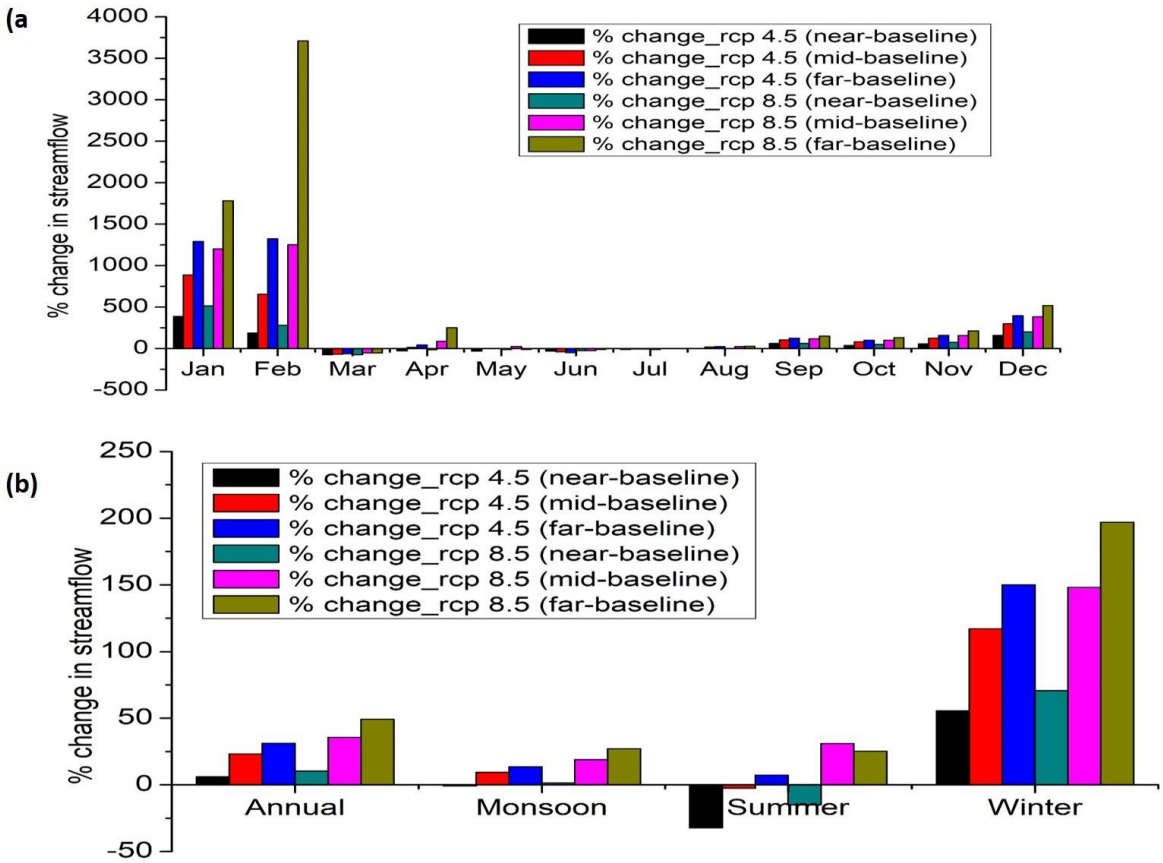

Fig. 5.41 Variation in streamflow owing to CC (a) mean monthly (b) mean seasonal and annual in the GRB.

5.2.6 Combined impacts of LULC and climate change on streamflow

In the earlier sections, the impacts of LULC variation alone with constant climate parameters and then constant LULC and varying climate parameters are found. These two cases enable us to understand the impacts of LULC and climate on hydrology. However, in the actual situation in the river basin, change is happening in LULC and climate. This occurs simultaneously, and both impacts are found in hydrological variables such as streamflow and ET. In this study, to carry out the analysis of both LULC and climate change, three different scenarios have been set up: (i) near (2011-2040) – baseline (T1); (ii) mid (2041-2070) – baseline (T2); and (iii) far (2071-2100) – baseline (T3). The baseline as climate 1981-2010 by using 2016 LULC (near to present) and for the future period, it is near, mid and far scenarios are considered like the climate of 2011-2040 by using 2030 LULC (for the T1 scenario), climate 2041- 2070 by using

2050 LULC (for the T2 scenario), climate 2071-2100 by using 2075 LULC (for T3 scenario) have been developed. The spatial distribution of rainfall considered is presented in the Fig. 5.42 for ARB and found very similar trend of historical rainfall at sub-basin scale. Still, it showed an increasing trend in all scenarios. It is seen that downstream rainfall will be more in comparison to the mid part of the basin and upstream.

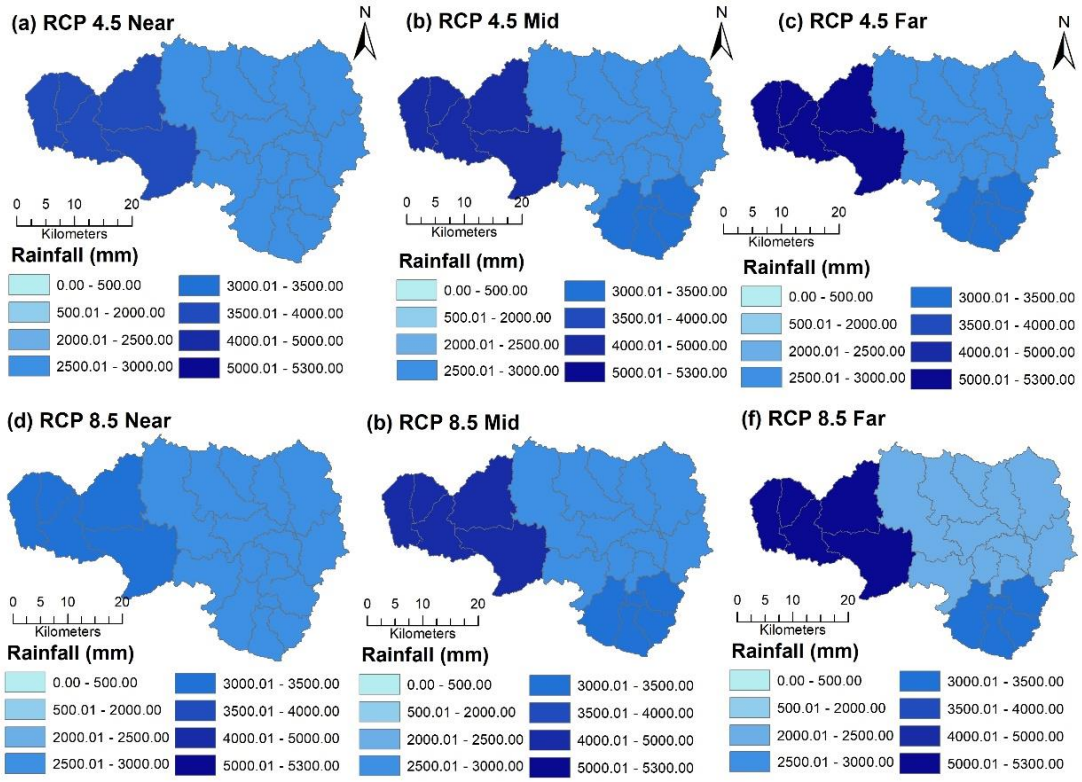

Fig. 5.42 Spatial distribution of rainfall of RCP emission scenarios for ARB.

Fig. 5.43 represents the spatial distribution of rainfall of VRB and found very similar trend of historical rainfall at the sub-basin scale with an increasing trend in all scenarios. It is seen that rainfall will be more in North West regions in the basin than other areas.

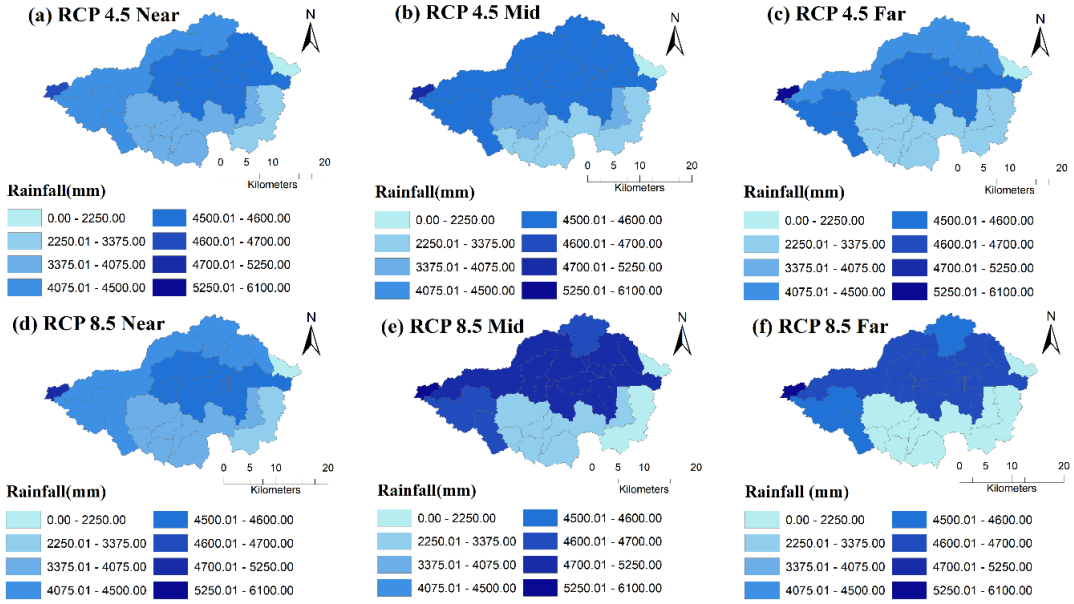

Fig. 5.43 Spatial distribution of rainfall of RCP emission scenarios for VRB.

The spatial distribution of rainfall for GRB is presented in the Fig. 5.44 and found very similar trend of historical rainfall at the sub-basin scale. Still, it showed an increasing trend in all-time slices for both RCP scenarios. It is seen that in the middle part of the basin, rainfall will be more in comparison to downstream of the basin and upstream.

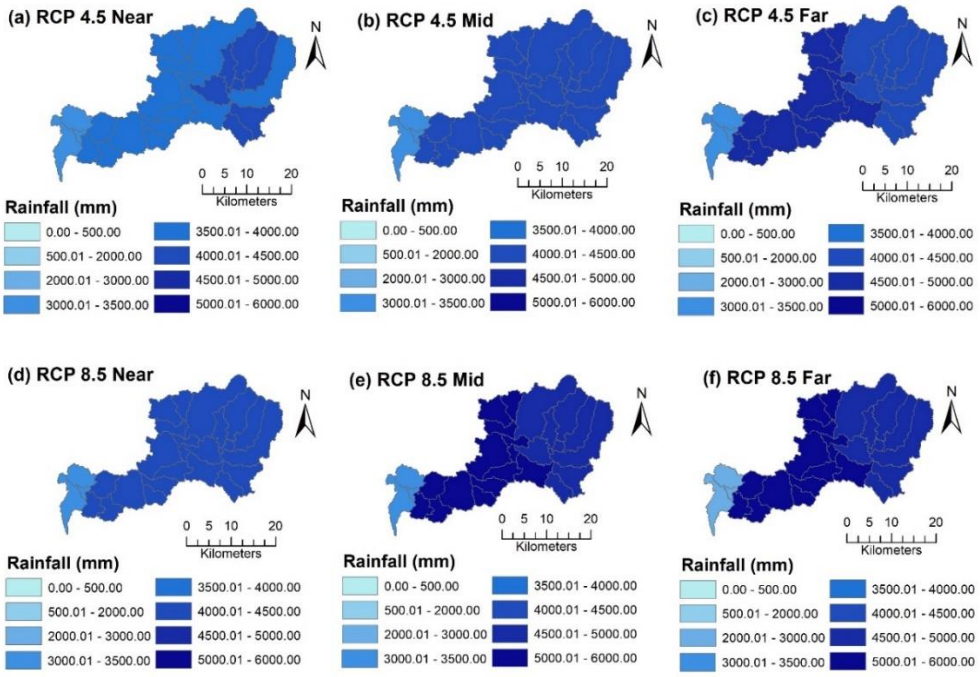

Fig. 5.44 Spatial distribution of rainfall of RCP emission scenarios for GRB.

The spatial distribution of ET is presented in Fig. 5.45 at the sub-basin scale for both RCPs scenarios for ARB. The Figure shows more ET in the coastal areas (downstream) and less in the upstream and southeast parts of the basin. Fig. 5.46 represents the spatial distribution of ET for VRB. The Figure shows more ET in the areas adjacent to the reservoir and less in the downstream areas. Whereas Fig. 5.47 exhibits more ET in the coastal areas (downstream) and less in the upstream and southeast parts of the basin for GRB.

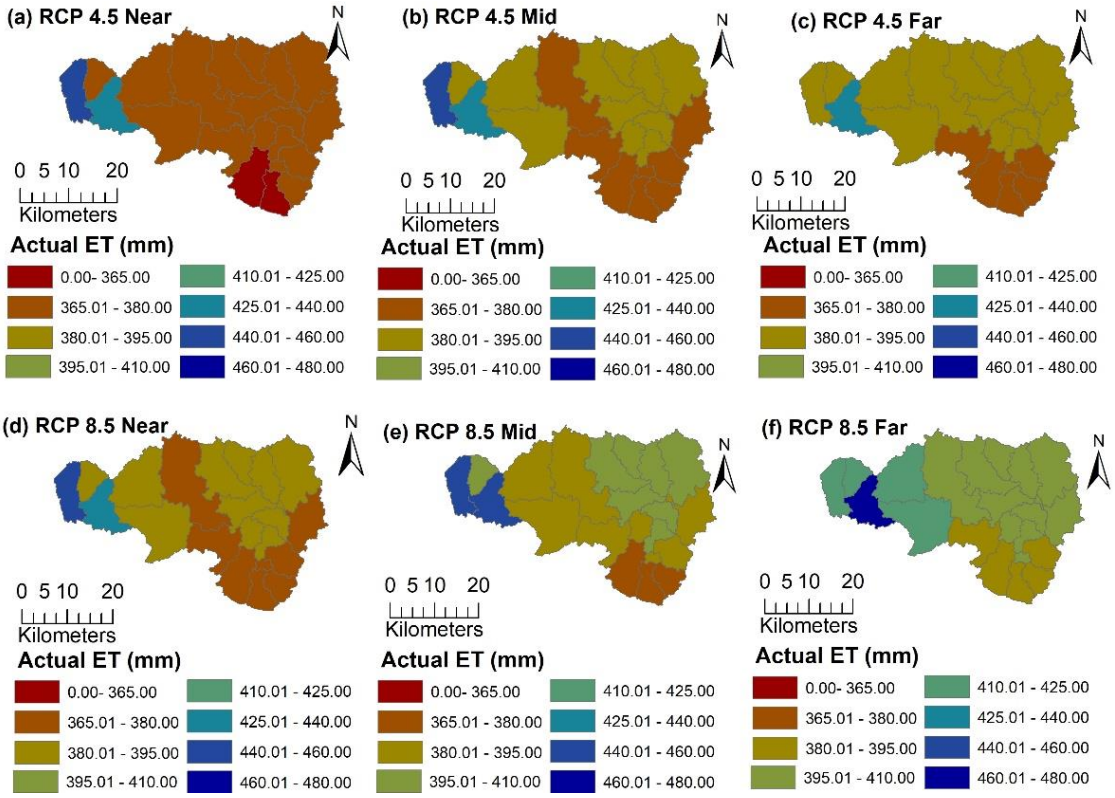

Fig. 5.45 Spatial distribution of actual ET for RCP emission scenarios in ARB.

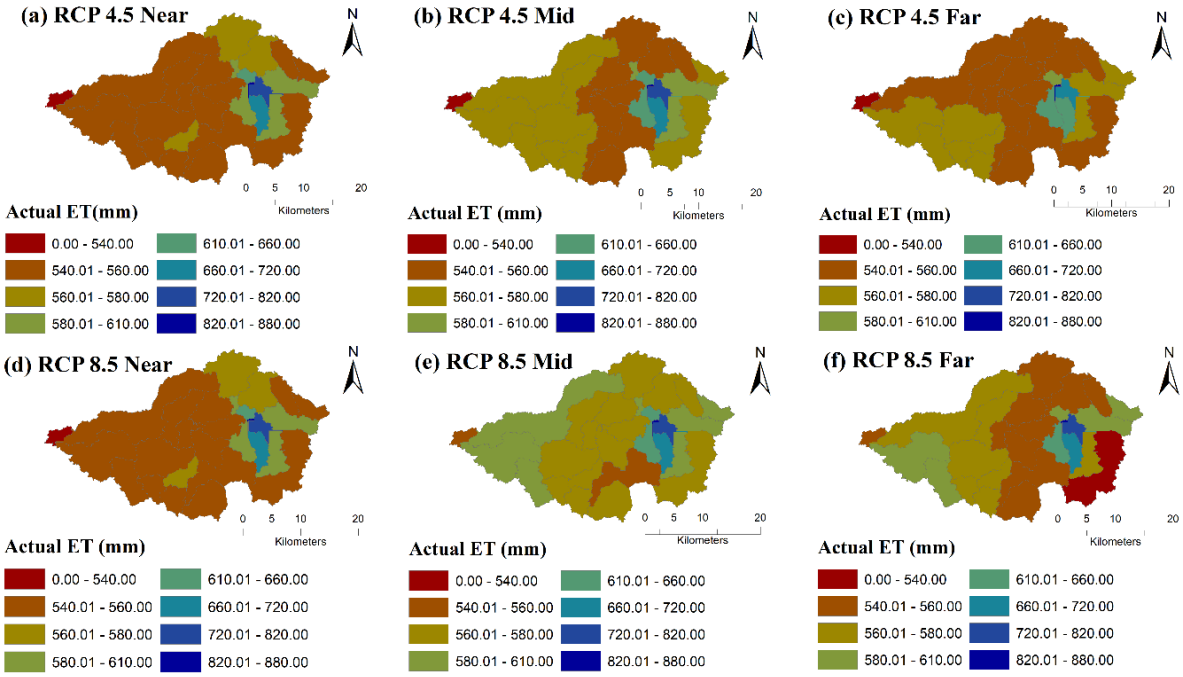

Fig. 5.46 Spatial distribution of actual ET for RCP emission scenarios in VRB.

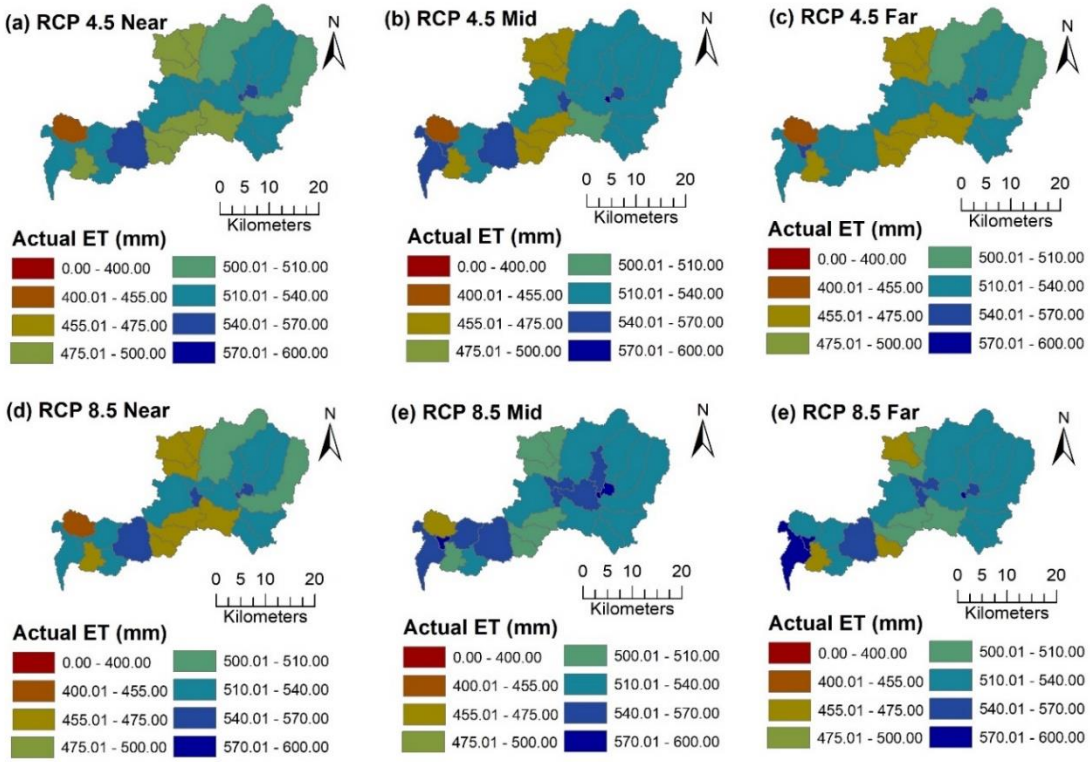

Fig. 5.47 Spatial distribution of actual ET for RCP emission scenarios in GRB.

Fig. 5.48 for ARB shows the regional patterns of change in surface runoff from baseline to future for RCP scenarios at the sub-basin scale. Results from the surface runoff suggest that the combined impacts showing a decreasing trend in T1, T2 and T3 scenarios of RCP 4.5 by 18.91%, 13.32% and 6.28% respectively compared with baseline. In the case of RCP 8.5, a decreasing trend was also predicted by 16.61% in the T1 and by 9.19%, 16.70% in the T2 and T3, respectively. This is because of the high variation in precipitation in the respective scenarios. From Fig. 5.48, it can be seen that most sub-basins show a decreasing trend of surface runoff in the future compared with the baseline, whereas as the time period moves to the T3, the decreasing trend reduces ARB which resembles with the precipitation pattern.

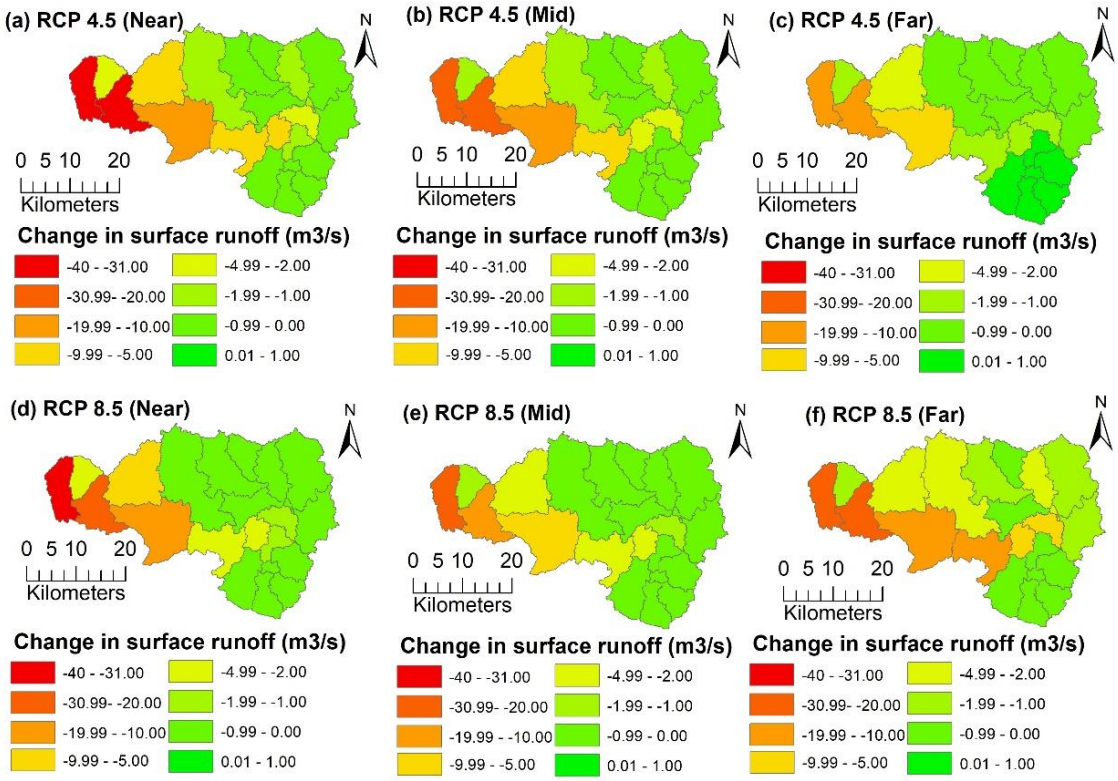

Fig. 5.48 Sub-basin level distribution of change in the surface runoff for the combined impact of LULC and CC in the ARB.

Fig. 5.49 represents the sub-basin level distributions of change in surface runoff from baseline condition to future for VRB. It is observed that the combined impacts show an increasing trend in all scenarios of RCP 4.5 by 12.65%, 8.2 9% and 6.82%

respectively. There is an increasing trend by 9.80% in the T1 and 5.24% in the T2 and decreasing by 0.90% in the T1 under RCP 8.5 emission scenarios. The surface runoff reduced at the sub-basins that receive less rainfall whereas more increased surface runoff is predicted in the sub-basin with more rainfall. Also, it is observed that as the time period moves to the T3 the decreasing trend increases in VRB which resembles the precipitation pattern.

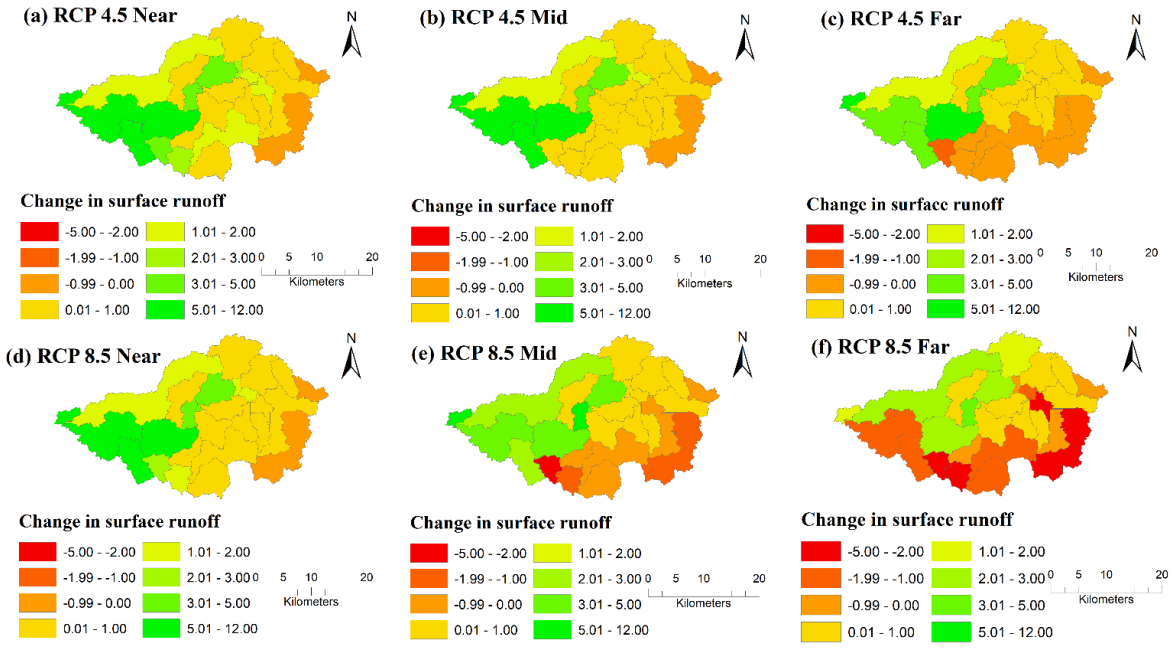

Fig. 5.49 Sub-basin level distribution of change in the surface runoff for the combined impact of LULC and CC in the VRB.

The spatial distributions of change in surface runoff from baseline condition to future, for GRB are shown in Fig. 5.50. Results replicate that the combined impacts show an increasing trend in T1, T2 and T3 scenarios of RCP 4.5 by 6.04%, 20.26%, and 28.49%, respectively, compared with baseline. In the case of RCP 8.5, an increasing trend was also predicted by 10.26% in the T1 and by 32.75% and 46.48% in the T2 and T3, respectively. This is because of the high variation in precipitation in the respective scenarios. It is also noted that CC is more dominant than LULC change in all the scenarios for both RCPs for GRB. Regarding LULC, it is noticed from the analysis that streamflow is highly sensitive to barren and urban areas. From Fig. 5.50, it can be seen that most sub-basins show an increasing trend of surface runoff and more towards the

downstream part of the GRB, in which more urban expansion is seen. Although positive trends in streamflow may be perceived beneficial in terms of water scarcity, it is important to note the timing and availability concerning agriculture and allied sectors. The National Food Security Mission (Government of India) provides a detailed cropping calendar specific to each state in India to aid with optimal times for sowing and harvest as agriculture in India is highly dependent on monsoon rains. The variations in rainfall, streamflow, and water availability observed in this study could be expected to impact sowing and harvesting directly. Similar variations may also be expected in other rivers of the Western Ghats, which have a similar climatic profile as GRB, which are more intensively farmed.

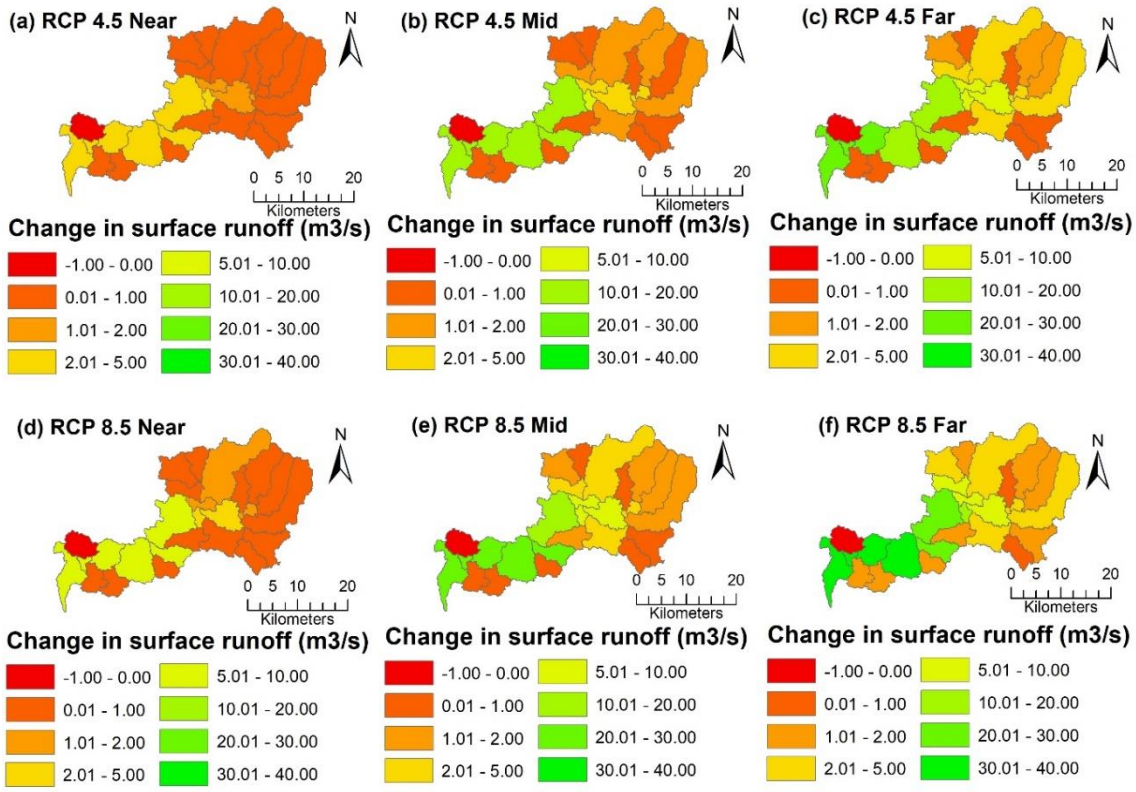

Fig. 5.50 Sub-basin level distribution of change in the surface runoff for the combined impact of LULC and CC in the GRB.

Fig. 5.51 shows the monthly, seasonally, and annual variation in streamflow in all scenarios for ARB. The results indicated that the monthly streamflow (Fig. 5.51 a) decreased from May to October and increased in September. The streamflow increases

in the rest of the months under all scenarios of RCP 4.5 and 8.5. The seasonal and annual variation of streamflow results gives a clear idea. It is clearly indicated that there is an increase in all seasons for all of the future periods (Fig. 5.51 b) except a decrease in winter for the T1 RCP 8.5 emission scenario.

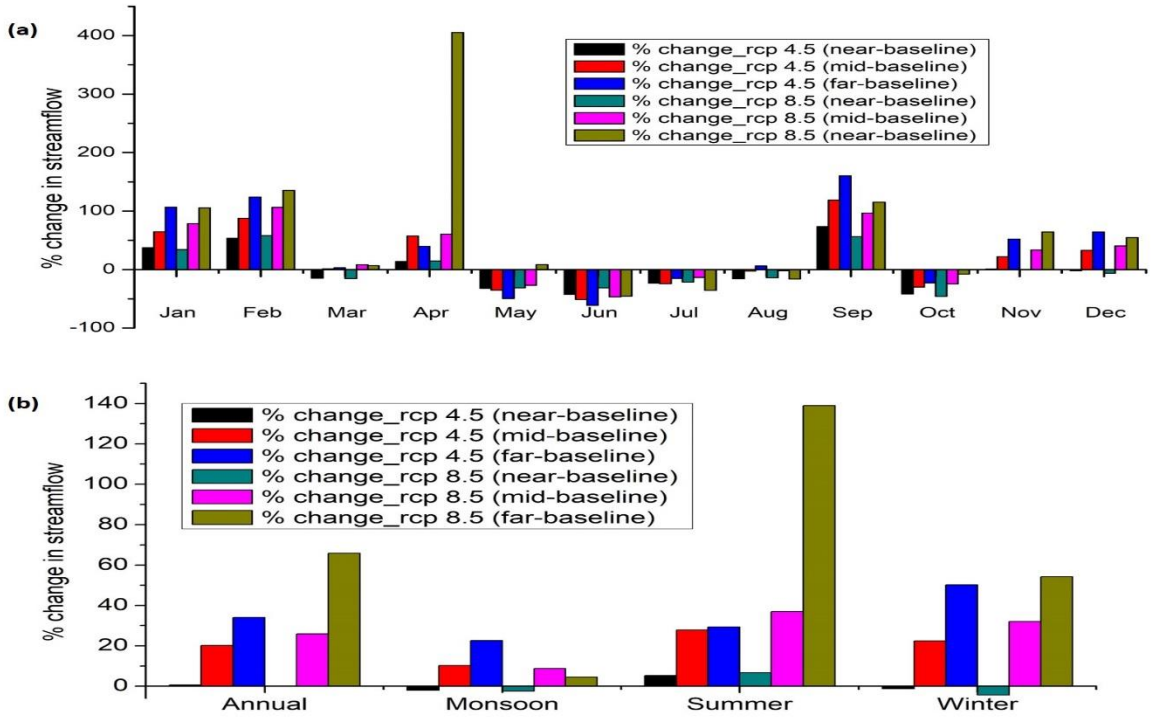

Fig. 5.51 Percentage change in streamflow due to LULC and climate change (a) mean monthly (b) mean seasonal and annual in the ARB.

The monthly, seasonally, and annual variation in streamflow for VRB is presented in fig 5.52. The results indicated that the monthly streamflow (Fig. 5.52 a) decreased during June and July. The streamflow increases in the rest of the months under all scenarios of RCP 4.5 and 8.5. It is observed that there is an increase in all seasons for all of the future periods (Fig. 5.52 b) except for a decrease in the monsoon season of the RCP 8.5 emission scenario.

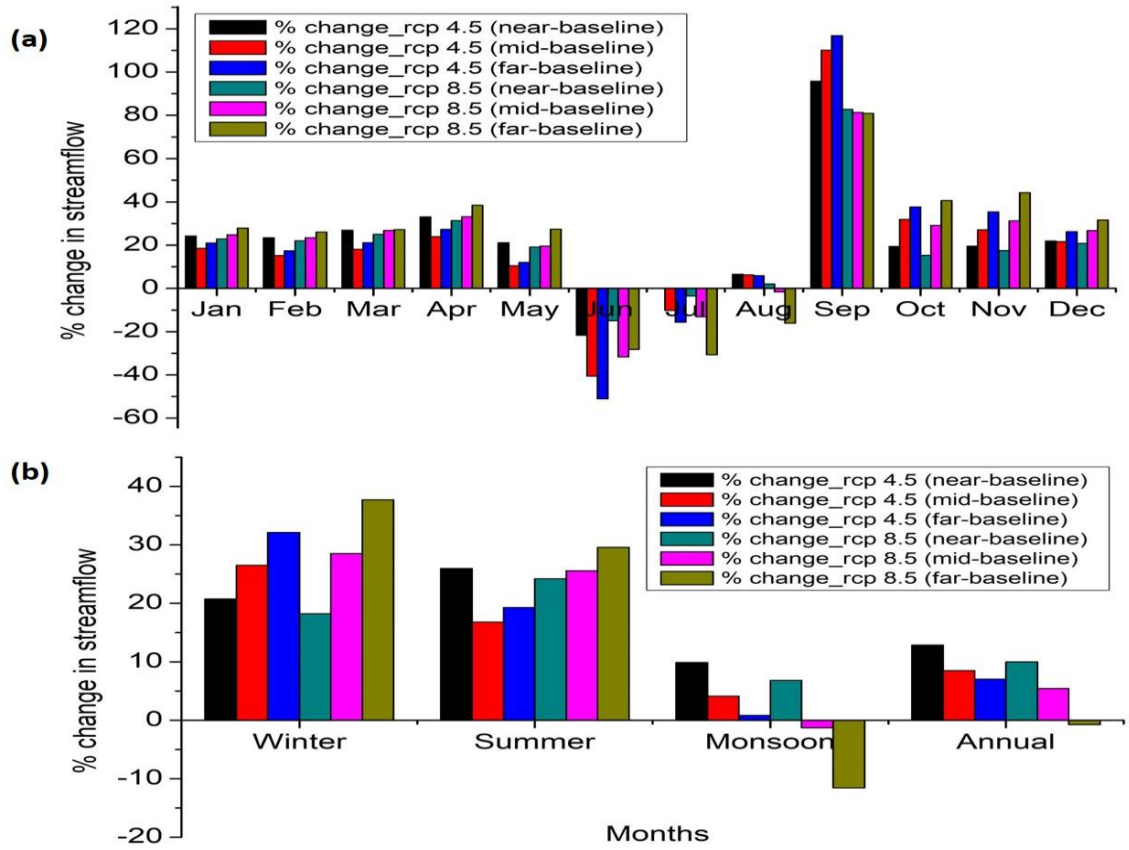

Fig. 5.52 Change in streamflow due to LULC and CC (a) mean monthly (b) mean seasonal and annual in the VRB.

For GRB, Fig. 5.53 shows the monthly, seasonally, and annual variation in streamflow. The monthly streamflow (Fig. 5.53 a) increased from September to February, decreasing in March. The streamflow has no significant variations in the rest of the months under all scenarios of RCP 4.5 and 8.5. There is an increase in flow in all seasons for all future periods under both emission scenarios except a decrease in summer in T1 under both RCP 4.5 and RCP 8.5 (Fig.5.53 b).

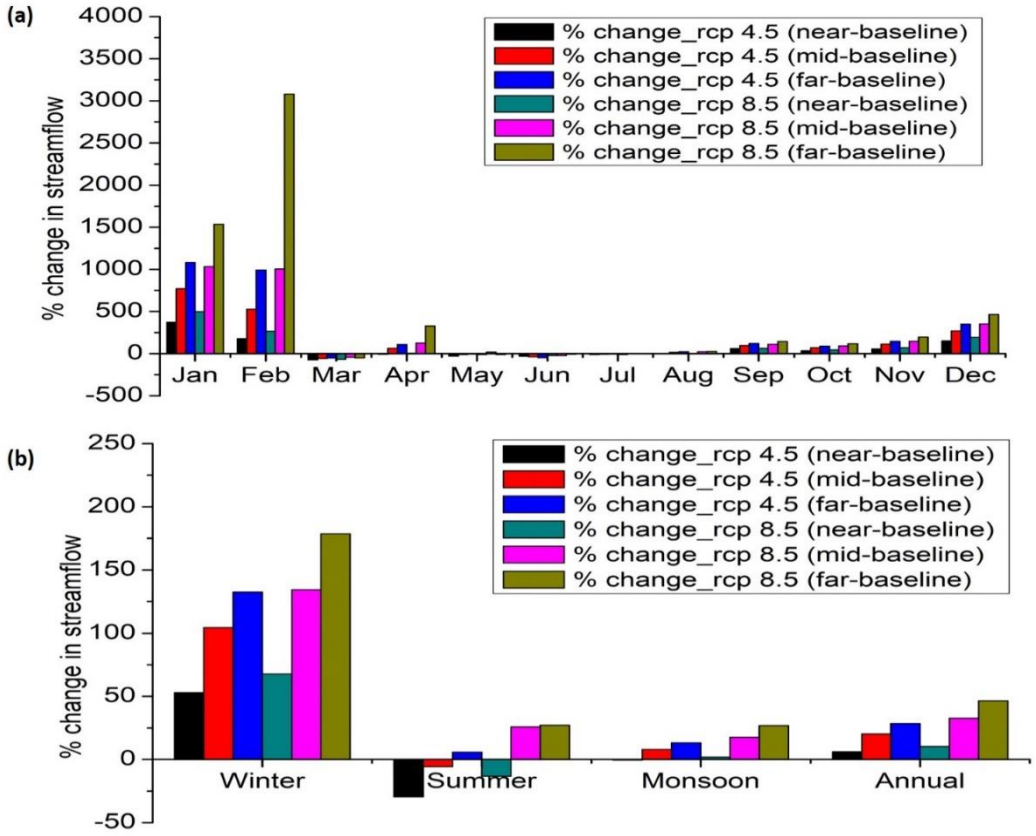

Fig. 5.53 Change in streamflow due to LULC and CC (a) mean monthly (b) mean seasonal and annual in the GRB.

CHAPTER 6

BASIN-SCALE WATER AVAILABILITY AND VULNERABILITY ASSESSMENT

6.1 METHODOLOGY

A scenario analysis approach was conducted to assess water scarcity in the Aghanashini, Varahi, and Gurupura river basins. Three climate window periods representing near-future (T1) (2006-2040), mid-future (T2) (2041-2070), and far-future (T3) (2071-2100) were framed for the scenario analysis of water scarcity. The freshwater scarcity was then quantified within each window period in terms of blue and green water. The sum of surface water and groundwater was estimated as Blue Water Flow (BWF). BWF translates to surface runoff, lateral, and return flows in terms of a basin scale. Naturally infiltrated water is considered the green water in the basin. Green water constitutes two components, namely Green Water Storage (GWS), which accounts for the available soil moisture, and Green Water Flow (GWF), which accounts for the actual evapotranspiration (Swain *et al* 2020).

Water scarcity is the inadequacy of enough water availability in a given river basin to fulfil water consumption needs in the region. However, granular data on sectoral water demands are not readily available for river basins. Thus, the water-scarce vulnerability assessment for the above river basins was carried out using baseline water demands which is the relative change in streamflow (ΔQ) and water availability (ΔWA) under Representative Concentration Pathway 4.5 (RCP 4.5) and RCP 8.5 scenarios. Water availability at the basin scale does not necessarily follow streamflow patterns as it is an integrated interaction between streamflow and basin storage components. The changes to streamflow and water availability in this study are computed, taking into account an ideal balance between water demand and water availability (Swain *et al.* 2020).

$$\Delta Q = \frac{Q_a - Q_b}{Q_b} \qquad (6.1)$$

$$\Delta WA = \frac{WA_a - WA_b}{WA_b} \quad (6.2)$$

where ΔQ = relative change in streamflow; Q_a and Q_b = average streamflows for the assessment and baseline periods, respectively; ΔWA = relative change in water availability, and WA_a and WA_b = average water availabilities for the assessment and baseline periods, respectively.

Based on ΔWA and ΔQ, four vulnerable sectors were identified as suggested by Garrote *et al.* (2018). The criteria for potential zoning of water scarcity risk assessment are outlined below:

Zone-1 (Z1) = ($\Delta Q > 0$, $\Delta WA > 0$) = Low risk (6.3)

Zone-2 (Z2) = ($\Delta Q < 0$, $\Delta WA > 0$) = Moderate risk (6.4)

Zone-3 (Z3) = ($\Delta Q > 0$, $\Delta WA < 0$) = High risk (6.5)

Zone-4 (Z4) = ($\Delta Q < 0$, $\Delta WA < 0$) = Extreme risk (6.6)

6.2 RESULTS AND DISCUSSION

6.2.1 Basin-scale water availability and vulnerability assessment

The Blue Water Flow (BWF), Green Water Flow (GWF), and Green Water Storage (GWS) under combined LU and CC were estimated at the basin scale and are given in Table 6.1. Using these estimates of BWF, GWF, and GWS, the water scarcity in the river basins was calculated as suggested by Swain *et al.* (2020). From Table 6.1, it may be observed from RCP 4.5 to RCP 8.5 scenarios that the BWF is almost the same for the T1 in the ARB with an increase in T2 and a decline in T3. Whereas in the case of VRB, BWF increased only in the case of the T1, with a decline in the T2 and T3 for both emission scenarios. However, in the GRB, an increase in BWF was observed for all climate windows across RCP 4.5 to RCP 8.5. The GWF and GWS increased for all the basins in all the climatic windows except for a slight decline in GWS in the T1 in the ARB and GWF in the T1 in VRB.

Table 6.1 Basin-scale estimates of precipitation, Blue Water Flow (BWF), Green Water Flow (GWF), and Green Water Storage (GWS)

Variable	Climate window	ARB		VRB		GRB	
		RCP 4.5	RCP 8.5	RCP 4.5	RCP 8.5	RCP 4.5	RCP 8.5
Precipitation	T1	2994.4	2995.9	4467.5	4566.9	3887.5	4004.1
	T2	3309.2	3465.9	4465.1	4374.3	4329.9	4739.8
	T3	3614.7	3359.8	4481.3	4098.7	4591.9	5205.8
Blue Water Flow (BWF)	T1	2444.65	2441.15	2397.71	2489.84	2298.83	2322.82
	T2	2732.05	2866	2442.97	2312.34	2656.73	2928.13
	T3	3034.5	2749.11	2434.82	2016.45	2882.64	3311.53
Green Water Flow (GWF)	T1	377.9	385.3	598.7	587.9	492	551.9
	T2	385.4	397.3	594.7	609.60	504.9	516
	T3	385.9	405.6	610.9	618.00	511.1	525.4
Green Water Storage (GWS)	T1	178.2	175.83	1471.35	1489.27	1196.39	1229.96
	T2	198.29	209.21	1427.61	1452.52	1271.32	1404.16
	T3	200.77	211.56	1435.78	1464.40	1302.22	1480.32

The GWF was found to be more than the GWS in the ARB, implying water loss as evapotranspiration in the basin and decreased soil moisture. On the other hand, GWS was higher than GWF in the VRB and GRB, which may be attributed to lesser evapotranspiration resulting from decreased forest cover and an increase in urbanized areas. Large vegetated areas lead to the soil's more excellent water storage capability and thereby enhance the infiltration and groundwater recharge (Guevara- Escobar *et al*., 2007; Marhaento *et al*., 2018).

Fig. 6.1 represents the relative change in streamflow and water availability for the three basins. ΔQ and ΔWA lesser than zero correspond to extremely vulnerable, and greater than zero corresponds to the less vulnerable sector. Similarly, ΔQ less than zero and ΔWA greater than zero refer to moderate vulnerability. A high vulnerable zone is referred to if ΔQ is greater than zero and ΔWA is less than zero (Garrote *et al.* 2018). ARB was classified as extremely vulnerable in the T1 climate window and less vulnerable over T2 and T3 windows.

Additionally, increasing temperature could result in increased evaporation, and lowering of soil moisture may lead to extreme events such as drought (Mukherjee *et al*., 2018; Whan *et al*., 2015). In the case of VRB, the relative changes to ΔQ and ΔWA were higher than zero and, therefore, classified under the low vulnerable category. However, for RCP 8.5 the VRB falls under moderate risk.

In the case of GRB, the increase in the BWF was attributed to the increase in urbanized areas and is also in accordance with previous studies (Giri *et al*., 2018). The relative changes to ΔQ and ΔWA were higher than zero, and therefore, the GRB was classified under the low vulnerable category as per the vulnerability classification.

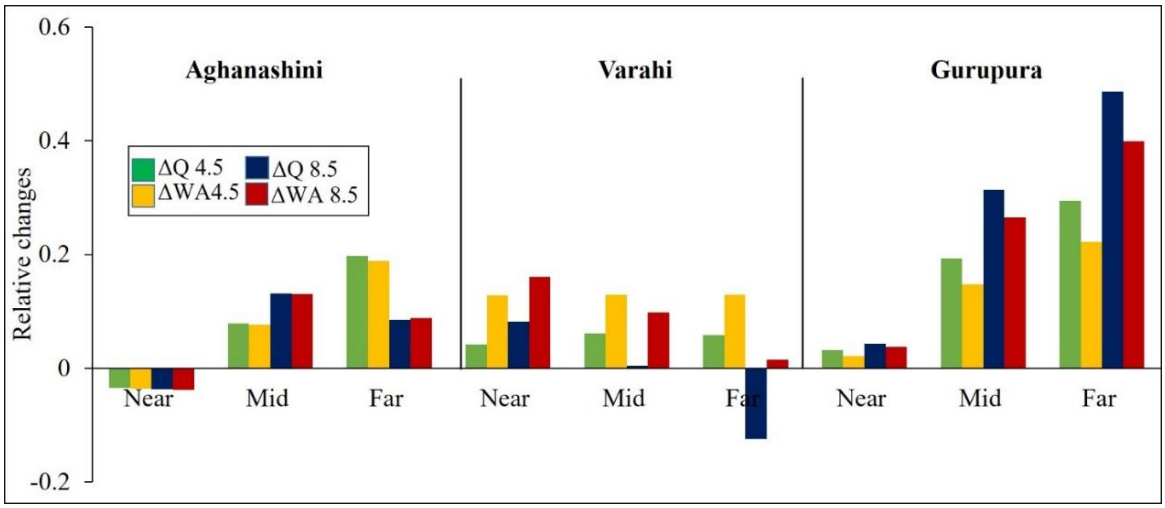

Fig. 6.1 Changes in water scarcity for the three climate windows

6.3 Keen observervation for the River Basin

The basin is classified into three primary zones based on observations, findings, and the level of LULC and CC impacts on surface runoff. The first zone is an upper region (upstream), the second zone is the middle region, and the third zone is the basins lower (downstream) region. The adaptation measures for each basin is described below:

6.3.1 Keen observation for Aghanashini River Basin

Fig. 6.2 represents different zone for water resource management in the ARB. For ARB, major changes are in forest areas and plantations in the first and second zone, while in the third (lower) zone considerable amount of wetlands has been noticed.

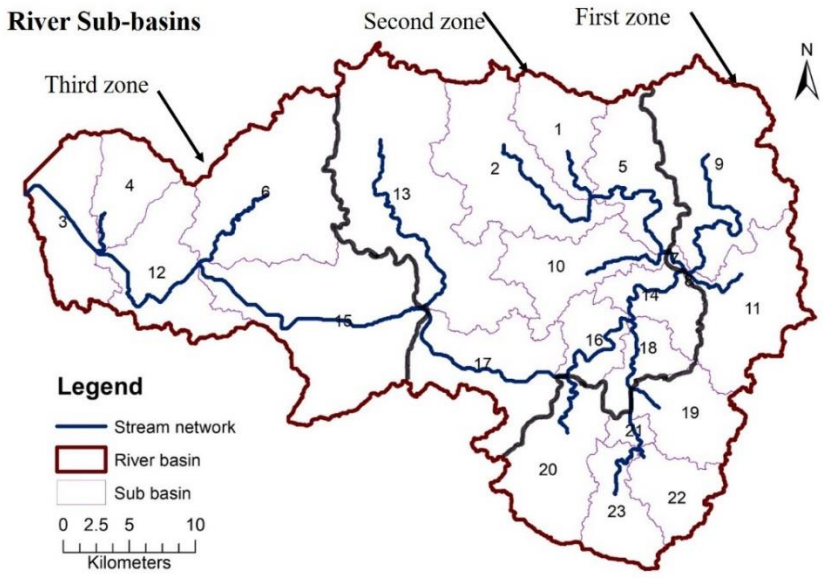

Fig. 6.2 River boundary, sub-basins, and different zone for water resource management in the ARB.

Based on the analysis of LULC impacts, it is found that very minute variation over the spatial variation. In contrast, the monthly and seasonal analysis observed a noticeable change in surface runoff. The Aghanashini river basin, characterized by its rich mudflats/tidal flats caused an increase in wetlands from 1.47% to 5.87% from 2016 to 2075. These mudflats are formed owing to organic matter/nutrients being transported from the forested region upstream of the basin. A decrease in forests generally tends to increase wetlands in small/medium undammed basins such as the Aghanashini.

However, it is essential to note that earlier studies on the wetlands of the Aghanashini river report more than 120 species of birds contribute to the productivity of mudflats through nutrient cycling in the form of potash and nitrogen source (Bhat *et al*. 2014; Boominathan *et al*. 2014, 2008). A decrease in forested areas and conversion of forests to plantation land in the ARB, as shown in the present study, could be inferred as a potential threat to these mudflats. These might be because of deforestation and high vegetative runoff that are known to be associated with higher transport of nutrient-rich sediments leading to eutrophication in aquatic environments. These changes also influence freshwater scarcity which causes nutrient-rich water that is not very fit for human and livestock consumption. It was found that the maximum change in streamflow was found from 1988 to 2003 (0.02%) historical and from 2016 to 2100 (0.01%) for the future. It is observed that change in annual surface runoff due to CC for all the time slices is moderate to highly significant for future CC scenarios. The Qclim decreased from the baseline period by 19.09%, 13.35%, and 6.37% in RCP 4.5 from the T1, T2, and T3 periods. In the case of RCP 8.5 there is a decrease in Qclim by 16.46% for T1 and a decrease by 9.29% and 16.78% for T2 and T3, respectively.

Also found that a decrease in streamflow in May, June, July, August, and October and an increase in streamflow for the other months in all scenarios. Seasonal change shows a rising trend in winter, summer, and monsoon and a decreasing trend in winter and monsoon season in all the T1 time slices compared to the baseline period. Therefore, it is essential to plan and recommend spatial variation and monthly, seasonal, and annual variation for future water resource management in ARB.

Combined impacts of LULC and climate change on surface runoff suggest a decreasing trend in T1, T2 and T3 scenarios of RCP 4.5 by 18.91%, 13.32%, and 6.28%, respectively, compared with baseline. In the case of RCP 8.5, a decreasing trend was also predicted by 16.61% in the T1 and by 9.19% and 16.70% in the T2 and T3, respectively. This is because of the high variation in precipitation in the respective scenarios (Table 6.2). The results indicated that the monthly streamflow decreased from May to October with an increase in September. The streamflow increases in the rest of the months under all scenarios of RCP 4.5 and 8.5.

6.3.2 Keen observation for the Varahi River Basin

Fig. 6.3 represents different zone for water resource management in the VRB. In the first and second zone, major changes are in forest and barren areas, while third (lower) zone, considerable conversion of barren land into the agricultural area has been noticed.

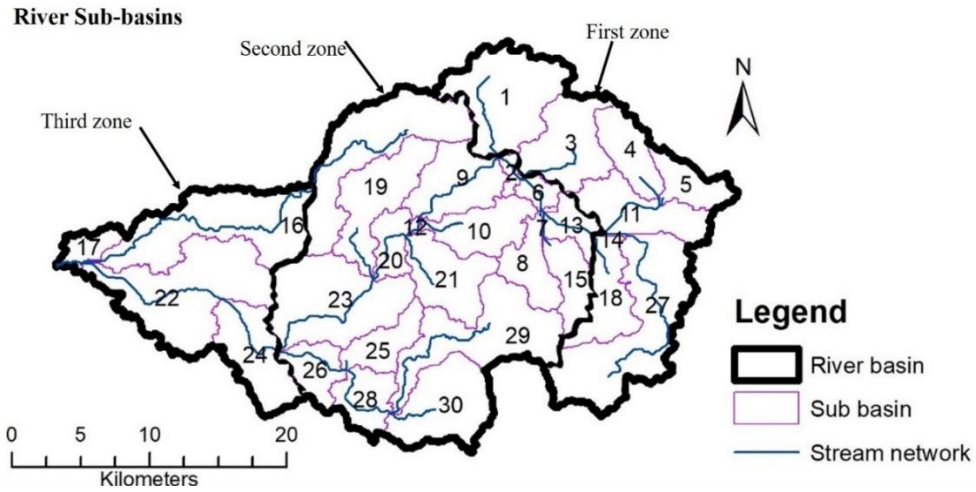

Fig. 6.3 River boundary, sub-basins, and different zone for water resource management in the VRB.

Based on the analysis of LULC impacts, it is found that water scarcity may happen due to high rainwater runoff, loss of forest cover, reclamation, expansion of the agricultural field, etc. It was observed that due to LULC change, even under the normal rainfall conditions, the lowland area of the basin may experience severe floods and meteorological drought due to high runoff more often than in the earlier times in the future period. The maximum change in streamflow was found from 1988 to 1995 (0.28%) in historical and from 2050 to 2075 (0.16%) in the future. Compared to the present LULC, the average streamflow will be increased by 0.09% by LULC 2030. However, the average annual streamflow increased by 0.318% from the current LULC (2016) to the projected LULC (2100) in the VRB. In particular, the Qclim increased from the baseline period by 12.7%, 9.0%, and 7.09% in RCP 4.5 from the T1, T2, and T3 periods respectively. Qclim increased from the baseline period by 10.01% and 5.81% in RCP 8.5 on the T1 and T2 time scale and decreased by 0.27% on a T3 time scale. Regarding impact of CC, a decrease in streamflow was observed in June and July.

There is an increase in streamflow for the other months in all scenarios except a reduction in August month during the T3 of the RCP 8.5 emission scenario. Seasonal change shows an increasing trend in winter, summer, and monsoon seasons in all the time slices compared to the baseline period, except for a decrease in monsoon during the T3 of the RCP 8.5 emission scenario.

Combined impacts of LULC and CC on surface runoff suggest an increasing trend in all scenarios of RCP 4.5 by 12.65%, 8.29%, and 6.82%, respectively. There is an increasing trend of 9.80% in the T1 and 5.24% in the T2, and decreasing of 0.90% in the T3 under RCP 8.5 emission scenarios. This is because of the variation in precipitation in the respective scenarios (Table 6.2). The results indicated a monthly streamflow decrease during June and July under RCP scenarios. The streamflow increases in the rest of the months under all scenarios of RCP 4.5 and 8.5. The seasonal and annual variation of streamflow gives a more precise idea. It indicates streamflow increase in all seasons for all future periods except a decrease in the monsoon season of the RCP 8.5 emission scenario.

6.3.3 Keen observation for the Gurupura River Basin

Fig. 6.4 represents different zone for water resource management in the GRB. In the first and second zone, significant changes are in forest areas, while third (lower) zone considerable amount of agricultural land conversion to the urban area has been noticed. Based on the analysis of LULC impacts, it is found that water scarcity may happen due to high rainwater runoff, loss of forest cover, reclamation, expansion of the vegetative field, etc. Due to LULC change, even under the normal rainfall conditions, the cities in the lowland area of the basin may experience severe floods and meteorological drought due to high runoff more often than the earlier times future period. Based on the analysis of LULC impacts, slight variation over the spatial variation is found.

In contrast, the monthly and seasonal analysis observed a noticeable change in surface runoff. The maximum shift in streamflow was found from 1988 to 2003 (0.08%) in historical and from 2016 to 2050 (0.03%) in the future. The Qclim increased from the baseline period by 6.11%, 23.24%, and 31.19% in RCP 4.5 from T1, T2, and T3

periods respectively. In the case of RCP 8.5 there is an increase in Qclim by 10.32% for T1, 35.77% for T2, and 49.18% for T3, respectively. Regarding impact of CC, there is an increase in streamflow in January and February, with a slight increase from September to December in all scenarios. A slight decline during March with minor changes in the monsoon months can be observed. Seasonal change shows an increasing trend in winter and monsoon seasons compared to the baseline period in all the time slices.

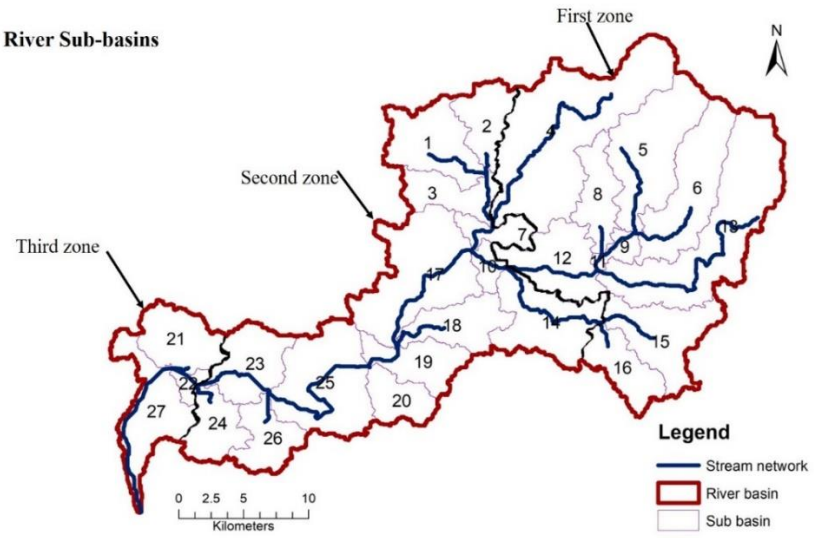

Fig. 6.4 River boundary, sub-basins, and different water resource management zones in the GRB.

Combined impacts of LULC and climate change on surface runoff suggest an increasing trend in T1, T2 and T3 scenarios of RCP 4.5 by 6.04%, 20.26%, and 28.49%, respectively, compared with baseline. In the case of RCP 8.5, an increasing trend was also predicted by 10.26% in the T1 and by 32.75% and 46.48% in the T2 and T3, respectively. This is because of the high variation in precipitation in the respective scenarios (Table 6.2). The results indicated that the monthly streamflow (Fig. 53 a) increased from September to February and decreased in March. The streamflow has no significant variations in the rest of the months under all scenarios of RCP 4.5 and 8.5. The seasonal and annual variation of streamflow results gives a more precise idea.

Table 6.2 Change in rainfall and surface runoff due to LULC and climate change for RCP 4.5 and 8.5.

River Basin	Scenarios	Scenarios	Time slice	Change in Rainfall (%)	Change in Surface Runoff (%)
Aghanashini River Basin	RCP 4.5	T1	2011-2040	-19.09	-18.91
		T2	2041-2070	-11.96	-13.32
		T3	2071-2100	-4.78	-6.28
	RCP 8.5	T1	2011-2040	-17.95	-16.61
		T2	2041-2070	-7.96	-9.19
		T3	2071-2100	-12.16	-16.70
Varahi River Basin	RCP 4.5	T1	2011-2040	4.95	12.65
		T2	2041-2070	6.07	8.29
		T3	2071-2100	7.83	6.82
	RCP 8.5	T1	2011-2040	4.42	9.80
		T2	2041-2070	10.16	5.24
		T3	2071-2100	11.03	-0.90
Gurupura River Basin	RCP 4.5	T1	2011-2040	-3.57	6.04
		T2	2041-2070	7.74	20.26
		T3	2071-2100	10.67	28.49
	RCP 8.5	T1	2011-2040	0.42	10.26
		T2	2041-2070	19.31	32.75
		T3	2071-2100	27.08	46.48

CHAPTER 7

SUMMARY AND CONCLUSIONS

This research aimed to determine the effects of LULC and CC on rivers that originate in the Western Ghats and flows through the west coast of Karnataka. Three river basins, namely Aghanashini, Varahi, and Gurupura, were chosen to represent the rivers on the west coast of Karnataka. The SWAT hydrological model was used to estimate the hydrology of river basins based on climatic variables, and the Dyna CLUE model was used to predict future land-use scenarios. Also, the study investigated the capability of four datasets of rainfall viz., IMD rainfall, TRMM, CHIRPS-0.25, and CHIRPS-0.05, in simulating streamflow under different calibration scenarios in a typical medium-sized river basin (Gurupura river) among the study area. The water scarcity analysis was carried out for these three river basins under the combined effect of long-term changes to land use and climate for vulnerability zonation.

The findings of the investigations are presented in this chapter. For clarity, the findings are provided in the order in which they were framed. The recommendations/ adaptation measures to cope with future climate change in the river basins are highlighted. The limitations of the current study and the need for more research are also discussed.

7.1 EVALUATION OF SATELLITE PRECIPITATION PRODUCTS IN SIMULATING STREAMFLOW

This work is aimed to investigate the capability of four datasets of rainfall viz., IMD rainfall, TRMM, CHIRPS-0.25, and CHIRPS-0.05, in simulating streamflow under different calibration scenarios in a typical medium sized river basin (Gurupura river) in the West coast of India. Soil and Water Assessment Tool (SWAT) was used for simulating streamflow and validating them against the flows generated by driving India Meteorological Department (IMD) rainfall dataset. Distinct testing scenarios for

simulating streamflow were made to check the suitability of these satellite precipitation data, and the following outcomes were obtained from this study:

- From categorical and continuous statistical results, TRMM detected better rainfall than CHIRPS with respect to IMD rainfall data.

- All rainfall datasets are forced into the SWAT hydrological model and calibrated separately to obtain the optimized parameters. The performance rating was found to be in the following order IMD, TRMM, CHIRPS-0.05, and CHIRPS-0.25.

- As the spatial resolution of the CHIRPS dataset increases, the model's performance in simulating the streamflow also increases.

- The performance indicators R^2, NSE, and PBIAS, were in the range 0.56 to 0.86, 0.54 to 0.86, and -14.98 to 10.71, respectively, which shows that all datasets are in the acceptable range for the streamflow generation.

- It could be inferred from the hydrological simulations that calibrated sensitive parameters of the gauge, or IMD dataset should not be used to calibrate the model with other satellite precipitation products; instead, each satellite dataset should be calibrated separately.

- It was evident that precipitation is one of the main components in the hydrological model which has a significant effect on streamflow simulations because the runoff simulations were greatly affected with the change in precipitation dataset by maintaining other datasets (Topography, Soil, Land use and other climatic parameters) constant for different simulations.

7.2 RIVER BASIN RESPONSE ON EFFECTS OF LAND USE AND CLIMATE CHANGE

This study aimed to investigate the impacts of past and future LULC and climate change on streamflow in the three west-flowing rivers of the Western Ghats, representing different levels of anthropogenic influence that spread over the northern (Aghanashini),

middle (Varahi), and southern portion (Gurupura) of the west coast Karnataka. The SWAT model was calibrated and executed for hydrological modeling of the river basins. The detection and analysis of LU were carried out using Landsat satellite imagery. Future LU maps were predicted using the Dyna-CLUE model, and future climate projections were derived from an average of five Global Circulation Models (GCMs). LULC changes impact streamflow by keeping the climatology constant to understand the hydrological effects of man-made LULC variations. The climate change analysis was carried out for three different time horizons: near-future (T1) (2006–2040), mid-future (T2) (2041–2070), and far-future (T3) (2071–2100) under RCP 4.5 and RCP 8.5 scenarios keeping LULC constant. To carry out the combined impact of LULC and CC, the T1, T2 and T3 scenarios are considered like the climate of 2011-2040 by using 2030 LULC (for the T1 scenario), climate 2041- 2070 by using 2050 LULC (for the T2 scenario), climate 2071-2100 by using 2075 LULC (for the T3 scenario) and the following outcomes may be inferred from this study:

- In ARB and VRB, the transition matrix of land use changes indicates that forest land converts to the plantation. It is observed that the expansion of agriculture, urban, and deforestation is highly sensitive to streamflow.
- In GRB, the transition matrix of land use changes indicates that forest land converts to plantation and agriculture into urban and barren lands.
- Out of five GCMs, it is observed that CNRM and MPI_LR are giving good results in comparison to other GCMs for ARB. But for VRB, CNRM and MPI_LR are providing good results. In the case of GRB, MPI_MR and MPI_LR are giving better performance.
- Compared to the present LULC (2016), the average streamflow will be decreased by 0.017% by LULC 2030 and 0.01% by 2100 for ARB. In VRB and GRB, the average streamflow will be increased by 0.09%, 0.06 % by LULC 2030, and 0.318%, 0.14% by 2100.
- It could be observed that the impact on streamflow due to only LULC is significantly less when compared with climate change impact. However, deforestation and the conversion of other LULC into an unorganized plantation/ agriculture with urban expansion increase streamflow.

- Due to LULC change, the surface runoff will decrease in 2030, 2050, 2075, and 2100 by 0.017%, 0.018%, 0.02%, and 0.01% in ARB, 0.1%, 0.13%, 0.30%, and 0.32% in VRB and 0.06%, 0.09%, 0.12%, and 0.14% in GRB in comparison to baseline (2016) land use.
- For climate change, only the impact ensemble of surface runoff decreased from the baseline period by 19.09%, 13.35%, and 6.37% in RCP 4.5 from the T1, T2, and T3 periods respectively. In the case of RCP 8.5, there is a decrease in Qclim by 16.46% for T1 and a decrease by 9.29% and 16.78% for T2 and T3, respectively, for ARB.
- Ensemble of surface runoff increased from the baseline period by 12.7%, 9.0%, and 7.09% from T1, T2, and T3 periods respectively, under RCP 4.5 and Qclim increased from the baseline period by 10.01% and 5.81% in RCP 8.5 in T1 and T2 time scale and decreased by 0.27% in the T3 time scale for VRB.
- In GRB, surface runoff increased from the baseline period by 6.11%, 23.24%, 31.19%, and an increase by 10.32%, 35.77%, and 49.18% in RCP 4.5 and RCP 8.5 from T1, T2, and T3 period respectively.
- Combined impacts of LULC and CC on surface runoff for ARB suggest a decreasing trend in T1, T2 and T3 scenarios of RCP 4.5 by 18.91%, 13.32%, and 6.28%, respectively, compared with baseline. The RCP 8.5 also predicted a decreasing trend of 16.61% in the T1 and 9.19% and 16.70% in the T2 and T3, respectively.
- An increasing trend in all scenarios of RCP 4.5 by 12.65%, 8.29%, and 6.82%, respectively, was observed under the combined impact on VRB. There is an increasing trend of 9.80% in the T1 and 5.24% in the T2 and decreasing by 0.90% in T1 under RCP 8.5 emission scenarios in VRB.
- Combined impacts suggest an increasing trend in T1, T2 and T3 scenarios of RCP 4.5 by 6.04%, 20.26%, and 28.49%, respectively, compared with baseline. In the case of RCP 8.5, an increasing trend was also predicted by 10.26% in the T1 and by 32.75% to 46.48% in the T2 and T3, respectively, in GRB.

- Understanding how future climate and LULC changes affect streamflow is critical for long-term water resource planning and management. In the future, ARB's annual streamflow is predicted to worsen.
- In ARB, monthly streamflow decreased from May to October under both RCP scenarios, with a rise in September. The streamflow increases in the rest of the months under all scenarios of RCP 4.5 and 8.5. The seasonal and annual variation of streamflow results gives a more precise idea. It indicated that increase in streamflow in all seasons for all future periods except a decrease in winter for the T1 RCP 8.5 emission scenario.
- Monthly streamflow decreases during June and July and increases in the rest of the months under all scenarios of RCP 4.5 and 8.5 for VRB. For VRB, streamflow increases in all seasons for all future periods except a decrease in the monsoon season of the RCP 8.5 emission scenario.
- In GRB, monthly streamflow increased from September to February and decreased in March. The streamflow has no significant variations in the rest of the months and observed an increase in flow in all seasons for all future periods.
- From the overall analysis it is found that climate change has more impact on streamflow than LULC change in the river basins.

7.3 BASIN-SCALE WATER AVAILABILITY AND VULNERABILITY ASSESSMENT

This study aimed to investigate water scarcity in the above three river basins due to the combined impacts of LU and CC under three climate window periods representing near-future (T1) (2006-2040), mid-future (T2) (2041-2070), and far-future (T3) (2071-2100). The freshwater scarcity was then quantified within each window period in terms of blue and green water. The sum of surface water and groundwater was estimated as Blue Water Flow (BWF). Naturally infiltrated water is considered the green water in the basin. Green water constitutes two components: Green Water Storage (GWS), which accounts for the available soil moisture, and Green Water Flow (GWF), which accounts for the actual evapotranspiration. The water-scarce vulnerability assessment for the above river basins was carried out using baseline water demands which are the

relative change in streamflow (ΔQ) and water availability (ΔWA) under Representative Concentration Pathway 4.5 (RCP 4.5) and RCP 8.5 scenarios and four vulnerable sectors were identified. The following results may be drawn from this study:

- It may be observed from RCP 4.5 to RCP 8.5 scenarios that the BWF is almost the same for the T1 in the ARB with an increase in T2 and a decline in T3.
- In the case of VRB, BWF increased only in the case of the T1, with a decline in the T2 and T3 for both emission scenarios.
- In GRB, an increase in BWF was observed for all climate windows across RCP 4.5 to RCP 8.5.
- The GWF and GWS increased for both the basins in all the climatic windows except for a slight decline in GWS in the T1 in the ARB and GWF in the T1 in VRB.
- The GWF was more than the GWS in the ARB, implying water loss as evapotranspiration in the basin and decreased soil moisture.
- GWS was higher than GWF in the VRB and GRB, which may be attributed to lesser evapotranspiration resulting from decreased forest cover and an increase in urbanized areas.
- ARB was classified as extremely vulnerable in the T1 climate window and less vulnerable over T2 and T3 windows.
- In the case of VRB, the relative changes to ΔQ and ΔWA were higher than zero and, therefore, classified under the low vulnerable category. However, for RCP 8.5, the VRB falls under moderate risk.
- In the case of GRB, the increase in the BWF was attributed to the increase in urbanized areas. The relative changes to ΔQ and ΔWA were higher than zero, and therefore, the Gurupura river basin was classified under the low vulnerable category as per the vulnerability classification.

7.4 LIMITATIONS OF THE STUDY

1. SWAT models were calibrated using data from a single river gauge for each river. If a more extensive database had been available, the SWAT model could have been calibrated at multiple locations (multi-gauges).
2. During the SWAT model's calibration and validation, it was observed that the model was unable to simulate extreme streamflow occurrences at particular period.
3. This research aims to shed information on the typical behaviour of rivers under changing land use and climatic circumstances rather than extreme events. Furthermore, the study of uncertainty was not the primary goal.
4. One of the study's flaws was the lack of examination of groundwater recharge under changing climate conditions.

7.5 SCOPE FOR FUTURE RESEARCH

1. Reduced streamflow might potentially increase water pollution; hence changes in water quality could be considered in climate change scenarios.
2. Extreme rainfall events can be investigated for their hydrological and ecological implications.
3. The extreme events under LULC and CC scenarios may be investigated.
4. Nutrient transport and crop management studies could make the model more general.
5. CMIP6 data, which describes shared socioeconomic pathways (SSPs) instead of CMIP5, could generate better results as the model deviation is reduced.

REFERENCES

Abbaspour, K. C., Yang, J., Maximov, I., Siber, R., Bogner, K., Mieleitner, J., Zobrist, J., and Srinivasan, R. (2007). "Modelling hydrology and water quality in the pre-alpine/alpine Thur watershed using SWAT." *J. Hydrol.*, 333(2–4), 413–430.

Arnold, J. G., Srinivasan, R., Muttiah, R. S., and Williams, J. R. (1998). "Large Area Hydrologic Modeling And Assessment Part I : Model Development." *J. Am. Water Resour. Assoc.*, 34(1), 73–89.

Ashouri, H., Hsu, K. L., Sorooshian, S., Braithwaite, D. K., Knapp, K. R., Cecil, L. D., Nelson, B. R., and Prat, O. P. (2015). "PERSIANN-CDR: Daily precipitation climate data record from multisatellite observations for hydrological and climate studies." *Bull. Am. Meteorol. Soc.*, 96(1), 69–83.

Babar, S., and Ramesh, H. (2014). "Analysis of extreme rainfall events over Nethravathi basin." *ISH J. Hydraul. Eng.*, 20(2), 212–221.

Beck, H. E., Vergopolan, N., Pan, M., Levizzani, V., Dijk, A. I. J. M. Van, Weedon, G. P., Brocca, L., Pappenberger, F., Huffman, G. J., and Wood, E. F. (2017). "Global-scale evaluation of 22 precipitation datasets using gauge observations and hydrological modeling." *Hydrol. Earth Syst. Sci.*, 21(12), 6201–6217.

Behera, M. D., Tripathi, P., Das, P., Srivastava, S. K., Roy, P. S., Joshi, C., Behera, P. R., Deka, J., Kumar, P., Khan, M. L., Tripathi, O. P., Dash, T., and Krishnamurthy, Y. V. N. (2018). "Remote sensing based deforestation analysis in Mahanadi and Brahmaputra river basin in India since 1985." *J. Environ. Manage.*, 206, 1192–1203.

Behera, N. K., and Behera, M. D. (2020). "Predicting land use and land cover scenario in Indian national river basin: the Ganga." *Trop. Ecol.*, 61(1), 51–64.

Bennett, J. C., Grose, M. R., Post, D. A., Ling, F. L. N., Corney, S. P., and Bindoff, N. L. (2011). "Performance of quantile-quantile bias-correction for use in hydroclimatological projections." *MODSIM 2011 - 19th Int. Congr. Model. Simul. - Sustain. Our Futur. Underst. Living with Uncertain.*, (December), 2668–2675.

Bhat M., V. N. Nayak, M. D. S. C. and T. V. R. (2014). "Impact of hydroelectric projects on finfish diversity in the Sharavathi River estuary of Uttara Kannada District, central west coast of India." *Int. J. Environ. Sci.*, 5(1), 1–9.

Bitew, M. M., and Gebremichael, M. (2011). "Evaluation of satellite rainfall

products through hydrologic simulation in a fully distributed hydrologic model." *Water Resour. Res.*, 47(6), 1–11.

Boominathan, M., G., R., M. D. Subash, C., and T. V., R. (2014). "Impact of Hydroelectric Projects on Bivalve Clams in the Sharavathi Estuary of Indian West Coast." *Open Ecol. J.*, 7(1), 52–58.

Boominathan, M., Subash Chandran, M. D., and Ramachandra, T. V. (2008). "Economic Valuation of Bivalves in the Aghanashini Estuary, West Coast, Karnataka." *Sahyadri Conserv. Ser. 9*, 33.

Boretti, A., and Rosa, L. (2019). "Reassessing the projections of the World Water Development Report." NPJ *Clean Water*, 2(1).

Bryan C Pijanowski, Daniel G Brown, Bradley A Shellito, G. A. M. (2002). "Using neural networks and GIS to forecast land use changes: a Land Transformation Mode." *Comput. Environ. Urban Syst.*, 26(6), 553–575.

Chappell, A., Renzullo, L. H., Raupach, T. J., and Haylock, M. (2013). "Evaluating geostatistical methods of blending satellite and gauge data to estimate near real-time daily rainfall for Australia." *J. Hydrol.*, 493, 105–114.

Chen, Q., Chen, H., Zhang, J., Hou, Y., Shen, M., Chen, J., and Xu, C. (2020). "Impacts of climate change and LULC change on runoff in the Jinsha River Basin." *J. Geogr. Sci.*, 30(1), 85–102.

Cover, F. (1993). "Members of the study team." *J. Clin. Epidemiol.*, 46(8), VII.

Diodato, N. (2005). "The influence of topographic co-variables on the spatial variability of precipitation over small regions of complex terrain." *Int. J. Climatol.*, 25(3), 351–363.

Dixon, B., and Earls, J. (2012). "Effects of urbanization on streamflow using SWAT with real and simulated meteorological data." *Appl. Geogr.*, 35(1–2), 174–190.

Ebert, B. Y. E. E., Janowiak, J. E., and Kidd, C. (2007). "Numerical Models." *Am. Meteorol. Soc.*, 88(January), 47–64.

Fadnavis, S., Mahajan, A. S., Choudhury, A. D., Roy, C., Singh, M., and Biswas, M. S. (2020). *Atmospheric aerosols and trace gases*. *Assess. Clim. Chang. over Indian Reg. A Rep., Minist. Earth Sci. (MoES), Gov. India*.

Franczyk, J., and Chang, H., (2009). "The effects of climate change and urbanization on the runoff of the Rock Creek basin in the Portland metropolitan

area, Oregon, USA." *Hydrol. Process.*, 23(November 2008), 805–815.

Fuka, D. R., Walter, M. T., Macalister, C., Degaetano, A. T., Steenhuis, T. S., and Easton, Z. M. (2014). "Using the Climate Forecast System Reanalysis as weather input data for watershed models." *Hydrol. Process.*, 28(22), 5613–5623.

Funk, C., Peterson, P., Landsfeld, M., Pedreros, D., Verdin, J., Shukla, S., Husak, G., Rowland, J., Harrison, L., Hoell, A., and Michaelsen, J. (2015). "The climate hazards infrared precipitation with stations - A new environmental record for monitoring extremes." *Sci. Data*, 2, 1–21.

Gao, F., Zhang, Y., Chen, Q., Wang, P., Yang, H., and Yao, Y. (2018). "Comparison of two long-term and high-resolution satellite precipitation datasets in Xinjiang , China." *Atmos. Res.*, 212(October 2017), 150–157.

Garg, V., Nikam, B. R., Thakur, P. K., Aggarwal, S. P., Gupta, P. K., and Srivastav, S. K. (2019). "Human-induced land use land cover change and its impact on hydrology." *HydroResearch*, 1, 48–56.

Garrote, L., Iglesias, A., and Granados, A. (2018). "Country-level assessment of future risk of water scarcity in Europe." *Proc. IAHS.*, 455–462.

Gaur, S., Mittal, A., Bandyopadhyay, A., Holman, I., and Singh, R. (2020). "Spatio-temporal analysis of land use and land cover change: a systematic model inter-comparison driven by integrated modelling techniques." *Int. J. Remote Sens.*, 41(23), 9229–9255.

Geist, H. J., and Lambin, E. F. (2006). "Proximate Causes and Underlying Driving Forces of Tropical Deforestation." *Bioscience*, 52(2), 143

Gerten, D., Hoff, H., Bondeau, A., Lucht, W., Smith, P., and Zaehle, S. (2005). "Contemporary 'green' water flows: Simulations with a dynamic global vegetation and water balance model." *Phys. Chem. Earth*, 30(6-7 SPEC. ISS.), 334–338.

Ghaffari, G., Keesstra, S., Ghodousi, J., and Ahmadi, H. (2010). "SWAT-simulated hydrological impact of land-use change in the Zanjanrood Basin, Northwest Iran." *Hydrol. Process.*, 24(7), 892–903.

Ghimire, S., Choudhary, A., and Dimri, A. P. (2015). "International Centre for Integrated Mountain Development Assessment of the performance of CORDEX-South Asia experiments for monsoonal precipitation over the Himalayan region during present climate." 1–24.

Ghosh, S., Das, D., Kao, S. C., and Ganguly, A. R. (2012). "Lack of uniform trends but increasing spatial variability in observed Indian rainfall extremes." *Nat. Clim. Chang.*, 2(2), 86–91.

Giri, S., Arbab, N. N., and Lathrop, R. G. (2018). "Water security assessment of current and future scenarios through an integrated modeling framework in the Neshanic River Watershed." *J. Hydrol.*, 563, 1025–1041.

Guevara-Escobar, A., Gonzalez-Sosa, E., Ramos-Salinas, M., and Hernandez-Delgado, G. D. (2007). "Experimental analysis of drainage and water storage of litter layers." *Hydrol. Earth Syst. Sci.*, 11(5), 1703–1716.

Hersperger, A. M., Gennaio, M., and Verburg, P. H. (2010). "<Hersperger et al_2010_Linking land change with driving forces and Actors_four conceptual models.pdf>." 15(4).

Himanshu, S. K., Pandey, A., and Patil, A. (2018). "Hydrologic evaluation of the TMPA-3B42V7 precipitation data set over an agricultural watershed using the SWAT model." *J. Hydrol. Eng.*, 23(4), 1–17.

Huang, W. R., Liu, P. Y., Chang, Y. H., and Liu, C. Y. (2020). "Evaluation and application of satellite precipitation products in studying the summer precipitation variations over Taiwan." *Remote Sens.*, 12(3), 1-17.

Huffman, G. J., Adler, R. F., Bolvin, D. T., Gu, G., Nelkin, E. J., Bowman, K. P., Hong, Y., Stocker, E. F., and Wolff, D. B. (2007). "The TRMM Multisatellite Precipitation Analysis (TMPA): Quasi-global, multiyear, combined-sensor precipitation estimates at fine scales." *J. Hydrometeorol.*, 8(1), 38–55.

Hung, C. L. J., James, L. A., Carbone, G. J., and Williams, J. M. (2020). "Impacts of combined land-use and climate change on streamflow in two nested catchments in the Southeastern United States." *Ecol. Eng.*, 143(February 2019), 1-24.

Iizumi, T., Takikawa, H., Hirabayashi, Y., Hanasaki, N., and Nishimori, M. (2017). "Contributions of different bias-correction methods and reference meteorological forcing data sets to uncertainty in projected temperature and precipitation extremes." *J. Geophys. Res.*, 122(15), 7800–7819.

Ilstedt, U., Bargués Tobella, A., Bazié, H. R., Bayala, J., Verbeeten, E., Nyberg, G., Sanou, J., Benegas, L., Murdiyarso, D., Laudon, H., Sheil, D., and Malmer, A. (2016). "Intermediate tree cover can maximize groundwater recharge in the

seasonally dry tropics." *Sci. Rep.*, 6(February), 1–12.

IPCC (Intergovernmental Panel on Climate Change). (2007). M. L. Parry, O. F. Canziani, J. P. Palutikof, P. J. van der Linden, and C. E. Hanson, eds. Climate Change 2007: Impacts, Adaptation and Vulnerability. Contribution of Working Group II to the Fourth Assessment Report of the Intergovernmental Panel on Climate Change. Cambridge University Press, Cambridge, UK.

IPCC (Intergovernmental Panel on Climate Change). (2012). Field, C. B., II, C.-C. W. G., Institution, C., Science, F., Barros, V., II, C.-C. W. G. Managing the Risks of Extreme Events and Disasters to Advance Climate Change Adaptation: Special Report of the Intergovernmental Panel on Climate Change. Cambridge University Press, Cambridge, UK.

IPCC (Intergovernmental Panel on Climate Change). (2018). Masson-Delmotte, V., Pörtner, H.-O., Skea, Jim, P. Z., Roberts, D., Shukla, P. R., & Pirani, A. (2018). Global warming? The Intergovernmental Panel on Climate Change, (5813), 630pp.

Islam, M. A. (2018). "Statistical comparison of satellite-retrieved precipitation products with rain gauge observations over Bangladesh." *Int. J. Remote Sens.*, 39(9), 2906–2936.

Jiang, Q., Li, W., Wen, J., Qiu, C., Sun, W., Fang, Q., Xu, M., Tan, J. (2018). "Accuracy Evaluation of Two High-Resolution Satellite-Based Rainfall Products : TRMM 3B42V7." *Water*, 10(10), 1–15.

Jiang, D., and Wang, K. (2019). "The role of satellite-based remote sensing in improving simulated streamflow: A review." *Water (Switzerland)*, 11(8), 10–14.

Kannan, S., and Ghosh, S. (2013). "A nonparametric kernel regression model for downscaling multisite daily precipitation in the Mahanadi basin." *Water Resour. Res.*, 49(3), 1360–1385.

Kerle, N., and Oppenheimer, C. (2002). "Satellite remote sensing as a tool in lahar disaster management." *Disasters*, 26(2), 140–160.

Khairul, I. M., Mastrantonas, N., Rasmy, M., Koike, T., and Takeuchi, K. (2018). "Inter-Comparison of Gauge-Corrected Global Satellite Rainfall Estimates and Their Applicability for Effective Water Resource Management in a Transboundary River Basin: The Case of the Meghna River Basin." *Remote Sens.*, 10(6), 1-32.

Khoi, D. N., and Thom, V. T. (2015). "Parameter uncertainty analysis for

simulating streamflow in a river catchment of Vietnam." *Glob. Ecol. Conserv.*, 4, 538–548.

Khoury, A. El. (2012). "Modeling Land-Use Changes in the South Nation Watershed using Dyna-CLUE." *Master Thesis*, Department of Civil Engineering,University of Ottawa, Canada.

Kidd, C., and Levizzani, V. (2011). "Status of satellite precipitation retrievals." *Hydrol. Earth Syst. Sci.*, 15(4), 1109–1116.

Kim, J., Choi, J., Choi, C., and Park, S. (2013). "Impacts of changes in climate and land use/land cover under IPCC RCP scenarios on streamflow in the Hoeya River Basin, Korea." *Sci. Total Environ.*, 452–453, 181–195.

Kindu, M., Schneider, T., Teketay, D., and Knoke, T. (2015). "Drivers of land use/land cover changes in Munessa-Shashemene landscape of the south-central highlands of Ethiopia." Environ. Monit. Assess., 187(7).

Kiprotich, P., Wei, X., Zhang, Z., Ngigi, T., Qiu, F., and Wang, L. (2021). "Assessing the impact of land use and climate change on surface runoff response using gridded observations and SWAT+." *Hydrology*, 8(1), 1–29.

Koch, J., Wimmer, F., Schaldach, R., and Onigkeit, J. (2012). "An Integrated Land-Use System Model for the Jordan River Region." Environ. L. Use Plan.

Kolluru, V., Kolluru, S., and Konkathi, P. (2020). "Evaluation and integration of reanalysis rainfall products under contrasting climatic conditions in India." *Atmos. Res.*, 246(July), 105121.

Krishnakumar, K. N., Prasada Rao, G. S. L. H. V., and Gopakumar, C. S. (2009). "Rainfall trends in twentieth century over Kerala, India." *Atmos. Environ.*, 43(11), 1940–1944.

Kumar, B., and Lakshmi, V. (2018). "Accessing the capability of TRMM 3B42 V7 to simulate streamflow during extreme rain events: Case study for a Himalayan River Basin." *J. Earth Syst. Sci.*, 127(2), 1–15.

Li, H., Sheffield, J., & Wood, E. F. (2010). "Bias correction of monthly precipitation and temperature fields from Intergovernmental Panel on Climate Change AR4 models using equidistant quantile matching". J.Geophys.Res.Atmos., 115(D10), 1-20.

Li, D., Christakos, G., Ding, X., and Wu, J. (2018). "Adequacy of TRMM satellite

rainfall data in driving the SWAT modeling of Tiaoxi catchment (Taihu lake basin, China).” *J. Hydrol.*, 556, 1139–1152.

Liew, M. W. Van, and Garbrecht, J. (2003). “Hydrologic Simulation Of The Little Washita River Experimental Watershed Using SWAT 1.” *J. Am. Water Resour. Assoc*, 73036, 413–426.

Li, W., and Wu, C. (2013). “A spatially explicit method to examine the impact of urbanisation on natural ecosystem service values.” J. Spat. Sci., 58(2), 275–289.

Lin, Y. P., Chu, H. J., Wu, C. F., and Verburg, P. H. (2011). “Predictive ability of logistic regression, auto-logistic regression and neural network models in empirical land-use change modeling - a case study.” Int. J. Geogr. Inf. Sci., 25(1), 65–87.

Malagò, A., Pagliero, L., Bouraoui, F., and Franchini, M. (2015). “Comparaison de jeux de paramètres calés de modèles SWAT pour les péninsules ibérique et Scandinave.” *Hydrol. Sci. J.*, 60(5), 949–967.

Mao, G., Liu, J., Han, F., Meng, Y., Tian, Y., Zheng, Y., and Zheng, C. (2018). “Assessing Green and Blue Water: Understanding Interactions and Making Balance between Human and Nature.” *Hydrol. Earth Syst. Sci. Discuss.*, (May), 193, 1–26.

Marhaento, H., Booij, M. J., and Hoekstra, A. Y. (2018). “Hydrological response to future land-use change and climate change in a tropical catchment.” *Hydrol. Sci. J.*, 63(9), 1368–1385.

Marquez, A. M., Guevara, E., and Rey, D. (2019). “Hybrid Model for Forecasting of Changes in Land Use and Land Cover Using Satellite Techniques.” *IEEE J. Sel. Top. Appl. Earth Obs. Remote Sens.*, 12(1), 252–273.

Me, W., Abell, J. M., and Hamilton, D. P. (2015). “Effects of hydrologic conditions on SWAT model performance and parameter sensitivity for a small, mixed land use catchment in New Zealand.” *Hydrol. Earth Syst. Sci.*, 19(10), 4127–4147.

Mekonnen, H. Daba Zerfu, Bazie and Ayalanesh, B. (2018). “Effects of Climate Change on Soil and Water Resources : A Review.” *J. Environ. Earth Sci.*, 8(7), 71–80.

Michaelides, S., Levizzani, V., Anagnostou, E., Bauer, P., Kasparis, T., and Lane, J. E. (2009). “Precipitation: Measurement, remote sensing, climatology and modeling.” *Atmos. Res.*, 94(4), 512–533.

Milly, P. C. D., Betancourt, J., Falkenmark, M., Hirsch, R. M., Kundzewicz, Z. W.,

Lettenmaier, D. P., and Stouffer, R. J. (2008). “Climate change: Stationarity is dead: Whither water management?” *Science (80-.).*, 319(5863), 573–574.

Moriasi, D. N., Arnold, J. G., Liew, M. W. Van, Bingner, R. L., Harmel, R. D., and Veith, T. L. (2007). “Model Evaluation Guidelines For Systematic Quantification Of Accuracy In Watershed Simulations.” *Trans. ASABE 2007*, 50(3), 885–900.

Mudbhatkal, A., and Amai, M. (2018a). “Regional climate trends and topographic influence over the Western Ghat catchments of India.” *Int. J. Climatol.*, 38(5), 2265–2279.

Mudbhatkal, A., and Mahesha, A. (2018b). “Bias Correction Methods for Hydrologic Impact Studies over India’s Western Ghat Basins.” *J. Hydrol. Eng.*, 23(2), 05017030.

Mudbhatkal, A., Raikar, R. V., Venkatesh, B., and Mahesha, A. (2017). “Impacts of climate change on varied River-Flow regimes of southern india.” *J. Hydrol. Eng.*, 22(9), 05017017.

Mukherjee, S., Mishra, A., and Trenberth, K. E. (2018). “Climate Change and Drought: a Perspective on Drought Indices.” *Curr. Clim. Chang. Reports*, 4(2), 145–163.

Musie, M., Sen, S., and Srivastava, P. (2019). “Comparison and evaluation of gridded precipitation datasets for streamflow simulation in data scarce watersheds of Ethiopia.” *J. Hydrol.*, 579(September), 124168.

Niehoff, D., Fritsch, U., and Bronstert, A. (2002). “Land-use impacts on storm-runoff generation: Scenarios of land-use change and simulation of hydrological response in a meso-scale catchment in SW-Germany.” *J. Hydrol.*, 267(1–2), 80–93.

Ochoa, A., Pineda, L., Crespo, P., and Willems, P. (2014). “Evaluation of TRMM 3B42 precipitation estimates and WRF retrospective precipitation simulation over the Pacific-Andean region of Ecuador and Peru.” *Hydrol. Earth Syst. Sci.*, 18(8), 3179–3193.

Overmars, K. P., and Verburg, P. H. (2005). “Analysis of land use drivers at the watershed and household level: Linking two paradigms at the Philippine forest fringe.” Int. J. Geogr. Inf. Sci., 19(2), 125–152.

Pai, D. S., Sridhar, L., Rajeevan, M., Sreejith, O. P., Satbhai, N. S., and Mukhopadhyay, B. (2014). “(1901-2010) daily gridded rainfall data set over India

and its comparison with existing data sets over the region." *Mausam*, 1(January), 1–18.

Pakoksung, K., and Takagi, M. (2016). "Effect of satellite based rainfall products on river basin responses of runoff simulation on flood event." *Model. Earth Syst. Environ.*, 2(3), 1–14.

Papalexiou, S. M., Rajulapati, C. R., Clark, M. P., and Lehner, F. (2020). "Robustness of CMIP6 Historical Global Mean Temperature Simulations: Trends, Long-Term Persistence, Autocorrelation, and Distributional Shape." *Earth's Futur.*, 8(10).

Pechlivanidis, I. G., Jackson, B. M., Mcintyre, N. R., and Wheater, H. S. (2011). "Catchment scale hydrological modelling: A review of model types, calibration approaches and uncertainty analysis methods in the context of recent developments in technology and applications." *Glob. Nest J.*, 13(3), 193–214.

Pervez, M. S., and Henebry, G. M. (2015). "Assessing the impacts of climate and land use and land cover change on the freshwater availability in the Brahmaputra River basin." *J. Hydrol. Reg. Stud.*, 3, 285–311.

Phung, Q. A., Thompson, A. L., Baffaut, C., Costello, C., Sadler, E. J., Svoma, B. M., Lupo, A., and Gautam, S. (2019). "Climate and Land Use Effects on Hydrologic Processes in a Primarily Rain-Fed, Agricultural Watershed." *J. Am. Water Resour. Assoc.*, 55(5), 1196–1215.

Pierce, D. W., Barnett, T. P., Santer, B. D., and Gleckler, P. J. (2009). "Selecting global climate models for regional climate change studies." *Proc. Natl. Acad. Sci. U. S. A.*, 106(21), 8441–8446.

Raju, K. S., and Kumar, D. N. (2020). "Review of approaches for selection and ensembling of GCMS." *J. Water Clim. Chang.*, 11(3), 577–599.

Rajulapati, C. R., Papalexiou, S. M., Clark, M. P., Razavi, S., Tang, G., and Pomeroy, J. W. (2020). "Assessment of extremes in global precipitation products: How reliable are they?" *J. Hydrometeorol.*, 21(12), 2855–2873.

Ramesh, K., and Goswami, P. (2007). "The shrinking Indian summer monsoon." *Geophys. Res. Lett.*, 34, 1–6.

Raneesh, K. Y., and Santosh, G. T. (2011). "A study on the impact of climate change on streamflow at the watershed scale in the humid tropics." *Hydrol. Sci. J.*,

56(6), 946–965.

Roy, A., and Inamdar, A. B. (2019). "Multi-temporal Land Use Land Cover (LULC) change analysis of a dry semi-arid river basin in western India following a robust multi-sensor satellite image calibration strategy." *Heliyon*, 5(4), e01478.

Sajikumar, N., and Remya, R. S. (2015). "Impact of land cover and land use change on runoff characteristics." *J. Environ. Manage.*, 161, 460–468.

Salvi, K., S., K., and Ghosh, S. (2013). "High-resolution multisite daily rainfall projections in India with statistical downscaling for climate change impacts assessment." *J. Geophys. Res. Atmos.*, 118(9), 3557–3578.

Satge, F., Ruelland, D., Bonnet, M., Molina, J., Pillco, R., Hydrosciences, U. M. R., Bataillon, P. E., Cedex, M., Hydrosciences, U. M. R., Bataillon, P. E., and Cedex, M. (2019). "Consistency of satellite-based precipitation products in space and over time compared with gauge observations and snow- hydrological modelling in the Lake Titicaca region." 595–619.

Schuol, J., Abbaspour, K. C., Yang, H., Srinivasan, R., and Zehnder, A. J. B. (2008). "Modeling blue and green water availability in Africa." *Water Resour. Res.*, 44(7), 1–18.

Schuster, G., Ebert, E. E., Stevenson, M. A., Corner, R. J., and Johansen, C. A. (2011). "Application of satellite precipitation data to analyse and model arbovirus activity in the tropics." *Int. J. Health Geogr.*, 10(1), 8.

Seyyedi, H. (2010). "Comparing satellite derived rainfall with ground based radar for North-western Europe." *Master's Thesis, Faculty of Geo-Information and Earth Observation, University of Twente, Enschede, The Netherlands*, , 1–100.

Sharannya, T. M., Al-ansari, N., Barma, S. D., and Mahesha, A. (2020). "Evaluation of Satellite Precipitation Products in Simulating Streamflow in a Humid Tropical Catchment of India using a Semi-Distributed Hydrological Model." *Water*, 12(2400), 1–22.

Sharannya, T. M., Mudbhatkal, A., and Mahesha, A. (2018). "Assessing climate change impacts on river hydrology – A case study in the Western Ghats of India." *J. Earth Syst. Sci.*, 127(6), 1–11.

Sharannya, T. M., Sreelakshmi, C. M., and Drissia, T. K. (2016). "Discharge Simulation for Thuthapuzha Subbasin of Bharathapuzha River Basin in Kerala."

Proc. of International Conference on Hydraulics, Water Resources and Coastal Engineering (HYDRO 2016), 699–704.

Sharannya, T. M., Venkatesh, K., Mudbhatkal, A., Dineshkumar, M., and Mahesha, A. (2021). "Effects of land use and climate change on water scarcity in rivers of the Western Ghats of India." *Environ. Monit. Assess.*, 193(12).

Shrestha, M., Shrestha, S., and Shrestha, P. K. (2020). "Evaluation of land use change and its impact on water yield in Songkhram River basin, Thailand." *Int. J. River Basin Manag.*, 18(1), 23–31.

Shrestha, N. K., Qamer, F. M., Pedreros, D., Murthy, M. S. R., Wahid, S. M., and Shrestha, M. (2017). "Evaluating the accuracy of Climate Hazard Group (CHG) satellite rainfall estimates for precipitation based drought monitoring in Koshi basin, Nepal." *J. Hydrol. Reg. Stud.*, 13(February), 138–151.

Shrestha, S., Bhatta, B., Shrestha, M., and Shrestha, P. K. (2018). "Integrated assessment of the climate and landuse change impact on hydrology and water quality in the Songkhram River Basin, Thailand." *Sci. Total Environ.*, 643(September), 1610–1622.

Shrestha, S., and Htut, A. Y. (2016). "Land Use and Climate Change Impacts on the Hydrology of the Bago River Basin, Myanmar." *Environ. Model. Assess.*, 21(6), 819–833.

Singh, S., Ghosh, S., Sahana, A. S., Vittal, H., and Karmakar, S. (2017). "Do dynamic regional models add value to the global model projections of Indian monsoon?" *Clim. Dyn.*, 48(3–4), 1375–1397.

Sinha, R. K., and Eldho, T. I. (2018). "Effects of historical and projected land use/cover change on runoff and sediment yield in the Netravati river basin, Western Ghats, India." *Environ. Earth Sci.*, 77(3).

Sinha, R. K., Eldho, T. I., and Subimal, G. (2020). "Assessing the impacts of land use/land cover and climate change on surface runoff of a humid tropical river basin in Western Ghats, India." *Int. J. River Basin Manag.*, 0(0), 1–12.

Srivastava, M. R. and S. R. K. (2009). "Development of a high resolution daily gridded temperature data set (1969 – 2005) for the Indian region." *Atmos. Sci. Lett.*, 10(October), 249–254.

Stagl, J.; Mayr, E.; Koch, H.; Hattermann, F.F.; Huang, S. Effects of climate change

on the hydrological cycle in central and eastern Europe. In Managing Protected Areas in Central and Eastern Europe under Climate Change; *Springer: Dordrecht, The Netherlands,* 31–43.

Status, G., Needs, A. A., and Indicator, F. O. R. S. D. G. (2021). "Progress on the level of water stress: Global status and acceleration needs for SDG indicator 6.4.2." *FAO and UN Water,*Rome, Italy.

Su, Y., Zhao, C., Wang, Y., and Ma, Z. (2020). "Spatiotemporal variations of precipitation in China using surface gauge observations from 1961 to 2016." *Atmosphere (Basel).*, 11(3), 303.

Swain, S. S., Mishra, A., Sahoo, B., and Chatterjee, C. (2020). "Water scarcity-risk assessment in data-scarce river basins under decadal climate change using a hydrological modelling approach." *J. Hydrol.*, 590, 125260.

Tarek, M., Brissette, F. P., Arsenault, R., De, É., and West, N. (2020). "Evaluation of the ERA5 reanalysis as a potential reference dataset for hydrological modelling over North America." 2527–2544.

Teutschbein, C., and Seibert, J. (2012). "Bias correction of regional climate model simulations for hydrological climate-change impact studies: Review and evaluation of different methods." *J. Hydrol.*, 456–457, 12–29.

Thiemig, V., Rojas, R., Zambrano-Bigiarini, M., and Roo, A. De. (2013). "Hydrological evaluation of satellite-based rainfall estimates over the Volta and Baro-Akobo Basin." *J. Hydrol.*, 499, 324–338.

Tomy, T., and Sumam, K. S. (2016). "Determining the Adequacy of CFSR Data for Rainfall-Runoff Modeling Using SWAT." *Procedia Technol.*, 24, 309–316.

Trisurat, Y., Alkemade, R., and Verburg, P. H. (2010). "Projecting land-use change and its consequences for biodiversity in northern thailand." *Environ. Manage.*, 45(3), 626–639.

Tuo, Y., Duan, Z., Disse, M., and Chiogna, G. (2016). "Evaluation of precipitation input for SWAT modeling in Alpine catchment: A case study in the Adige river basin (Italy)." *Sci. Total Environ.*, 573, 66–82.

Uniyal, B., Jha, M. K., and Verma, A. K. (2015). "Parameter identification and uncertainty analysis for simulating streamflow in a river basin of Eastern India." *Hydrol. Process.*, 29(17), 3744–3766.

Vanham, D. (2016). “Does the water footprint concept provide relevant information to address the water-food-energy-ecosystem nexus?” *Ecosyst. Serv.*, 17, 298–307.

Varghese, S. K., Veettil, P. C., Speelman, S., Buysse, J., and Huylenbroeck, G. Van. (2013). “Estimating the causal effect of water scarcity on the groundwater use efficiency of rice farming in South India.” *Ecol. Econ.*, 86, 55–64.

Veldkamp, A., and Fresco, L. O. (1996). “CLUE: A conceptual model to study the conversion of land use and its effects.” *Ecol. Modell.*, 85(2–3), 253–270.

Venkatesh, K., Preethi, K., and Ramesh, H. (2020a). “Evaluating the effects of forest fire on water balance using fire susceptibility maps.” *Ecol. Indic.*, 110(August 2019).

Venkatesh, K., and Ramesh, H. (2018). “Impact of land use land cover change on run off generation in tungabhadra river basin.” *ISPRS Ann. Photogramm. Remote Sens. Spat. Inf. Sci.*, 4(5), 367–374.

Venkatesh, K., Ramesh, H., and Das, P. (2020b). “Modelling stream flow and soil erosion response considering varied land practices in a cascading river basin.” *J. Environ. Manage.*, 264, 110448.

Verburg, P. H., and Overmars, K. P. (2009). “Combining top-down and bottom-up dynamics in land use modeling: Exploring the future of abandoned farmlands in Europe with the Dyna-CLUE model.” *Landsc. Ecol.*, 24(9), 1167–1181.

Visakh, S., Raju, P. V., Kulkarni, S. S., and Diwakar, P. G. (2019). “Inter-comparison of water balance components of river basins draining into selected delta districts of Eastern India.” *Sci. Total Environ.*, 654, 1258–1269.

Wagener, T., Wheater, H. S., and Gupta, H. V. (2011). “Identification and evaluation of watershed models.” *Water Sci. Appl.* 6, 29–47.

Wagle, N., Acharya, T. D., Kolluru, V., Huang, H., and Lee, D. H. (2020). “Multi-temporal land cover change mapping using google earth engine and ensemble learning methods.” *Appl. Sci.*, 10(22), 1–20.

Wang, H. M., Chen, J., Xu, C. Y., Zhang, J., and Chen, H. (2020). “A Framework to Quantify the Uncertainty Contribution of GCMs Over Multiple Sources in Hydrological Impacts of Climate Change.” *Earth’s Futur.*, 8(8).

Whan, K., Zscheischler, J., Orth, R., Shongwe, M., Rahimi, M., Asare, E. O., and Seneviratne, S. I. (2015). “Impact of soil moisture on extreme maximum

temperatures in Europe." *Weather Clim. Extrem.*, 9, 57–67.

Xu, R., Chen, N., Chen, Y., and Chen, Z. (2020). "Downscaling and Projection of Multi-CMIP5 Precipitation Using Machine Learning Methods in the Upper Han River Basin." *Adv. Meteorol.*, 2020.

Xue, X., Hong, Y., Limaye, A. S., Gourley, J. J., Huffman, G. J., Khan, S. I., Dorji, C., and Chen, S. (2013). "Statistical and hydrological evaluation of TRMM-based Multi-satellite Precipitation Analysis over the Wangchu Basin of Bhutan: Are the latest satellite precipitation products 3B42V7 ready for use in ungauged basins?" *J. Hydrol.*, 499, 91–99.

Yuan, F., Wang, B., Shi, C., Cui, W., Zhao, C., Liu, Y., Ren, L., Zhang, L., Zhu, Y., Chen, T., Jiang, S., and Yang, X. (2018). "Evaluation of hydrological utility of IMERG Final run V05 and TMPA 3B42V7 satellite precipitation products in the Yellow River source region, China." *J. Hydrol.*, 567(June), 696–711.

Zang, C., and Mao, G. (2019). "A spatial and temporal study of the green and blue water flow distribution in typical ecosystems and its ecosystem services function in an arid basin." *Water (Switzerland)*, 11(1).

Zhang, L., Nan, Z., Xu, Y., and Li, S. (2016). "Hydrological impacts of land use change and climate variability in the headwater region of the Heihe River Basin, northwest China." *PLoS One*, 11(6), 1–25.

Zhao, C., and Garrett, T. J. (2008). "Ground-based remote sensing of precipitation in the Arctic." *J. Geophys. Res. Atmos.*, 113(14), 1–10.

Zheng, X. Q., Zhao, L., Xiang, W. N., Li, N., Lv, L. N., and Yang, X. (2012). "A coupled model for simulating spatio-temporal dynamics of land-use change: A case study in Changqing, Jinan, China." *Landsc. Urban Plan.*, 106(1), 51–61.

PUBLICATIONS

International Journals

1. **Sharannya, T. M.**, Venkatesh, K., Mudbhatkal, A., Dineshkumar, M., and Mahesha, A. (2021). "Effects of land use and climate change on water scarcity in rivers of the Western Ghats of India." *Environ. Monit. Assess.*, 193(12). https://doi.org/10.1007/s10661-021-09598-7
2. **Sharannya, T. M.**, Al-Ansari, N., Barma, S. D., and Mahesha, A. (2020). "Evaluation of Satellite Precipitation Products in Simulating Streamflow in a Humid Tropical Catchment of India Using a Semi-Distributed Hydrological Model." *Water 2020,* 12(2400), 1–22. https://doi.org/10.3390/w12092400
3. **Sharannya, T. M.**, Acharya, T. D., Venkatesh, K., and Mahesha, A. (2022). "Enhanced streamflow simulations using nudging based optimization coupled with data-driven and hydrological models." *J. Hydrol. Reg. Stud,* 43 (101190), 1-14. https://doi.org/10.1016/j.ejrh.2022.101190.

Book Chapter

1. **Sharannya, T. M.,** and Mahesha, A. (2022). "Quantifying the Impact of Dynamic Land Cover and Climate Change on Sustainable Water Yield- A River Basin Scale Approach'. *Hydro-Environmental Impact Assessment of Climate and Land Use Change on Watersheds for Sustainable Development* edited by Eldho, T.I., Jha, M.K., North Carolina A&T University, USA, Cambridge Scholars Publishing (CSP). (Abstract submitted)

International Conferences

1. **Sharannya. T. M.**, and Mahesha, A. (2022). "Assessment of Streamflow under Climate Change Scenarios in Kariangode River Basin of Kerala". *International Conference on Water and Environmental Management (WEM-2022),* CWRDM.

2. **Sharannya. T. M.**, and Mahesha, A. (2021). “Hydrologic Impact of Climate Change on Gurupura Catchment - Western Ghats of India”. Canadian Geophysical Union Conference. Sponsored by *Canadian Geophysical Union* – Hydrology Section, Canadian Young Hydrologic Society, McGill University. Paper id-33.
3. **Sharannya. T. M.**, and Mahesha, A. (2020). “Application of RS and GIS to simulate runoff in a humid catchment”. *International Conference on Hydraulics, Water Resources and Coastal Engineering 25th HYDRO 2020*, NIT Rourkela, India, paper id-023.
4. **Sharannya. T. M.**, DineshKumar M., and A.Mahesha (2019). “Assessment of water balance of a humid tropical river Basin”. *Proc. Int. Conf. Hydraulic, Water Resources and Coastal Engg., (HYDRO 2019)*, Editors: Gopal Naik, M., Suresh Kumar N, Anjaneya Prasad, M, Raja Sekhar, P, Shashikanth K, Prasanna, SVSNDL and Harish Gupta, BS Publications, Hyderabad, ISBN: 978-93-8935-484-3,Vol. 1, 602-608.
5. Dinesh Kumar M., **Sharannya T.M.** and A. Mahesha, (2019). A comparative study on univariate and bivariate flood frequency analysis in Netravathi basin, Karnataka. Proc. Int. Conf. Hydraulic, Water Resources and Coastal Engg., (HYDRO 2019), Editors: Gopal Naik, M., Suresh Kumar N, Anjaneya Prasad, M, Raja Sekhar, P, Shashikanth K, Prasanna, SVSNDL and Harish Gupta, BS Publications, Hyderabad, ISBN: 978-93- 8935-484-3,Vol. 1, 609-617.

BRIEF BIO

Name **:** Sharannya T.M.

D.O.B. **:** 16/10/1992

Address **:** Divya Nivas,

B. Street, Mananthavady (P.O.),

Wayanad, Kerala. 670645

Current Designation: Scientist B

Hydrology and Climatology Research Group

Centre for Water Resources Development and Management

(CWRDM), Kerala.

Education **:** M.Tech (2017), Water Resources Engineering and Management,

National Institute of technology Karnataka, Surathkal.

B.Tech, Civil Engineering (2015),College of Engineering Trivandrum,

Kerala.

Contact **:** +91 9562286977

Email **:** sharannyatm@gmail.com